Università degli Studi di Ferrara

DOTTORATO DI RICERCA IN
SCIENZE DELL'INGEGNERIA

CICLO XXII

COORDINATORE Prof. Stefano Trillo

CORROSION BEHAVIOUR OF THE AZ31 MAGNESIUM ALLOY AND SURFACE TREATMENTS FOR ITS CORROSION PROTECTION

Settore Scientifico Disciplinare ING-IND/22

Dottorando
Dott. Federica Zanotto

Tutori
Chiarissimo Prof. Fabrizio Zucchi

Prof.ssa Cecilia Monticelli

_____

_____

Anni 2007/2009

To Francesco and Nicola

Contents

Preface

This thesis contains most of the research activity carried on during my PhD study at the Corrosion Study Centre "A. Daccò", University of Ferrara (Italy), from January 2007 to December 2009, with Professor Fabrizio Zucchi and Professor Cecilia Monticelli as my supervisors. The PhD was financed by the "Fondazione Aldo e Cele Daccò per la ricerca scientifica" – Lugano (Svizzera).

The main topic of my PhD has been the study of corrosion behaviour of magnesium alloys, in particular AZ31 alloy (a magnesium-aluminium alloy that find applications in the automotive fields) and the anti-corrosion methods, such as corrosion inhibition and surface treatments, for the protection of AZ31 alloy from corrosion.

Nowadays, the study of magnesium alloys is a topic of great relevance, because they are finding increasing attention by the automotive industry in reason of their low density associated with good mechanical properties. Environmental conservation has given impulse to magnesium alloys research and development, because it depends, to a great extent, on transportation industry, particularly CO_2 emissions produced by transport vehicles. As CO_2 emission is in direct proportion to fuel consumption, car weight has become a very important criterion of design efficiency assessments. Despite the numerous advantages in magnesium alloys usage as a structural material, their large diffusion has found limitation principally due to the poor corrosion resistance, the low capacity of strengthening and scarce ductility. Thus significant research is still

needed on processing, surface treatment, corrosion resistance, new alloy development and mechanical properties improvement.

Surface treatments are technologies currently used to protect magnesium alloys from corrosion and/or to favor the adhesion between the metallic substrate and the organic coatings. However, in the last recent years, efforts have been made to develop pretreatments with a low environmental impact to substitute chromate treatments, that present a serious environmental risk and are suspected carcinogens. Thus the development of eco-friendly surface treatments is a issue finding a considerable attention from the research and development community.

In the first chapter of this thesis the main aspects concerning corrosion behaviour and surface protection technologies of magnesium alloys will be presented.

In chapter 2 a comparative study between the corrosion behaviour of as-cast and hot rolled AZ31 magnesium alloy will be discussed in order to evaluate the effects of microstructure as well as phase chemical composition and distribution on the corrosion resistance of AZ31 alloy.

For the increasing interest in using environmentally friendly compounds, sodium salts of linear mono-carboxylic acids were firstly analyzed as inhibitors of AZ31 alloy corrosion in standard saline solution (Chapter 3) and successively, for the interesting results, tested as conversion coating promoters (Chapter 4), while their protective action was studied in diluted sulphate and chloride solutions.

Finally, the protective performance of coatings obtained by treating AZ31 specimens in 3-mercapto-propyl-trimethoxysilane baths modified with cerium nitrate (Chapter 5) or with nanoparticle oxides (Chapter 6), will be investigated.

The results of my PhD activity have been published or submitted for publication in national and international conference proceedings, as well as in international journals (see list of publication).

Acknowledgment

I wish to thank all the research group of the Corrosion Study Centre "A. Daccò", for their cooperation and encouragement. In particular gratitude goes to Professor Fabrizio Zucchi, who gave me the possibility to undertake this PhD studies.

I would especially like to thank the "Fondazione Aldo e Cele Daccò per la ricerca scientifica" for having financed this three years research activity.

A special thank goes to all my family, in particular to my parents and my husband Nicola, for their everyday concrete and moral sustain.

This thesis is dedicated to my son Francesco, because with his smiles and joy, give me the wish and the strength to improve myself. I hope that my husband and I will be able to transmit to him the desire and pleasure of learning.

Chapter 1

GENERAL ASPECTS ABOUT THE CORROSION BEHAVIOUR AND THE SURFACE PROTECTION TECHNOLOGIES OF MAGNESIUM ALLOYS

1.1 Introduction

Magnesium is the lightest of all the engineering metals, having a density of 1.7 g/cm^3. It is 35% lighter than aluminium (2.7 g/cm^3) and over four times lighter than steel (7.86 g/cm^3) [1]. It has an hexagonal crystal structure and, due to its favourable size factor (atomic diameter 0.320 nm), it is able to form a solid solution with a variety of elements including: Al, Zn, Li, Y, Ce, Ag, Zr and Th [2, 3].

Magnesium is widely distributed in the earth's crust as mineral deposits and in solution in sea water, this gives it a virtually unlimited supply, for example, it has been estimated that at current world use levels there is enough magnesium in the Dead Sea for at least 22,000 years [2, 3]. It is produced through either the metallothermic reduction of magnesium oxide with silicon or the electrolysis of magnesium chloride melts from seawater [1].

Magnesium alloys provide advantages when used as structural materials, because of their high strength-to-weight ratio, specific rigidity, good damping characteristics, and castability, which makes them applicable in various fields of modern engineering [2, 4]. Furthermore, magnesium and its alloys are non-magnetic, have relatively high thermal and electrical conductivity, and good vibration and shock adsorption ability [2].

Because of their low density and good mechanical properties combination, Magnesium alloys are of particular interest to the aerospace

and transport industry; for example, thorium-containing alloys have found applications in missiles and spacecrafts [2]. In the automotive industry, the requirement to reduce the weight of car components, as a result of legislation limiting emission, has increased interest towards magnesium alloys, in fact CO_2 emission is in direct proportion to fuel consumption [1]. A lightweight part made of magnesium on a car may cost more than that of aluminium, but Mg cost compensates for Al cost due to reduction in fuel and CO_2 emission [1, 5, 6]. General applications of magnesium alloys in the automotive industry are casting products, such as gear boxes, interior parts (car seat frame, instrument panel, brake and clutch pedal) [1, 5, 6]. Wrought alloys are currently used to a very limited extent, due to a lack of suitable alloys and some technological restrictions imposed by the hexagonal crystal structure of magnesium [1]. In fact, magnesium alloys possess poor formability at room temperature because of their hexagonal closed packed (h.c.p.) structure which results in limited deformation mechanisms [7, 8]. A further application in automotive industry of magnesium wrought products will depend mainly on improving of surface treatment, corrosion resistance, joining technique and cost reduction [9]. Magnesium alloys that will withstand higher temperatures are being developed for engine blocks and transmission housings. BMW manufactured a composite magnesium-aluminium alloy engine, the R6, that is the lightest 3.0 litre in-line six-cylinder gasoline engine in the world [1]. However, magnesium alloys usage as a structural material has been limited principally due to the poor corrosion resistance, the low capacity of strengthening and scarce ductility [2], thus significant research is still needed on processing, surface treatment, corrosion resistance, new alloy development, and

mechanical properties improvement, in order to increase its diffusion as engineering material.

1.2 Corrosion behaviour

The standard electrode potential of magnesium $E^{\circ}_{Mg^{2+}/Mg}$ is -2.37 V, but in 3% sodium chloride the electrode potential is -1.63 V/SCE. Therefore magnesium is often used as a sacrificial anode [10]. When magnesium alloys are employed as engineering material, in particular in automotive industry, they may be subjected to serious environments, thus their corrosion behaviour is one of the main critical aspect. The poor corrosion properties of magnesium and its alloys in wet environments deals with two aspects: 1) the almost-passive hydroxide films forming on surface are not perfect and protective; 2) the internal galvanic corrosion caused by impurities and secondary phases such as $Mg_{17}Al_{12}$, AlMn, AlsMnS, $Mg_{12}Nd$, Mg_2Pb [2, 10-12].

Magnesium dissolution in wet environments generally proceeds by an electrochemical reaction with water to produce magnesium hydroxide and molecular hydrogen (H_2), thus magnesium corrosion is relatively insensitive to oxygen concentration [2, 13].

The overall corrosion reaction is [2, 13]:

$$Mg + 2H_2O \rightarrow Mg(OH)_2 + H_2 \qquad\qquad (1)$$
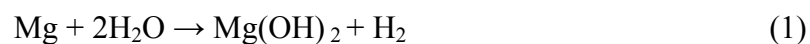
The overall corrosion reaction (1) may be expressed as the sum of the following partial reactions:

$$Mg \rightarrow Mg^{2+} + 2\,e^- \qquad \text{(anodic reaction)} \qquad (2)$$

$$2H_2O + 2\,e^- \rightarrow H_2 + 2OH^- \qquad \text{(cathodic reaction)} \qquad (3)$$

$$Mg^{2+} + 2OH^- \rightarrow Mg(OH)_2 \qquad \text{(product formation)} \qquad (4)$$

3
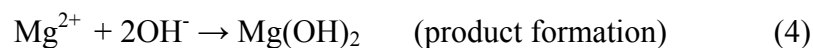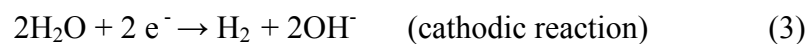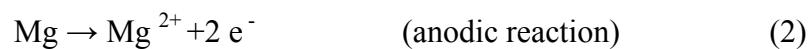
The anodic reaction (2) probably involves intermediate steps which may produce the monovalent magnesium ion (Mg^+) that has a short lifetime [20]. Low overvoltage cathodes (such as Ni, Fe, and Cu) facilitate hydrogen evolution, causing substantial corrosion rates [2].

The formation of a surface layer of $Mg(OH)_2$ or perhaps MgO, causes the difference between the theoretical standard potential and the actual measured corrosion potential [2]. Assuming that the protective film on magnesium is $Mg(OH)_2$, in figure 1.1 is reported the Pourbaix diagram showing the pH-potential stability range of this film.

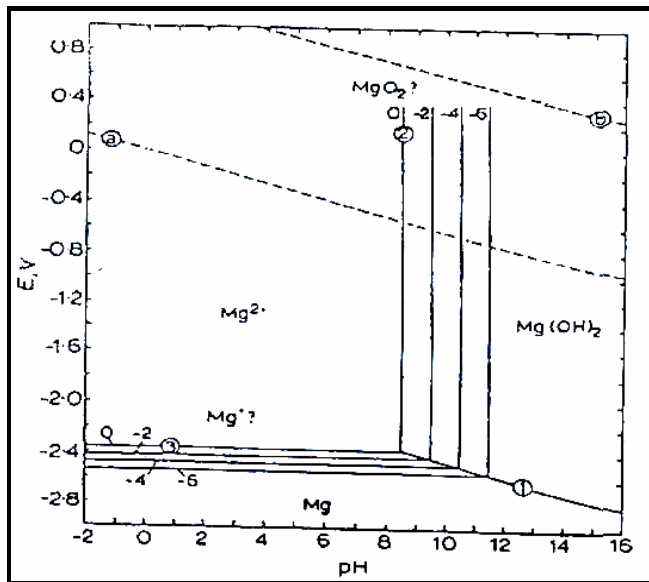**Fig. 1.1** – *Pourbaix diagram for the Mg-H_2O system at 25°C [1] . The region of water stability lies between the lines marked (a) and (b). The different regions are separated by the following reactions:*

        (1)   Mg + 2H_2O => Mg(OH) $_2$ + H_2

        (2)   Mg $^{2+}$ +H_2O => MgO + 2 H $^+$

        (3)   Mg => Mg $^{2+}$ +2 e^-

Anyway, Perrault affirmed that Pourbaix diagram needed to include the thermodynamic data for magnesium hydrides (MgH_2) and monovalent magnesium ion (Mg^+) and concluded that a thermodynamic equilibrium could not exist for a magnesium electrode in contact with an aqueous solution [2]. Song et al. [13], in a study of the polarization behaviour and the cathodic hydrogen evolution rates of pure magnesium in HCl and H_2SO_4 acidic solutions, found that on film-free surface, the experimental data were consistent with the involvement of the intermediate species Mg^+ in the magnesium dissolution process: magnesium is first oxidized to the intermediate species Mg^+, which, successively, chemically reacts with water to produce molecular hydrogen and Mg^{2+} ions.

The Mg^+ intermediate formation during magnesium dissolution process is also included as one of the model (monovalent magnesium ion model) used to partially explain the Negative Difference Effect (NDE): an electrochemical phenomenon exhibited by magnesium and its alloys [2, 13]. At the corrosion potential, the anodic (1) and cathodic (2) reactions involved in the overall magnesium corrosion process occurs with the same rate. When the potential is shifted to a more positive value (positive polarization), the rate of the anodic partial reaction would be expected to increase and the cathodic one to decrease. However, it was experimentally found that, with increasing of potential, both the magnesium corrosion rate increases and also the hydrogen evolution reaction rate (HER) increases rather than decreases. Thus, for this conditions, there is a negative difference effect due to the fact that the actual hydrogen evolution rate corresponds to a value higher than the expected one [2]. Moreover, a second experimental observation linked to this phenomenon was that the measured weight loss, with increasing of

the applied potential, was greater than the magnesium dissolution rate expected from the anodic polarization curve. Four different mechanisms have been proposed to explain the NDE phenomenon, anyway, they only partially succeed on this purpose [2, 13].

Generally, the corrosion of magnesium depends also on the characteristics of its surface film [2]. However, there are still limited information available on the nature of passive layers on magnesium in different solutions. Lunder et al. [21] reported that in dry environments, pure magnesium is protected by a stable air-formed oxide, whereas in wet environments, the air formed MgO is replaced by a less stable, hydrated oxide resulting from electrochemical metal oxidation. More recently, some researchers analyzed the initial film grown on mechanically polished Mg electrodes in water solution in a large range of pH values [22]. The XPS data showed the presence of an external $Mg(OH)_2$ layer, whose thickness was a function of immersion time, and of an underlying ultra-thin MgO layer probably of constant thickness after long immersion time in neutral aqueous solution. They also suggested that the thicker hydroxide layer formed at room temperature was porous.

The analysis of films formed when magnesium alloys containing Al, Mn or Zn exposed to the atmosphere, showed and enrichment of the secondary constituents [2]. In particular, Lunder et al.[29] considered that when the content of aluminium reaches 8% (mass fraction), the corrosion resistance of magnesium alloy could be greatly improved. It is likely that the beneficial effect of Al content is also related to the strong tendency for Al to form a stable passive film [2].

6

1.2.1 Types of corrosion

If exposed to normal ambient temperature in dry atmospheric environments, magnesium shows good resistance to oxidation [2, 11], however, corrosion susceptibility increases with the relative humidity and the temperature [14]. Corrosion resistance is especially low when magnesium alloys contain specific metallic impurities or when are exposed to aggressive electrolyte species such as Cl⁻ ions [2].

Magnesium alloys are highly susceptible to galvanic corrosion, mainly due to impurities and second phase presence (internal galvanic corrosion), but also due to a not correct assemblage or design (external galvanic corrosion) [2, 11]. If the cathodic element, present as impurities or as metal in contact with magnesium, are metals with low hydrogen overvoltage, such as Ni, Fe and Cu, they can constitute efficient cathodes for magnesium, causing severe galvanic corrosion, whereas metals that combine an active corrosion potential with a high hydrogen overpotential, such as Al, Zn, Cd and Sn are less dangerous [10].

The early magnesium alloys suffered rapid attack in moist conditions mainly due to the presence of impurities, chiefly iron, nichel and copper, creating micro-cells with the anodic magnesium matrix [4]. Recently high-purity alloys have been developed, with a controlled impurities content below a critical concentration. They shows a corrosion resistance to salt water higher than alloys of normal purity [15].

The galvanic corrosion rate is increased by the high conductivity of the electrolyte, the large potential difference between the anode and cathode, large chatodic to anodic area ratio and small distance from anode to cathode [2].

Magnesium is a naturally passive metal. Pitting corrosion will occur at its free corrosion potential, Ecorr, when exposed to chloride ions in a non-oxidizing medium, for example in neutral or alkaline solutions [2, 10]. It is generally observed that corrosion pits initiate near to the secondary phase particles such as $Mg_{17}Al_{12}$ and AlMn as a result of the local passive layer breakdown [2]. This is followed by the formation of an electrolytic cell in which the secondary phase particles are the cathode and the surrounding Mg matrix is the anode.

Figure 1.1 reports a model of pitting corrosion mechanism occurring on an extruded AM60 magnesium alloy in 3.5% NaCl aqueous solution [10].
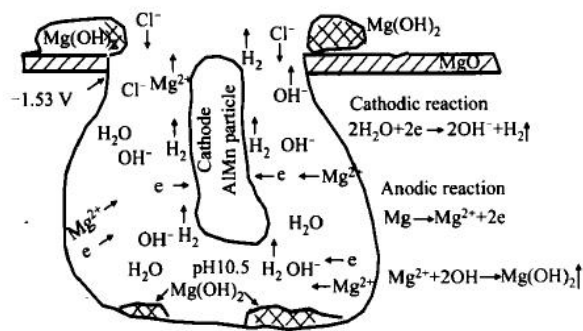
Fig. 1.2 – *Scheme of pitting corrosion mechanism for AM60 magnesium alloy in natural 3.5% NaCl solution [9].*

When AM60 alloy is immersed in a sodium chloride aqueous solution, Cl^- ions will absorb on the α-matrix areas bordering the intermetallic particles (i.e. AlMn particles). If the breakdown potential of the oxide film (previously formed in contact with air) reaches its corrosion potential (-1.53 V/SCE for the AM60), the α-matrix areas becomes anodic compared to the intermetallic particles and start to dissolve, thus a

corrosion nucleus may form adjacent to the AlMn particle. From this nucleus a corrosion pit develops, where the anodic and cathodic electrochemical reactions proceeds, leading to $Mg(OH)_2$ precipitation on the anodic areas and H_2 evolution on the cathodic ones [10].

Filiform corrosion, that is a type of localized corrosion generally occurring under protective coatings or anodized layers [2, 23], usually does not occur on uncoated pure magnesium [2]. However, the earlier stage of corrosion for an uncoated AZ91 magnesium alloy shows pitting and filiform corrosion morphology [16], due to the relatively resistant oxide film that can naturally form on this alloy [2].

It is generally reputed [2, 10] that magnesium alloys are immune to intergranular corrosion, even if secondary phases and intermetallics mainly can precipitate at grain boundaries during solidification. The reason is, as previously anticipated, that intermetallic compounds and secondary phases are cathodic to the grain interior. Corrosion tends to be concentrated in the area adjacent to the grain boundary until eventually the grain may be undercut and fall out [2].

Another type of corrosion that can affect magnesium alloys, particularly that used for automotive applications, is stress corrosion cracking (SSC); in fact automobiles components are often subjected to stress in a corrosive environment. SSC in magnesium and magnesium alloys is mainly transgranular. Sometimes intergranular SSC occurs in Mg-Al-Zn alloys, related to localized galvanic attack of the matrix when coupled with cathodic $Mg_{17}Al_{12}$ grain-boundary precipitates [10]. SSC is more marked in wrought alloys where it appears to follow the twinning plane [2]. Alloying addiction such as Al and Zn promote stress corrosion cracking [2]. Song et al. [17] studied the susceptibility to SSC, in various

solutions, of the AZ31 magnesium alloy, one of the most popular wrought magnesium alloys, usually supplied as sheet material with small thickness. AZ31 magnesium alloy is most susceptible to SCC when tested in 0.1M NaCl solution, whereas less susceptible in distilled water in spite of the not large difference. This can be probably attributed to Cl^- ions that promote the corrosion and the concomitant hydrogen production by the associated cathodic reaction. Some hydrogen atoms penetrate into the magnesium alloy, causing a reduction of the material cohesive strength, hence resulting in hydrogen embrittlement [10, 17]. In many related works it was reported that the role of the anodic dissolution is to produce surface defects which promote hydrogen production and entry into the material [17, 18].

Corrosion fatigue, that is caused by the simultaneous action of a cyclic stress application and a moderately aggressive environment exposure [23], is also an important corrosion mechanism that can affect magnesium alloys for engineering applications. It was found that corrosion fatigue cracks propagate in a mixed transgranular-intergranular mode and that the fatigue crack growth rate was accelerated by the same environments that accelerate SSC growth. Also in the case of corrosion fatigue, the addiction of alloying elements, such as Al, can increase the sensitivity to the corrosive environment [19].

Concerning corrosion at elevated temperature, it was reported [2] that, in oxygen, the oxidation rate of magnesium is a linear function of time, indicating a non-protective oxide on magnesium surface. Most alloying elements, such as Al and Zn, increase the rate of oxidation [2]. An alloy containing small amounts of cerium and lanthanum has been found to have an oxidation rate considerably below that of pure magnesium [2].

10

1.3 Factors influencing the corrosion behaviour

The corrosion behaviour of magnesium alloys depends on their metallurgy and on environmental factors. Concerning the metallurgical aspects, an important role is played by the alloying and impurity elements, the constituent phases and the microstructure.

1.3.1 Impurity elements

Some elements are extremely detrimental to the corrosion performance of magnesium alloys and they are termed impurity elements. In particular, is reported in literature [2] that Fe, Cu, and Ni are extremely deleterious because they have low solid solubility limits and provide active cathodic sites. At the same concentration the detrimental effect decreases as follows: Ni > Fe > Cu [2]. However, iron is generally of most concern since it is introduced to the melt from steel pots and casting moulds and is present as an impurity in the alloying elements [3]. In figure 1.3 is reported the tolerance limit of iron in pure magnesium (3% NaCl solution) [3]. When the impurity exceeds the tolerance limit, the corrosion rate is greatly accelerated. The tolerance limits are influenced by the manufacture method and the solidification rate [2], but also by the presence of third elements, such as manganese in the Mg-Al alloys [2, 3]. In fact manganese added in small amounts improves the corrosion resistance of these alloys [3, 10]. In this case, iron tolerance limit is equal to 0.032 of the manganese concentration (by weight) [2]. As reported in literature [21], Mn reduces the corrosion rate of magnesium alloys firstly because it combines with the iron in molten magnesium alloy during melting and forms an intermetallic compound which settles to the melt bottom, thus lowering the iron content in the alloy; secondly,

manganese encapsulates iron particles that remain in the metal during solidification, therefore making them less active as cathodic sites (magnesium-manganese galvanic coupling is less effective than the magnesium-iron one [2]).

Nickel is more harmful than iron, both in pure magnesium and in magnesium alloys, because of it has a lower tolerance limit [2]. Nickel tolerance limit was found independent from other alloying elements addition, but affected by the casting method [2].

The addiction of copper to Mg-Al-Zn alloys showed a detrimental effect on corrosion resistance, likely due to its incorporation in the eutectic phase [2].
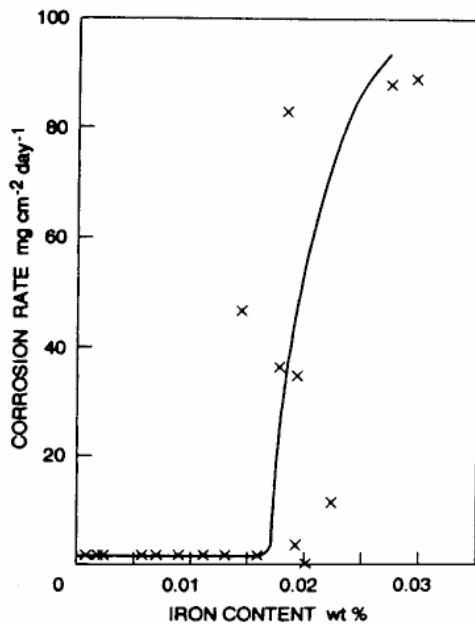

Fig. 1.3 *– Effect of iron on the corrosion of pure magnesium (3% NaCl solution) [3].*

12

1.3.2 Principal alloying elements

In accordance with their chemical composition magnesium alloys belong to two main alloying systems, namely, Mg – Al – Zn – Mn and Mg – Zn – Zr. There are also magnesium-lithium alloys but they have a specificity and limited use [24]. In the standard designation for magnesium alloys, the first two letters identify the two most important alloying elements, these are followed by their nominal concentrations in wt. % [3]. For example AZ31: A and Z correspond to aluminium and zinc respectively, which are contained in the alloy with a nominal concentration of 3 % and 1 % respectively.

When magnesium is alloyed with zirconium, generally posses good corrosion resistance in salt solutions and are relatively insensitive to iron and nickel. In fact these impurities are maintained to very low level by precipitation with zirconium before casting [2]. The solubility of Zr in magnesium is lower therefore it is a remarkable grain refiner for magnesium alloys [25].

Aluminium is partly present in solid solution, and partly precipitated as a continuous β phase ($Mg_{17}Al_{12}$) along grain boundaries as well as in the eutectic phase, constituted by a lamellar structure [2]. Alloying magnesium with aluminium in general improves the corrosion resistance [11]. It is reported that corrosion rate decreases rapidly with increasing of aluminium up to 4%, but further addiction up to 9% results only in a modest improvement in corrosion resistance [2]. The beneficial role of aluminium is generally attributed to β phase precipitation, that, depending on its distribution, can show a barrier effect to corrosion [26, 27], and to the increasing of the passive film stability [28]. The aluminium enrichment in anodic films with increasing of aluminium

content in the substrate was suggested to be the reason of the higher passive film stability for Mg-Al alloys [28].

However, it was also found that aluminium can have a negative influence on corrosion, because this metal reduced iron tolerance limit almost linearly with increasing of its content [2].

The aluminium concentration in the α phase is also crucial to the overall corrosion performance of dual phase alloys [2, 29]. For effect of segregation during solidification process, the aluminium concentration can vary from a few percent in the grain interior to 10% in the vicinity of the β phase, thus Lunder et al. [29] proposed that aluminium accelerates anodic dissolution below 8%, whereas decreases corrosion above 10%. Mathieu et al. [30] suggested that the semi-solid process (SSP), leading to an Al enrichment of the α phases, would be a way to reduce the AZ91 alloy corrosion. In fact, the galvanic corrosion rate between the two main constituents (α and β) resulted decreased with increasing of Al content.

The presence of zinc in magnesium alloys can increase the tolerance limits and reduce the effect of impurity once the tolerance limit has been exceeded [2]. Lunder et al. [29] found that generally zinc seemed to render α and β phase more noble. However the sensitivity of AZ alloys to filiform corrosion increases as the zinc content increases in the range of 0-3% [2].

Generally, an improvement in microstructure and mechanical properties of magnesium alloys can be achieved by the addition of minor alloying elements, such as rare earth elements [31-33]. In particular, rare earth element can improve strength at elevated temperature as well as creep resistance [33]. In addition to favourable high temperature properties, certain Mg-RE alloys present good corrosion resistance [1]. Zucchi et al.

14

[34] analyzed the corrosion behaviour of a WE43 magnesium alloy (3.92% Y, 2.09% Nd and 0.48% Zr) in sulphate and chloride solutions, they observed an improvement of the protective performances of the corrosion product film provided by RE elements. Moreover, the formation of less cathodic intermetallic compounds can justify the higher corrosion resistance exhibited by the Mg-RE alloys [1].

1.3.3 The role of phases

In general, the corrosion performance of magnesium alloys is mostly dependent on chemical composition and distribution of its constituent phases. The Mg-Al-Zn alloy are mainly constituted by two phases: the α phase, a substitutional solid solution of aluminium in magnesium, and the β phase, the intermetallic compound ($Mg_{17}Al_{12}$), present as precipitates along the grain boundaries. Researchers [27, 29, 30] have demonstrated that the study of the corrosion behaviour of α and β phases is the foundation for understanding the corrosion processes of Mg-Al-Zn alloys and the effects on corrosion of others factors such as alloying elements and impurities. It is reported in literature [2, 27], that β phase in AZ91 acts as inert corrosion barrier so that its presence improves the corrosion resistance; however there is also the opposite opinion that $Mg_{17}Al_{12}$ precipitates, being cathodic with respect to the α matrix, are detrimental for corrosion resistance. Song et al. [26, 27], measuring the polarization curves for α and β phases in 1N NaCl solution, found that the corrosion current density of β phase was much lower than that of α phase. This findings led these researchers to the conclusion that β phase was very stable in NaCl solutions and was inert to corrosion. However the β phase is also an effective cathode for the α matrix, thus they suggested that the

β phase mainly served as a galvanic cathode and accelerated the corrosion process of the α matrix, if its volume fraction was small. On the contrary, if β phase volume fraction was high, it may act as an anodic barrier to inhibit the overall corrosion of the alloy, because in this case corrosion only occurs on limited surface area on α phase.

As already discussed in paragraph 1.3.2, also the α phase composition and compositional distribution can influence the corrosion behaviour and morphology of Mg-Al alloys. Figure 1.4 reports a microstructure of a die cast AZ91D alloy [26]. The microstructure consisted of primary α grains surrounded by a eutectic mixture of α and β ($Mg_{17}Al_{12}$). The primary α and the eutectic α phases have different electrochemical behaviour depending on their different aluminium contents [26, 30]. As a matter of fact, Song et al. proposed for the die cast AZ91D alloy [26] that primary α grains were preferentially dissolved, then β intermetallics were undermined due to the dissolution of eutectic α phase.
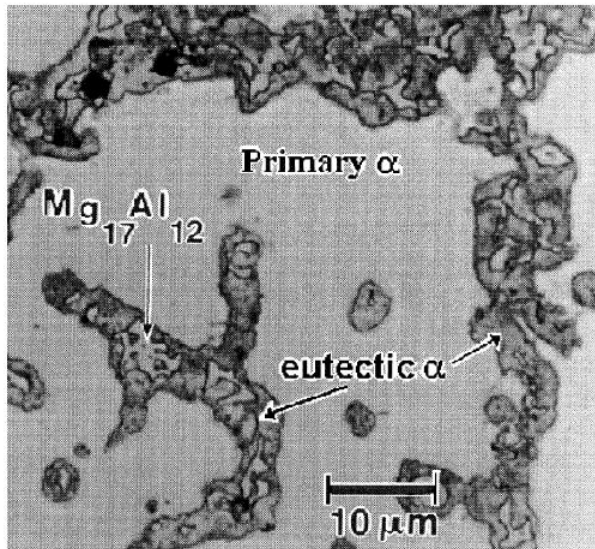

Fig. 1.4 – *Optical microstructure of a die cast AZ91D alloy [24].*

16

1.3.4 Effect of microstructure

Microstructural parameters such as grain size and phase distribution also have influence on corrosion behaviour [2]. The microstructure varies with the method of processing or the subsequent heat treatments, however, also the same production techniques conducted by different researchers might determine quite different microstructures and leading to apparent contradictory electrochemical behaviours [35]. Even for the same specimen, the microstructures can vary depending on the examined sections. For example, Song et al. [26] in a study on the effect of the microstructure on the corrosion behaviour of a die-cast AZ91D alloy, found that the skin of die cast alloy showed better corrosion resistance than the interior. This was attributed to a combination of a higher volume fraction of the β phase, to a more continuous β phase distribution around finer α grains and to a lower porosity in the skin layer than in the interior of the die casting. These authors concluded that the casting method strongly influences the corrosion performance through a microstructure control, with higher solidification rates being of potential benefit. In fact, [2] rapid solidification generally improves corrosion resistance since it leads to a significant grains refinement, a more homogenized microstructure than in the ingot metallurgy and increases the limit of solid solubility, allowing detrimental elements to exist in less harmful locations or phases.

Other researchers [36] analyzed the different corrosion behaviour of a die-cast and a ingot AZ91D alloy. The die-cast alloy showed higher corrosion resistance and better passivity than AZ91D ingot due to fine grain structure and a higher β phase volume fraction. Coring of aluminium also showed a more significant influence on corrosion

behaviour in ingot material. In fact, the lower aluminium content of eutectic α phase in ingot compared to die-cast, makes it susceptible to corrosion at longer exposure times that led to undermining of β phase, which was found to be high for ingot material from XRD data.

The semi-solid processing (thixomolding) is an innovative production technology, where magnesium alloys, maintained in a thixotropic semi-solid state by a vigorous stirring, are injected under pressure into a mould [37, 38]. In a comparative study about the corrosion behaviour of an AZ91D alloy produced by semi-solid processing (SSP) and the same produced by high pressure die-casting (HPDC) [42], it was observed that the corrosion resistance of semi-solid AZ91D alloy was somewhat higher than the same alloy produced by HPDC. In this case, the better corrosion resistance of the SSP AZ91D cannot be due to β phase acting as a barrier, since this phase is present as large discontinuous grains, but it was attributed mainly to the particular composition of the α phase resulting from the treatment of the semi-solid alloy prior to injection in the mould. In fact it is reported that [38] stirring determines breaking of the dendritic structure leading to rounded-shape pre-existing α grains with an Al content (about 3.7 wt.%) higher than that of the α solid solution (1.8 wt.% Al) of the die-cast alloy.

Micro-porosity presence in the magnesium alloy can also have a detrimental effect on corrosion resistance [2]. Castings usually have some porosity. The amount and form of porosity strongly depends on the alloy composition, the employed casting method, the design of the casting, thermal and feeding parameters [26]. Higher porosity means that the exposed surface is more active. As a matter of fact, usually micro-pores originate from defects, so they are active points for corrosion

18

reactions. Moreover, the formation of corrosion products inside a micro-pore can lead to the development of a auto-catalytic corrosion cell within the pores and thus to a serious localized corrosion breakdown [26].

Heat treatment can change the microstructure of magnesium alloys [10]. For example, it was observed [39] that a moderate temperature ageing of a die cast AZ91D led, in the early stages, to a rapid precipitation of β phase in the aluminium rich areas of the α matrix. The β phase precipitation occurred mainly on grain boundaries, so that it formed an almost continuous network along the grain boundaries. This β phase distribution, as also previously reported (paragraph 1.3.3), had a beneficial effect on corrosion resistance, acting as a barrier to corrosion propagation in the α matrix. However, in the later aging stages, the precipitation of rod shaped β phase further away from the grain boundaries, determined an aluminium content decreasing in the α grains; this effect made the α matrix more active, causing an increase of the alloy corrosion rate.

With increasing applications of magnesium alloy in aerospace, aircraft and automotive fields, also some post processing techniques such as laser welding will became important for these alloys. Evidently, welding process parameters may influence their corrosion resistance [40]. Generally, the high welding speed and fast cooling rate of the welds, as in the case for high power laser welding, could improve the corrosion resistance of the weld zone connected with the same material, because of its fine grain sizes and of solid solutions with higher aluminium content [10, 40]. The corrosion behaviour of Mg weld zone and the effects of the welding process parameters on corrosion, stress corrosion cracking and

19

corrosion fatigue, however, are not well known and further research remains to be done [10].

1.3.5 Influences of Environment

The corrosion resistance of materials always refers to some specific environments. Magnesium alloys are stable in fewer media in comparison with other materials, like steels and aluminium alloy. Following, only some information about the environmental influence on corrosion behaviour of magnesium and its alloys are reported.

Usually the corrosion resistance in aqueous solution is influenced not only by solute concentration and pH, but also by the volume, movement and temperature of the liquid [23]. In general magnesium alloys are stable in basic solutions, but in neutral and acidic media they dissolve at high rates [2]. In neutral and basic solutions the corrosion resistance is relatively high because of the formation of a partially protective $Mg(OH)_2$ layer on the alloy surface [2, 41]. Song et al. compared the electrochemical behaviour of magnesium in Na_2SO_4 and NaCl, they suggested that chloride ions presence could make the surface film more active or increase the film-free area, and might also accelerate the electrochemical reaction rate from magnesium to magnesium univalent ions (the intermediate species Mg^+) [42]. Thus the corrosion rate usually increases with increasing of Cl^- concentration. SO_4^{2-} is believed to have much less influence than Cl^- [42]. Ambat et al. [43] found that the corrosion rate for the ingot and die-cast AZ91D was very high in highly acidic solutions (pH 1÷2) as compared to that in neutral and highly alkaline solutions (pH 4.5÷12.0), and the rate increased with chloride ion concentration at all pH levels. They suggested that the increase in

20

corrosion rate with increasing chloride ion concentration at pH 7.25 and 12.0 may be attributed to the participation of chloride ions in the dissolution reaction. Chloride ions are aggressive for both magnesium and aluminium. The adsorption of chloride ions to oxide covered magnesium surface transforms $Mg(OH)_2$ to easily soluble $MgCl_2$.

Dissolved oxygen does not appear to influence magnesium and magnesium alloys corrosion in chloride solutions [2] or in sodium sulphate solution [44], whereas the corrosion rate of magnesium is dependent on HCO^{3-} concentration, naturally present in aerated solutions. In fact, it was observed [44] that in sodium sulphate solutions the presence of HCO^{3-} ions destabilized the MgO/Mg(OH)2 layer initially formed on the magnesium surface by formation of soluble salts. Evidently, in NaCl solutions the aggressiveness of chlorides masks the role of HCO^{3-} [44].

Neutral or alkaline fluorides from insoluble MgF_2 and are not appreciable corrosive. Magnesium fluoride is very insoluble in hydrofluoric acid and as a consequence magnesium does not dissolve in this acid [2]. However, in dilute aqueous hydrofluoric acid magnesium is not stable and it might undergo to pitting attack [2].

Magnesium is readily soluble in dilute sulphuric acid and no protective film is formed in this acid, so the attack is rapid [2].

A clean unprotected magnesium alloy surface exposed to indoor or outdoor atmospheres free from salt spray develops a gray film that protects the metal from corrosion [2]. Corrosion of magnesium alloys increases with the increase of relative humidity (RH). At low humidity levels the rate of the corrosion attack is negligible. At 30% humidity, only minor corrosion may occur. At 80% humidity, the surface may

21

exhibit considerable corrosion. In marine atmospheres heavily loaded with salt spray, magnesium alloys require protection for prolonged survival [45].

The presence of NaCl and/or CO_2 in the atmosphere affects the mechanism of corrosion of magnesium alloys in humid environments [14]. In fact, it was reported [46], that the sodium chloride-induced atmospheric corrosion of magnesium alloys is inhibited by ambient concentrations of CO_2. The inhibitive effect of CO_2 was partly attributed to the formation of a slightly protective carbonate-containing film.

1.4 Corrosion prevention

Following are reported the main successful corrosion prevention strategies [2]:

> ➢ High purity alloys. Decrease the impurities level below their tolerance limits.

> ➢ New alloys. Develop alloys with improved corrosion resistance by means of suitable elements addition and/or phases and microstructure distribution.

> ➢ Surface modification. This includes ion implantation and laser annealing.

> ➢ Protective coatings. These includes anodizing, electrochemical plating, conversion coatings, hydride coatings, organic coatings and vapor-phase processes.

One of the most effective ways to prevent corrosion of magnesium and its alloys is to create a barrier between the metal and its environment, through the formation of protective coatings and/or through the presence of corrosion inhibitors in them [47]. In order to provide adequate

22

corrosion protection, the coating must be uniform, well adhered, pore free and self-healing for applications where physical damage to the coating may occur. As already discussed, one of the problems with magnesium is its chemical reactivity. As soon as it comes in contact with air or water an oxide/hydroxide layer forms on the surface which can have a detrimental effect on coating adhesion and uniformity. Thus, the pre-cleaning process plays a critical role in the development of a good protective coating on magnesium and its alloys [47].

Among the above mentioned technologies available for coating magnesium and its alloys, organic coatings can offer an adequate barrier effect against atmospheric corrosion, in fact they are widely used for protecting aluminium, steel and zinc [48]. Organic coating systems can include a variety of different processes that make use of organic polymers, such as painting, powder coating, E-coating (cathodic epoxy electrocoating) and the application of lacquers, enamels and varnishes [47]. However organic coatings are usually the last step in a coating system, because their protective properties may be lost by the entrapping of water at the interface in the form of a thin layer or as blisters [48]. The adhesion and corrosion resistance of these coatings are inadequate without a suitable pretreatment. Therefore this problem has been mainly and successfully solved by means of chromating layers [49].

Chromate conversion coatings are formed by a chemical or an electrochemical treatment of metals or metallic coatings in solutions containing hexavalent chromium (Cr^{6+}) and, usually, other components. The process results in the formation of an amorphous protective coating composed of the substrate, complex chromium compounds, and other components of the processing bath [48]. These coatings provide

corrosion protection, not only presenting a non-reactive barrier to the environment, but also through their self-healing properties and the inhibiting effect of Cr(VI). In fact, during corrosion Cr(VI)?? is reduced to form an insoluble trivalent chromium species that terminates the oxidative attack [47]. However chromate coatings present a serious environmental risk and are suspected carcinogens. Thus in the last years efforts have been made to develop pre-treatments with a low environmental impact, like the chrome 3^+ (green chromate treatment), or fluorozirconate [49] or phosphate–permanganate, or stannate treatments [50-55]. Moreover, in recent times, also rare earth metal salts (REMS) and especially cerium species were tested as conversion coatings on magnesium and its alloys [56-59]. Corrosion inhibition by cerium salts is generally associated with the formation and precipitation of cerium oxides or hydroxides over cathodic sites on the metal surface. These precipitates, in turn, give rise to a blocking effect and reduce the rate of the reduction reactions [56, 58]. Dabalà et al. [58] from the analysis of the conversion coating morphology of a AZ63 magnesium alloy after cerium-based conversion treatment, observed that the conversion coating consisted of a thin and cracked coating with 'dry-mud' morphology with large agglomerates over cathodic intermetallic particles; thus they suggested that the local pH increase, favoured by the galvanic activity between the cathodic particles and the α matrix, induced the precipitation of hydrated cerium oxide.

With the objective to find an economic and eco-friendly alternative to the existing chromate treatments, in the last recent years layers based on silanes have been introduced. These layers have been studied as adhesion promoters and/or protective coatings [49]. With the term silanes are

indicated a group of silicon-based organic-inorganic chemicals. Trialkoxysilanes (or silanes), with the general formula $R'(CH_2)_nSi(OR)_3$ (where R' = organic functionality; and OR = hydrolyzable alkoxy group, e.g., methoxy (OCH3) or ethoxy (OC2H5)), have been used as effective coupling agents or adhesion promoters in glass/mineral-reinforced polymeric composites for decades [60]. Generally, silanes need to be hydrolyzed in diluted aqueous solutions before application:

$$-Si(OR)_3 \xrightarrow{\text{hydrolysis}} -Si(OH)_3$$
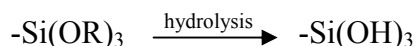
In fact they became "workable" once a sufficient number of silanols (SiOH) are generated [60]. The metallic surface pretreatment mechanism using the silanes is a rather simple mechanism. This consists in the immersion for a few minutes of the component in a solution (aqueous or alcoholic) diluted with the silane (generally 1-5 vol %), followed by an air drying process (or a thermal baking treatment) [49]. Before the drying step two key condensation reactions occur [49, 60].

One is the condensation between silanols (SiOH) from the silane solution and the metal hydroxides (MeOH) on the metal surface, forming covalent metallo-siloxane bonds (Me-O-Si) according to:

$$SiOH_{\text{(solution)}} + MeOH_{\text{(metal surface)}} = SiOMe_{\text{(interface)}} + H_2O$$
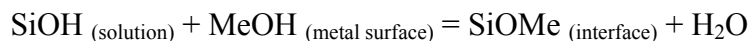
The other is the condensation among the excess SiOH groups adsorbed on the metals, forming a siloxane (SiOSi) film on the top:

$$SiOH_{\text{(solution)}} + SiOH_{\text{(solution)}} = SiOSi_{\text{(silane film)}} + H_2O$$
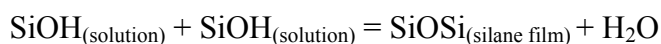
In figure 1.5 a simplified schematic bonding mechanism is reported [61]. Before condensation (figure 1.5, a), silane molecules are adsorbed onto the metal surface through hydrogen bonds formed between SiOH groups of the silane molecules and MeOH groups of the metal hydroxides. During the drying process (Figure 1.5, b) the condensation itself takes place with the consequent replacement of the weak bonds with the covalent Me-O-Si, giving excellent adhesion to the metal substrate, and Si-O-Si bonds.
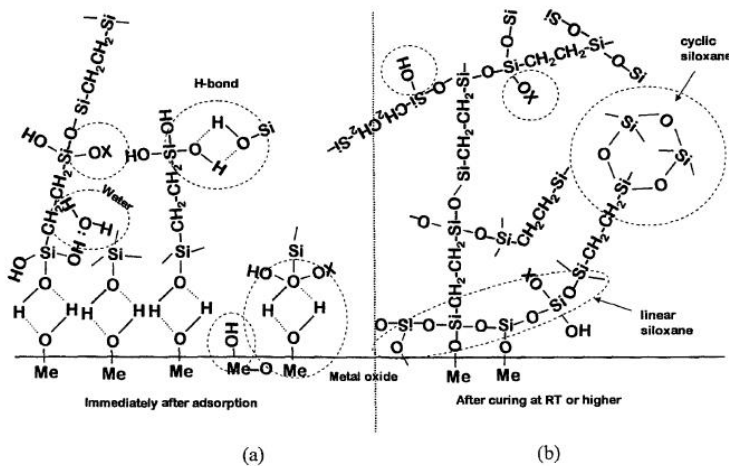

Fig. 1.5 *– Simplified schematic bonding mechanism between silane molecules and metal surface hydroxide layer: (a) before condensation: hydrogen-bonded interface; (b) after condensation: covalent-bonded interface [61].*

Furthermore, in the silane solution, another reaction could take place: the homopolymerization where the SiOH groups can condensate each other forming Si-O-Si bonds. This phenomenon does not seem to be positive since an homopolymerized molecule can no longer rely on the presence of the functional group which can bind with the organic layer. Nevertheless, this limitation can be avoided using proper immersion

time, in such a way that the silanes adhere to the surface, without having the time to bind each other [49].

The silanes suitable for corrosion protection can be divided into two major categories, i.e., "mono-silanes" (or organofunctional silanes, because have both organic and inorganic features [49]) and "bis-silanes" (or non-functional silanes [49]).

Mono-silanes are the silane coupling agents mentioned above with a general formula [60]:

$$R'(CH_2)_n Si(OR)_3$$
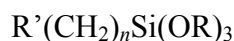
Where R' is the organofunctional group (for example amine or epoxy groups), which is able to form bonds with the polymeric materials [49], whereas OR is the hydrolyzable methoxy (OCH_3) or ethoxy (OC_2H_5) group [60]. For example, in this thesis, one of the most common organofunctional silanes has been studied, the 3-mercapto-propyl-trimethoxysilane having the following chemical structure:

$$HSCH_2CH_2CH_2Si(OCH_3)_3$$

In this case the thiol (SH) is the organofunctional group, and the methoxy (OCH_3) is the hydrolyzable group.

Bis-silanes, are mainly used as crosslinkers for silane coupling agents and have the following general formula [60]:

$$(RO)_3Si(CH_2)_n R'(CH_2)_n Si(OR)_3$$
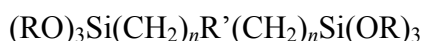
One of the difference between mono- and bis-silanes is that the number of hydrolysable OR groups in a bis-silane molecule is double that in a mono-silane molecule, as illustrated in figure 1.6 [61]. Thus they can be hydrolyzed more easily than the mono-silane and the possibility to form covalent bonds with the substrate seems to be accentuated [49]. However, apparently they are not able to form bonds with the polymeric materials, because their functional groups might bond only with metal and inorganic materials [49].
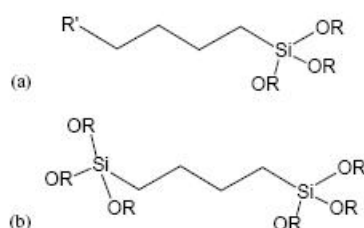

Fig. 1.6 – *Structures of mono-silane (a), and bis-silane molecule (b) [61].*

The call for a reduction of Volatile Organic Compounds (VOC) in metal-finishing industries, has given effort to the development of water-soluble silanes, that need only de-ionized water for treatment bath preparation.

Silane hydrolysis in water-based silane solution is very quick due to their hydrophilic nature [62]. Water-based silanes can be also mixed with resins. Such silane/resin systems are called "super-primers". The purpose of developing "super-primers" is to further enhance both corrosion protection and paint adhesion of metals [63].

In the last recent years the research on silane treatments has also focused on the development of nano-structured silane films and "self-healing" silane systems. Silica nano-particle filled silane film applied on an aluminium alloy was demonstrated to provide a high corrosion resistance

(also due to an inhibition effect of silica particles to the cathodic process) and to have improved mechanical properties (the interfacial layer is hardened by silica particles) [61]. Adding eco-friendly corrosion inhibitor, such as a cerium salt, into silane solutions can increase the corrosion resistance of the silane film and provide "self-healing" effect [64].

It is reported in literature [60] that silane film thickness has been found to be linearly proportional to the corresponding silane solution concentration. It was also demonstrated that the obtained film thickness was independent of contact time [60].

In this thesis the attention was principally focused on the development of treatments for the formation of protective surface films, such as conversion coatings and organic coatings. However, part of the experimental activity was dedicated also to the inhibition of magnesium alloys by means of environmentally friendly compounds. In fact, corrosion inhibition is another possibility of reducing magnesium alloys corrosion rate by adding the aggressive solution with suitable chemical compounds [23].

References

[1]   Mustafa Kemal Kulekci, *"Magnesium and its alloys applications in automotive industry"*, International Journal of Manufacture Technology (2008), 39, pp. 851-865.

[2]   G. L. Song, A. Atrens *"Corrosion Mechanism of Magnesium Alloys"* Advanced Engineering Materials (1999), 1, No. 1, Rev., pp. 11-33.

[3]   D. Eliezer, E. Aghion, F.H. (Sam) Froes, *"Magnesium Science, Technology and Applications"*, Advanced Performance Materials (1998), 5, pp. 201-212

[4]   E. F. Volkova, *"New Mg-based materials"*, Metal Science and Heat Treatment (2006), 48, pp. 11 – 12, Translated from Metallovedenie i Termicheskaya Obrabotka Metallov (2006), 11, pp. 5-9.

[5]   H Friedrich, S. Shumann, *"Research for a "new age of magnesium" in automotive industry"* Journal of Materials Processing Technoly (2001), 117, pp. 276-281.

[6]   E. Aghion, B. Bronfin, D. Eliezer , *"The role of the magnesium industry in protecting the environment"*, Journal of Materials Processing Technoly (2001), 117, pp. 381-385.

[7]   Bo-Ping Zhang , Yi-Fan Tu, Jing-Yi Chen, Hai-Long Zhang, Yong-Lin Kang, Hirowo G. Suzuki, *"Preparation and characterization of as-rolled AZ31 magnesium alloy sheets"*, Journal of Materials Processing Technology (2007), 184, pp. 102-107.

[8]   M. Easton, A. Beer, M. Barnett, C. Davies, G. Dunlop, Y. Durandet, S. Blacket, T. Hilditch, and P. Beggs *"Magnesium Alloy Applications in Automotive Structures"*, JOM Vol. 60 No. 11 *www.tms.org/jom.html*, pp. 57-62.

[9]   A. Stalmann, W. Sebastian, H. Friedrich, S. Shumann and K. Droder, *"Properties and Processing of Magnesium Wrought Products for Automotive Applications"*, Advanced Engineering Materials (2001), 3, No. 12., pp. 969-974.

[10] Zeng Rong-Chang,H Ang Jin, Huang Wei-Jiu, W. Dietzel, K. U. Kainer, C. Blawert, Ke Wei, *"Review of studies on corrosion of magnesium alloys"*, Transactions of Nonferrous Metals Society of China (2006), 16, pp. S763-S771.

[11] G. Song, A. Atrens, *"Understanding magnesium corrosion"*, Advanced Engineering Materials (2003),5(12), pp. 837-858.

[12] G. Song, *"Recent progress in corrosion and protection of magnesium alloys"*, Advanced Engineering Materials (2005), 7(7), pp. 563-586.

[13] G. Song, A. Atrens, D. StJhon, et al., *"The electrochemical corrosion of pure magnesium in 1 N NaCl"*, Corrosion Science 1997, vol 39, 5, pp. 855-875.

[14] S. Feliu Jr., A. Pardo , M.C. Merino, A.E. Coy, F. Viejo, R. Arrabal, *"Correlation between the surface chemistry and the atmospheric corrosion of AZ31, AZ80 and AZ91D magnesium alloys"*, Applied Surface Science (2009), 255, pp. 4102-4108.

[15] *"Magnesium – Alloys and Technology"*, Edited by K.U. Kainer, 2003 WILEY-VCH Verlag GmbH & Co. KG aA, Weinheim.

[16] O. Lunder, Lein J. E., Hesjevik S. M., Awe T. Kr, Nisancioglu, *"Corrosion morphologies on magnesium alloy AZ91"*, Werkstoffe und Korrosion (1994), 45, pp.331-340.

[17] G. Song, C. Blawert, W. Dietzel, A. Atrens, *"A study on stress corrosion cracking and hydrogen embrittlement of AZ31 magnesium alloy"*, Materials Science and Engineering A (2005), 399, pp. 308–317.

[18] R. Song, F. Yang, C. Blawert, W. Dietzel, "*Behavior of Stress Corrosion Cracking in a Magnesium Alloy*" Journal of Wuhan University of Technology - Material Science, Ed. Feb. 2009, pp. 111-113.

[19] Y. Uematsu, K. Tokaji, T. Ohashi, *"Corrosion fatigue behavior of extruded AZ80, AZ61, and AM60 magnesium alloys in distilled water"*, Strength of Materials (2008), Vol. 40, No. 1, pp.

[20] G. L. Makar, K. Kruger, *"Corrosion Studies of Rapidly Solidified Magnesium Alloys"*, Journal of Electrochemical Society (1990), 137(2), pp. 414-421.

[21] O. Lunder , T.Kr Aune, K. Nisancioglu, *"Effect of Mn additions on the corrosion behavior of mould-cast magnesium ASTM AZ91"*, Corrosion (1987), 43 (5), pp. 291-295.

[22] M. Santamaria, F. Di Quarto, S. Zanna, P. Marcus, *"Initial surface film on magnesium metal: A characterization by X-ray photoelectron spectroscopy (XPS) and photocurrent spectroscopy (PCS)"* Electrochimica Acta (2007), 53, pp. 1314–1324.

[23] G. Bianchi, F. Mazza, *"Corrosione e protezione dei metalli"*, 3° ed., AIM (Italy), 2005.

[24] E. F. Volkova, *"Modern magnesium-base deformable alloys and composite materials (a review)"*, Metal Science and Heat Treatment (2006) Vol. 48 (11, 12), pp. 473-478.

[25] Q. Ma; L. Zheng, D. Graham, M.T. Frost, D.H. StJohn, *"Settling of undissolved zirconium particles in pure magnesium melts"*, Journal of Light Metals (2001), 1 (3) pp. 157-165.

[26] G. Song, A. Atrens, M. Dargusch, *"Infuence of microstructure on the corrosion of diecast AZ91D"*, Corrosion Science (1999), 41, pp. 249-273

[27] G. Song, A. Atrens, Wu, Xianliang; Zhang, Bo, *"Corrosion behaviour of AZ21, AZ501 and AZ91 in sodium chloride"*, Corrosion science (1998) 40 (10), pp. 1769-1791.

[28] O. Khaselev, J. Yahalom, *"The anodic behavior of binary Mg-Al alloys in KOH-aluminate solutions"*, Corrosion science (1998), 40, pp. 1149-1160.

[29] O. Lunder, J.E. Lein, T. Kr. Aune, K. Nisancioglu, "The role of $Mg_{17}Al_{12}$ phase in the corrosion of Mg alloy AZ91", Corrosion (1989), 45 , pp. 741-748.

[30] S. Mathieu, C. Rapin, J. Steinmetz, P. Steinmetz, *"A corrosion study of the main constituent phases of AZ91 magnesium alloys"*, Corrosion Science (2003), 45, pp. 2741–2755.

[31] W. Mingxing, Z. Hong, W. Lin, *"Effect of Yttrium and Cerium Addition on Microstructure and Mechanical Properties of AM50 Magnesium Alloy"*, Journal of Rare Earths 2007,25 (2), April, pp. 233-237.

[32] Zhang, Ya; Zeng, Xiaoqin; Liu, Liufa; Lu, Chen; Zhou, Hantao; Li, Qiang; Zhu, Yanping *"Effects of yttrium on microstructure and mechanical properties of hot-extruded Mg–Zn–Y–Zr alloys"*, Materials Science and Engineering: A (2004), 373 (1-2), pp. 320-327.

[33] Yang, Mingbo; Pan, Fusheng, *"Effects of Y addition on as-cast microstructure and mechanical properties of Mg–3Sn–2Ca (wt.%) magnesium alloy"*, Materials Science & Engineering A (2009), 525 (1-2), pp. 112-120.

[34] F. Zucchi, V. Grassi, A. Frignani, C. Monticelli and G. Trabanelli *"Electrochemical behaviour of a magnesium alloy containing rare earth elements"*, Journal of Applied Electrochemistry (2006) , 36 pp. 195–204.

[35] A. Pardo, M.C. Merino, A.E. Coy, F. Viejo, R. Arrabal, S. Feliú Jr., *"Influence of microstructure and composition on the corrosion behaviour of Mg/Al alloys in chloride media"*, Electrochimica Acta (2008), 53, pp. 7890–7902.

[36] R. Ambat, N. Naing Aung, W. Zhou, *"Evaluation of microstructural effects on corrosion behaviour of AZ91D magnesium alloy"*, Corrosion Science (2000), 42, pp. 1433-1455.

[37] H. Kaufmann, P. J. Uggowitzer, *"Fundamentals of the New Rheocasting Process for Magnesium Alloys"*, Advanced Engineering Materials (2001), 3 (12), pp. 963-967.

[38] S. Mathieu, C. Rapin, J. Hazan, P. Steinmetz, *"Corrosion behaviour of high pressure die-cast and semi-solid cast AZ91D alloys"*, Corrosion Science (2002), 44, pp. 2737–2756.

[39] G. Song, A. L. Bowles, D. H. StJohn, *"Corrosion resistance of aged die cast magnesium alloy AZ91D"*, Materials Science and Engineering (2004) , A366, pp. 74–86.

[40] X. Cao, M. Jahazi, J.P. Immarigeon, W. Wallace, *"A review of laser welding techniques for magnesium alloys"*, Journal of Materials Processing Technology (2006), 171, pp. 188–204

[41] W.A. Badawy, N.H. Hilal, M. El-Rabiee, H. Nady, *"Electrochemical behavior of Mg and some Mg alloys in aqueous solutions of different pH"*, Electrochimica Acta (2008), doi:10.1016/j.electacta.2009.10.083.

[42] G. Song, A. Atrens, D. St John, X. Wu , J. Nairn, *"The anodic dissolution of magnesium in chloride and sulphate solutions"*, Corrosion science (1997), 39 (10-11), pp. 1981-2004.

[43] R. Ambat, N.N. Aung And W. Zhou, *"Studies on the infuence of chloride ion and pH on the corrosion and electrochemical behaviour of AZ91D magnesium alloy"*, Journal of Applied Electrochemistry (2000), 30, pp. 865-874.

[44] G. Baril, N. Pébère, *"The corrosion of pure magnesium in aerated deaerated sodium sulphate solutions"*, Corrosion Science (2001), 43, pp. 471- 484.

[45] A. Froats, T. Kr. Aune, D. Hawke, W. Unsworth, J. Hillis, *"Corrosion of Magnesium and Magnesium Alloys"*, Corrosion, Vol. 13 ASM Handbook, ASM International (1987).

[46] R. Lindstrfom, L. Johansson, G. E. Thompson, P. Skeldon, J. Svensson, *"Corrosion of magnesium in humid air"*, Corrosion Science (2004), 46, pp. 1141–1158.

[47] J.E. Gray, B. Luan, *"Protective coatings on magnesium and its alloys — a critical review"*, Journal of Alloys and Compounds (2002), 336, pp. 88–113.

[48] H. Leidheiser, Jr., *"Fundamentals of Corrosion Protection in Aqueous Solutions"*, Corrosion, Vol. 13 ASM Handbook, ASM International (1987).

[49] S. Rossi, F. Deflorian, *"Innovative Pretreatment of Metals to improbe the Adhesion Strength of the Organic Coatings: Silanes"*, Pitture e Vernici – European Coatings 1 (2006), pp.47-63.

[50] M.A. M.A Gonzáles-Núñez, C.A. Núñez-Lopez, P. Skeldon, G.E. Thompson, H. Karimzadeh, P. Lyon, T.E. Wilks, *"A non-chromate conversion coating for magnesium alloys and magnesium-based metal matrix composites"*, Corrosion Science (1995), 37, pp. 1763-1772.

[51] H. Huo, Y. Li, F. Wang, "*Corrosion of AZ91D magnesium alloy with a chemical conversion coating and electroless nickel layer"*, Corrosion Science (2004), 46, pp. 1467-1477.

[52] C.S. Lin, H.C. Lin, K.M. Lin, W.C. Lai, "*Formation and properties of stannate conversion coatings on AZ61 magnesium alloys"*, Corrosion Science (2006), 48, pp. 93-109.

[53] H. Umehara, M. Takaya, S. Terauchi, "*Chrome-free surface treatments for magnesium alloy"*, Surface and Coating Technology (2003),169-170, pp. 666-669.

[54] C.S. Lin, C.Y. Lee, W.C. Li, Y.S. Chen, G.N. Fang, "*Formation of Phosphate/Permanganate Conversion Coating on AZ31 Magnesium Alloy"*, Journal of Electrochemical Society (2006), 153(3), B90-B96.

[55] F. Zucchi, A. Frignani,G. Grassi, G. Trabanelli, C. Monticelli, "*Stannate and permanganate conversion coatings on AZ31 magnesium alloy"*, Corrosion Science (2007), 49, pp. 4542-4552.

[56] A.L. Rudd, C.B. Breslin, F. Mansfeld, *"The corrosion protection afforded by rare earth conversion coatings applied to magnesium"*, Corrosion Science, (2000), 42, pp. 275-288.

[57] M.F. Montemor, A.M. Simões, M.G.S. Ferreira and M.J. Carmezim, *"Composition and corrosion resistance of cerium conversion films on the AZ31 magnesium alloy and its relation to the salt anion"*, Applied Surface Science (2008), 254 (6), pp.1806-1814.

[58] M. Dabalà, K. Brunelli, E. Napolitani, M. Magrini, *"Cerium-based chemical conversion coating on AZ63 magnesium alloy"*, Surface and Coatings Technology (2003), 172, pp. 227-232.

[59] M.F. Montemor, M.G.S. Ferreira, *"Electrochemical study of modified bis-[triethoxysilylpropyl] tetrasulfide silane films applied on the AZ31 Mg alloy"*, Electrochimica Acta 52 (2007), pp. 7486-7495.

[60] W. J. van Ooij, D. Zhu, V. Palanivel, J. A. Lamar and M. Stacy , *"Overview: The Potential of silanes for chromate replacement in metal finishing industries"*, Silicon Chemistry (2006) , 3, pp.11–30.

[61] V. Palanivel, D. Zhu, W. J. van Ooij *"Nanoparticle-filled silane films as chromate replacements for aluminum alloys"*, Progress in Organic Coatings (2003), 47, pp. 384–392.

[62] D. Zhu, W. J. van Ooij, *"Corrosion protection of metals by water-based silane mixtures of bis-[trimethoxysilylpropyl]amine and vinyltriacetoxysilane"*, Progress in Organic Coatings (2004), 49, pp. 42–53.

[63] A. Seth, W.J. van Ooij, P. Puomi, Z. Yin, A. Ashirgade, S. Bafna, C. Shivane, *"Novel, one-step, chromate-free coatings containing anticorrosionpigments for metals - An overview and mechanistic study"*, Progress in Organic Coatings (2007), 58, pp. 136–145.

[64] V. Palanivel, Y. Huang, W. J. van Ooij, *"Effects of addition of corrosion inhibitors to silane films on the performance of AA2024-T3 in a 0.5M NaCl solution"*, Progress in Organic Coatings (2005), 53, pp. 153–168.

Chapter 2

EFFECT OF MICROSTRUCTURE ON CORROSION BEHAVIOUR OF AZ31 MAGNESIUM ALLOY

2.1 Introduction

As already reported in the Chapter 1, the corrosion resistance of magnesium alloys does not depend only on the environment, but also on microstructure [1, 2] as well as on the presence of impurity elements, i.e. Fe, Ni, Cu and Co, acting as efficient cathodic sites towards the metal surface [3].

The microstructure of Mg-Al alloys is constituted by the α phase, a substitutional solid solution of aluminium in magnesium, and the β phase, present as intermetallic compound ($Mg_{17}Al_{12}$) in the eutectic (α+β) composition [4]. However, the distribution, volume fraction and chemical composition of the constituent phases depends on production technology, in particular, on solidification rate and succeeding heat treatments [1].

The β phase can have a stimulating effect on corrosion rate if present as small discontinuous precipitates in the α matrix, acting as effective cathode for hydrogen evolution; whereas, if β is present as a continuous phase along the α grain boundaries, it can determine a corrosion rate reduction, once the α phase is completely dissolved and the β phase remains exposed to the test solution [5].

For the comprehension of magnesium alloys corrosion behaviour, the effect of coring, a microlevel segregation occurring during solidification of many commercial castings [6], has to be considered.

In the dendritic solidification process of a conventional cast AZ91 alloy, the amount of aluminium in the dendrite cores is very low. As the solidification proceeds, the liquid is enriched in aluminium up to the eutectic composition [7]. Thus the α phase is microscopically heterogeneous. In particular, it has been reported that the aluminium content of the primary α phase far from the β intermetallic compounds is lower than that near to the β phase [2, 8]; this difference in the composition determines a different electrochemical behaviour between these areas [1].

Currently, the principal production technology for magnesium alloys is pressure Die-Cast process, because of its high productivity and dimensional accuracy [9]. However, in the last few years, the need of high strength magnesium alloy sheets in the automotive and aerospace fields has given impulse to the research and development of rolled magnesium alloys. Among the different alloys used for this purpose, the Mg-Al-Zn alloys have shown the better behaviour in terms of age hardening, resulting from the precipitation of β phase [10].

The purpose of this work is to make a comparative study between the corrosion behaviour of as-cast and hot rolled AZ31 alloy, in order to evaluate the effect of the microstructural modification due to this metallurgical process.

42

2.2 Experimental part

The as-cast and hot-rolled AZ31 alloy (AZ31C and AZ31L respectively) were supplied as plates of 5 and 1 mm thickness respectively. Square coupons were obtained from these plates.

The nominal composition of the AZ31 alloy was: Al 2,5-3,5% ; Zn 0,7-1,3 ; Mn 0.2-1.0% ; Si <0.05% ; Cu <0.01%; Fe <0.002% ; Ni <0.001%.

Specimen surfaces for microstructural analysis were mechanically ground with SiC emery papers up to No. 1000, polished with a 1 μm Al_2O_3 colloidal suspension and finally degreased with acetone. Etching was performed at room temperature with a 10% HF solution [6]. The metallurgical structure was observed using Optical Microscope and analyzed with Scanning Electron Microscopy (SEM) equipped with an Energy dispersive X-ray spectrometer (EDX).

Weight loss measurements were performed exposing samples to 0.05M Na_2SO_4 and 0.1M NaCl solutions for 168 hours (7 days) at room temperature. Corrosion products were mechanically removed by means of sample immersion in acetone and ultrasonic treatment for few minutes up to constant weight. The corrosion rate was calculated in mdd. Afterward, samples were embedded into an epoxy resin and transversally sectioned. The exposed transversal surface was observed using Optical Microscope.

Microcorrosion tests were performed applying a droplet of 0,1 N NaCl solution on alloys surface. The corroded surfaces, resulting from the electrochemical activity within the droplet, were observed with Optical Microscopy after determined time intervals.

The electrochemical tests were conducted in a 250 ml glass cell, using a three electrode configuration, with saturated calomel electrode (SCE) as reference.

The working electrode consisted of a Teflon sample holder leaving a surface of 0,79 cm^2 exposed to the electrolyte. Surface polishing was carried out with SiC emery papers up to No. 1000. The test solutions were 0.05M sodium sulphate or sodium chloride in a concentration ranging from 0.01 to 0.1M.

The electrochemical impedance spectra (EIS) were obtained at the open circuit potential with an *ac* voltage perturbation of ± 10 V in the $10^5 \div 10^{-3}$ Hz frequency range. The potentiodynamic polarization curves were recorded with a scan rate of 0.2 mV/sec.

2.3 Results and discussion

2.3.1 Microstructure

Figure 2.1 and 2.2 show the microstructure of the two alloys after 10% HF etching. The microstructure of the alloy AZ31C (figure 2.1) is the result of a non-equilibrium dendritic solidification. It is characterized by the primary α matrix (light zones) and by the eutectic α phase (grey zones) and the eutectic precipitates β-$Mg_{17}Al_{12}$ (dark zones) both mainly concentrated on grain boundaries. The hot rolled alloy (figure 2.2) has a regular structure in which β phase particles and the other intermetallic compounds are dispersed. As reported in literature, hot rolling breaks eutectic precipitates and moves them from grain boundaries to the grain cores [10].
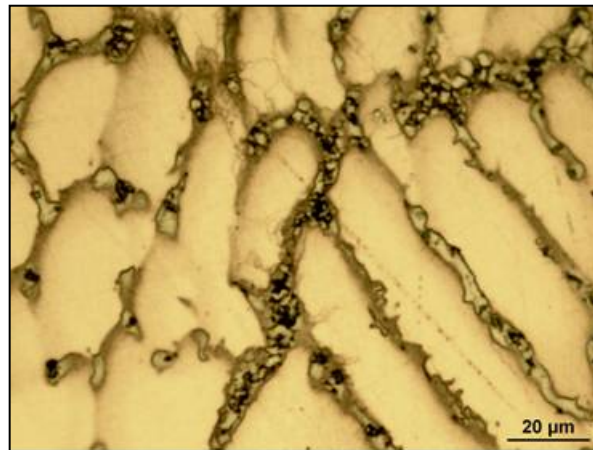
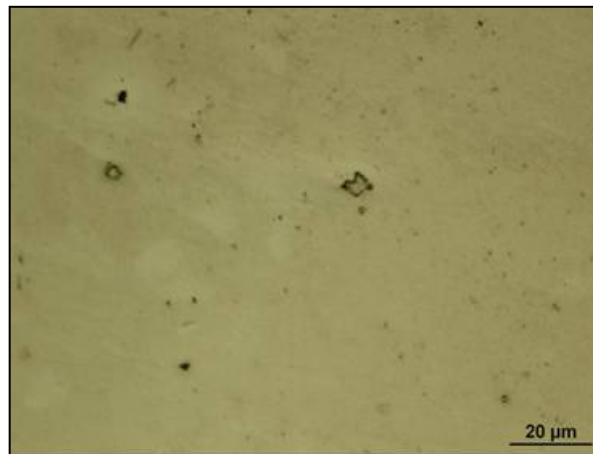***Fig. 2.1*** *– Micrograph of the as-cast AZ31 after etching with a 10% HF solution.*

Fig. 2.2 *– Micrograph of the hot-rolled AZ31 after etching with a 10% HF solution.*

The EDX spectra of AZ31C (figure 2.3) shows the presence of aluminium reach β phase and of Mn-Al reach intermetallic compounds on grain boundaries and on interdendritic zones (Spectrum 1 and 2). The presence of intermetallic compounds containing Mn, Fe and Al is well documented in literature [7].

45

EDX analysis confirms that the eutectic α phase, for coring effect, has an aluminium content higher than the primary α phase, in fact the aluminium concentration in the dendrite's core (Spectrum 4) is not detectable, whereas aluminium presence can be found in the α phase at dendrite's edge (Spectrum 3).
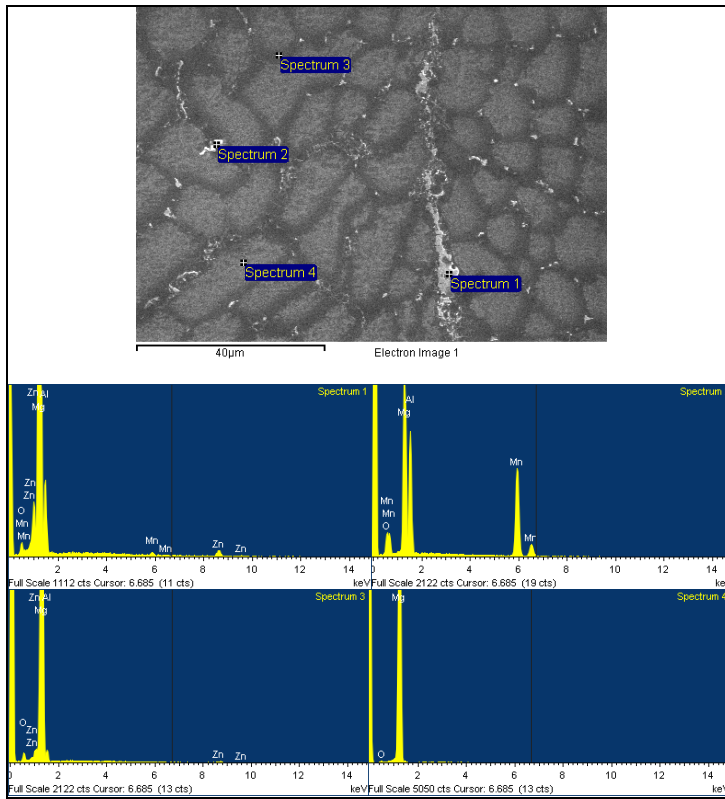
Fig. 2.3 – *SEM micrograph and EDX spectra of the AZ31C alloy.*

From EDX analysis and SEM micrographs of the hot rolled AZ31L alloy (figure 2.4) can be observed the presence of aluminium and manganese rich particles (Spectrum 1) dispersed in the α matrix (Spectrum 4).
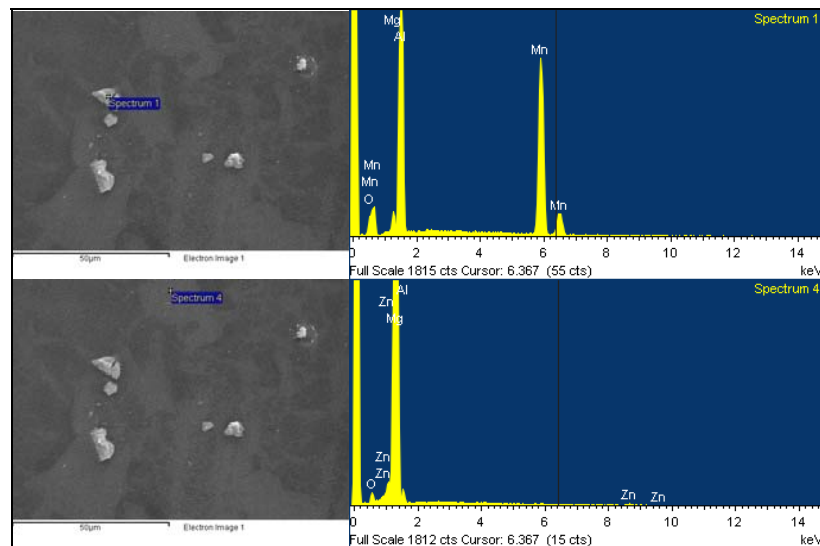
Fig. 2.4 *– SEM micrographs and EDX spectra of the AZ31L alloy.*

2.3.2 Weight loss measurement

The corrosion rates of the two m agnesium alloys obtained after exposure for 168 hours to 0.1M N aCl and 0.05M Na_2SO_4 solutions are reported in table 2.1.

It can be observed that the dissoluti on rate of the AZ31L alloy is higher than that of the AZ31C in both the so lutions, but with a higher difference in chloride solution.

The corrosion rate of AZ31C alloy is essentially equiv alent in chlo ride solution an d in sulph ate solu tion, whereas th e AZ31L alloy shows a corrosion rate higher in 0.1M sodium ch loride than in the 0.05M sodium sulphate solution.

Table 2.1 – *Corrosion rates from weight loss tests in solutio ns 0.1M NaCl and 0.05M Na$_2$SO$_4$.*

Electrolyte	Alloy	V$_{corr}$ (mdd)
NaCl 0.1M	AZ31C	1.36
	AZ31L	5.42
Na$_2$SO$_4$ 0.05M	AZ31C	1.48
	AZ31L	3.86

2.3.3 Microcorrosion test

The corrosion surfaces evolution, resulting from the electrochemical activity within the 0,1M NaCl droplet applied on the two alloys, is reported in figure 2.5 as sequential pictures taken with optical microscope after specific time intervals up to 20 hours testing.

For the as-cast AZ31C, the corrosion attack started on the primary α phase, while the α and β eutectic phases on dendrites edge and on grain boundaries were not affected by the aggressive solution. With passing of time, the primary α phase was more and more corroded, whereas the α+β eutectic phase remained on relief and became more discernible. This behaviour could be evidenced by means of a transversal section micrograph obtained from a AZ31C sample exposed to a solution of 0.1M NaCl for 28 hours (figure 2.6).
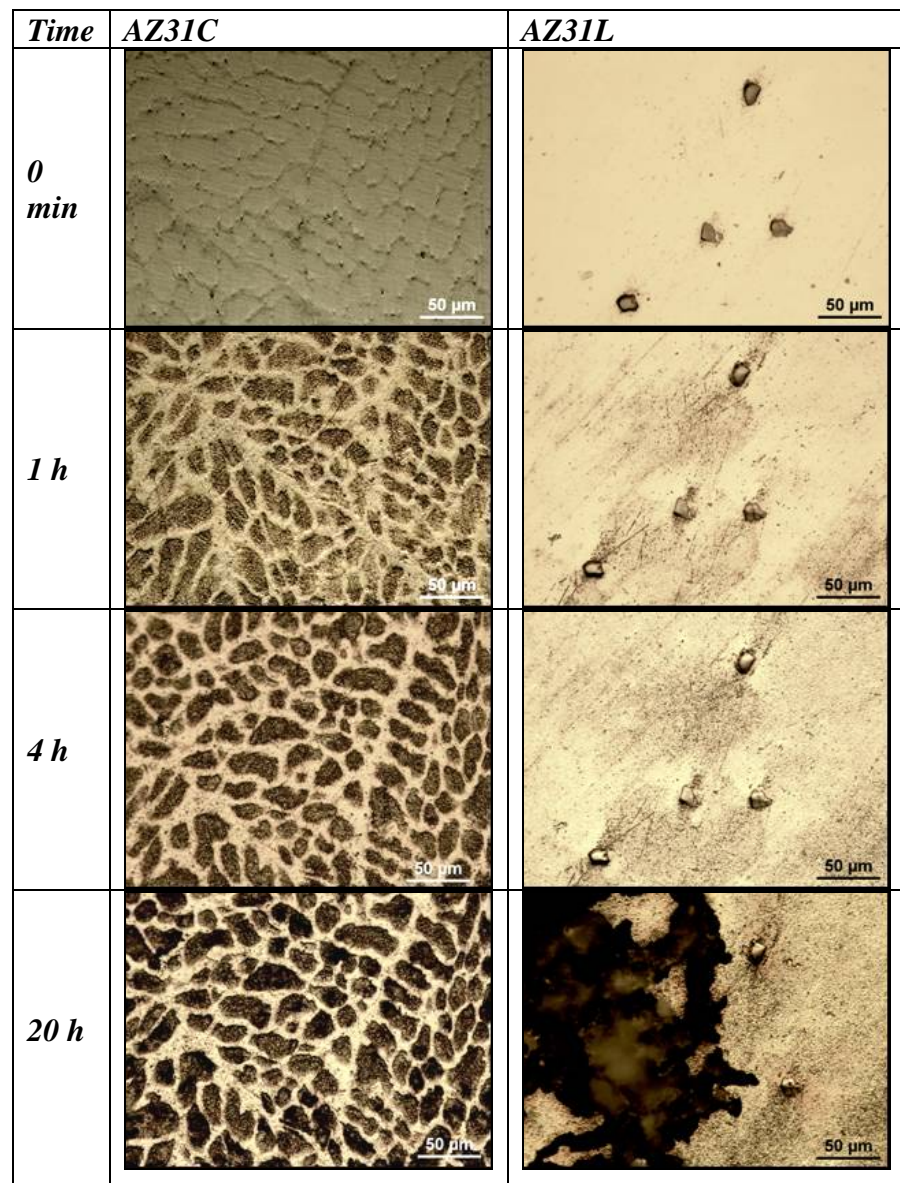
Time	AZ31C	AZ31L
0 min		
1 h		
4 h		
20 h		

Fig.2.5 – *Corrosion morphology evolution on sample exposed to a 0.1M NaCl solution.*
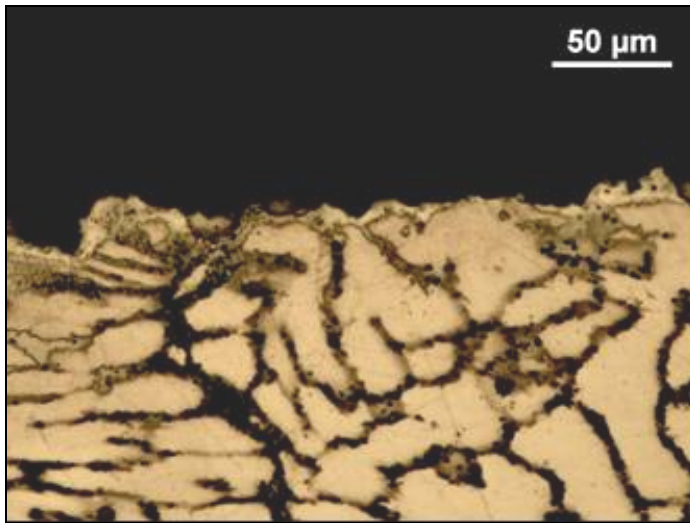
Fig. 2.6 – *Micrographs of the transversal section of AZ31C after exposition for 28 hours to a 0.1M NaCl solution.*

Concerning the hot rolled AZ31L, the β phase particles and the Mn-Al rich intermetallic compounds, acting as cathodic areas, remained almost unaltered in the first hours of exposition to the aggressive medium, whereas the α matrix was interested by a generalized corrosion attack. The increasing of contact time with the aggressive solution, resulted in a progressively deeper corrosive attack at β particles and intermetallic compounds interface, probably leading to the undermining of these particles, as it can be observed in the AZ31L transversal section micrograph (figure 2.7).
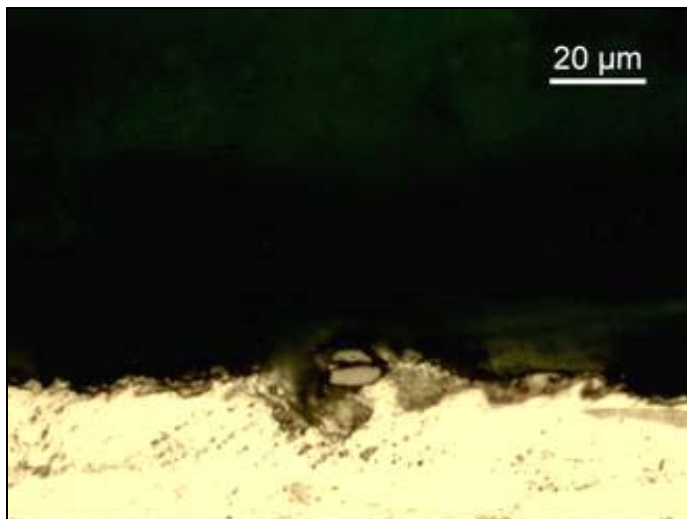
Fig. 2.7 – *Micrographs of the transversal section of AZ31L after exposition for 28 hours to a 0.1M NaCl solution.*

2.3.4 Polarization curves

In figure 7 the anodic and cathodic polarization curves recorded after 1 and 168 h immersion in the 0.05 M sodium sulphate solution, are reported. After 1 hour immersion, both the AZ31C and the AZ31L alloys, showed a certain tendency to the growing of a corrosion product layer on their surfaces. After 168 h this layer was characterized by a higher stability and protectiveness, as evidenced by the shifting of the anodic polarization curves towards lower currents values and from the higher slope in the first part of the anodic curve. However, the hot rolled alloy seemed to have a lower capacity to maintain a passive state, because its anodic curve was characterized by a lower slope and the cathodic one by higher current density for potential values near to the corrosion potential.
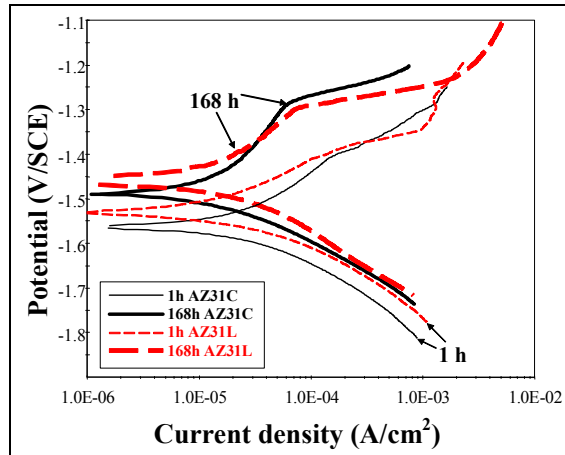
51

Fig. 2.8 *– Polarization curves recorded after 1 and 168 h immersion in 0.05 M Na$_2$SO$_4$ solution.*

With presence of chloride ions (solution 0.01 M NaCl) (figure 2.9), the as-cast AZ31 still presented a passive state, and showed a certain stability of the corrosion products layer up to 168 h. On the contrary, the hot rolled alloy, after 168 h, showed an anodic curve with a continuous trend and cathodic currents higher than that of the AZ31C.
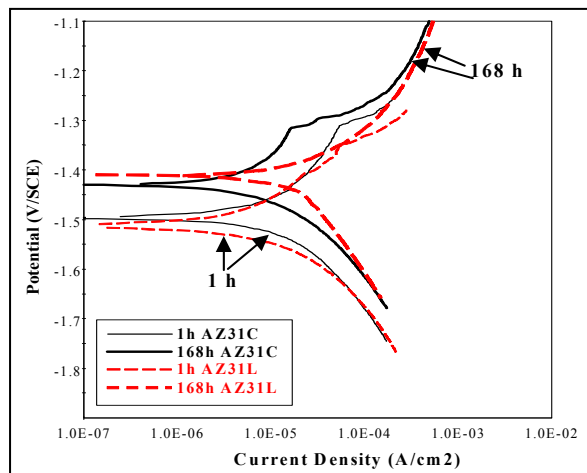

Fig. 2.9 *– Polarization curves recorded after 1and 168 h immersion in 0.01 M NaCl solution.*

52

Whit increasing of sodium chloride concentration (solution 0.1 M NaCl) (figure 2.10), the tendency to form a corrosion products layer on as cast specimen was hindered. The AZ31C anodic curve, after 1 h immersion, presented a low slope in its initial part, however the film underwent to a local breakdown after a little anodic polarization.
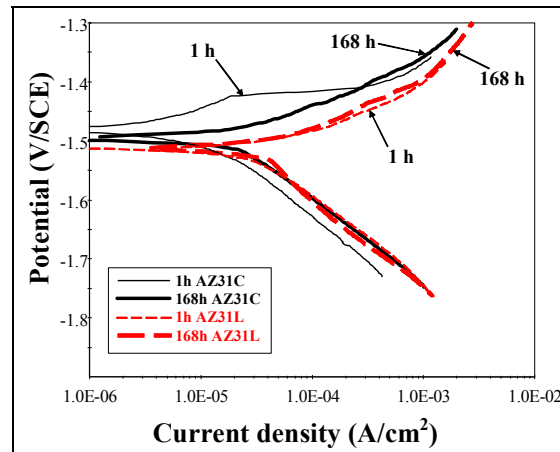

Fig. 2.10 – *Polarization curves recorded after 1and 168 h immersion in 0.1 M NaCl solution.*

The predisposition to the growing of an oxide and hydroxide layer on magnesium alloy surfaces exposed to aqueous solutions has been widely discussed in literature [11, 12] and differences in terms of surface stability depending on the electrolyte type has been evidenced [13, 14]. It is reputed that chloride ions favour a local breakdown of the layer and accelerate the electrochemical oxidation reaction to univalent magnesium, whereas sulphate ions are considered less aggressive [13]. The hot rolled alloy seem to have a higher susceptibility to Cl⁻ ions in comparison to the "as-cast" alloy, which, al least in diluted chloride, succeeded in maintaining a passive state up to 168 h immersion.
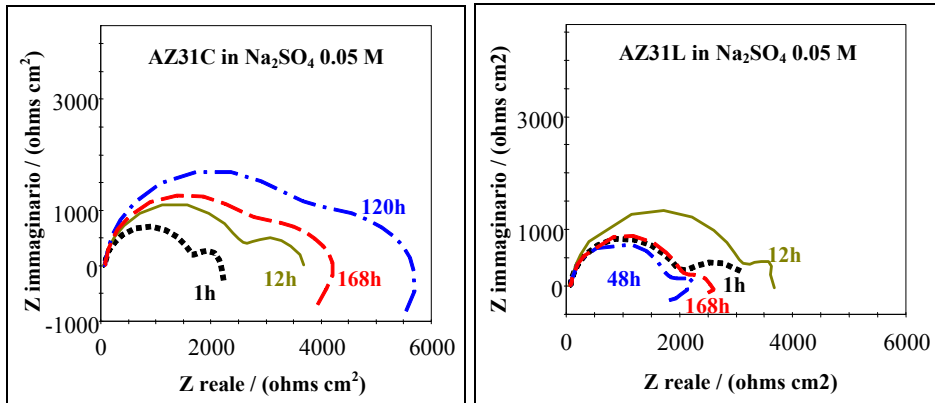
53

2.3.5 Electrochemical Impedance Spectra (EIS)

Fig. 2.11 – *EIS Spectra recorded in the 0.05 M Na$_2$SO$_4$ solution on the as-cast (left) and on the hot rolled (right) AZ31 electrode.*

In the sodium sulphate solution, the electrochemical impedance spectra (Nyquist plot) of the as-cast AZ31 alloy were characterized by two capacitive semicircles (high, *hf,* and low, *lf,* frequency respectively) followed by the beginning of an inductive loop at very low frequencies (< 10^{-1} Hz) (figure 2.11, left). The *hf* and *lf* semicircle diameters increased up to 120 h, but at the end of the test, 168 h, they presented a certain reduction. The shape of the spectra of the hot rolled AZ31 electrode was similar to that of the as-cast one; but the *lf* capacitive loop resulted scarcely defined (figure 2.11, right). In this case an increasing in the *hf* and *lf* semicircle diameter was observed only up to 12 h, then a gradual reduction ensued, followed by a system stabilization after 48 h. However, the hot rolling process determined a reduction, also remarkable, of the capacitive semicircle size.

In diluted (0.01 M) sodium chloride solution (figure 2.12, left), the AZ31C impedance spectra showed a shape and an evolution with time similar to that observed in 0.05 M sodium sulphate; in this case the size of the capacitive loops increased in the first 20 h immersion, with a successive gradual reduction.

On AZ31L (figure 2.12, right), the *lf* capacitive loop, after only 16 h immersion, was no more detectable, while the presence of localized corrosion was macroscopically observable on the specimen surface. Then, the *hf* capacitive loop amplitude decreased with time.
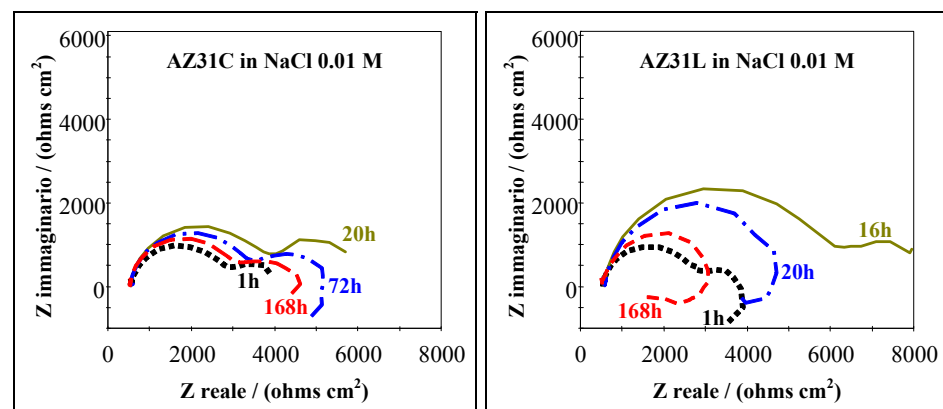

Fig. 2.12 *– EIS Spectra recorded in the 0.01 M NaCl solution on the as-cast (left) and on the hot rolled (right) AZ31 electrode.*

A higher chloride concentration (0.1 M) in the test solution determined the occurring of localized corrosion after only 2 h immersion for the AZ31C (figure 2.13, left) and from the first hour for the AZ31L (figure 2.13, right), i.e. the increased solution aggressiveness tended to mask the different electrochemical behaviour of the two alloys.
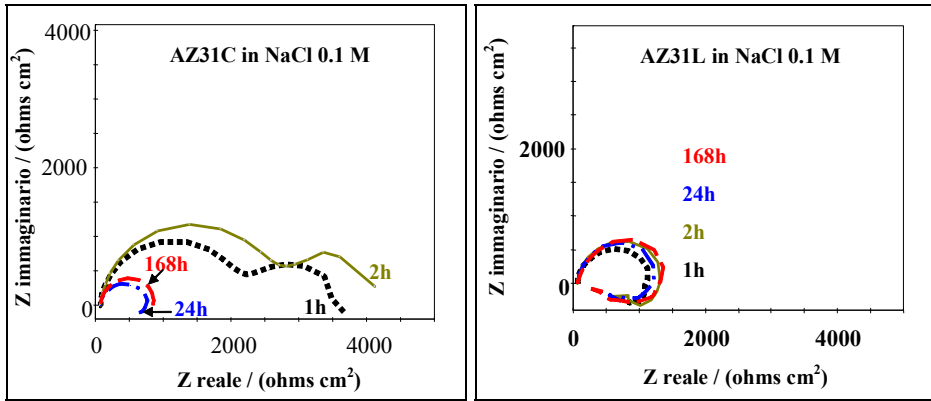
Fig. 2.13 *– EIS Spectra recorded in the 0.1 M NaCl solution on the as-cast (left) on the hot rolled (right) AZ31 electrode.*

In the case of the as-cast sample, the *lf* capacitive loop was detectable up to 2 h immersion and successively only the *hf* capacitive semicircle, but with a diameter noticeably inferior to that obtained in the former less aggressive solutions (0.05 M Na_2SO_4 and 0.01 M NaCl)

For the hot rolled sample, only one capacitive loop has detected during all the test period, with a practically constant diameter.

In general, the electrochemical impedance spectra recorded on the AZ31 showed a shape similar to that of the pure magnesium [15-17], mainly for the as-cast alloy. As previously proposed by other authors [15, 16, 18], the *hf* capacitive semicircle can be attributed to the charge transfer process and film resistance, the *lf* semicircle to the diffusion processes trough the corrosion products layer (likely Mg^+ ions) and finally the inductive loop to adsorbed intermediates. Thus the *hf* capacitive semicircle of the AZ31 was analyzed by means of an equivalent circuit composed by a series of two R-C element in parallel: the charge transfer resistance R_{CT} in parallel with the double layer capacitance C_{DL} and the

film resistance R_f in parallel with the film capacitance C_f, both linked to the corrosion products layer [15, 16, 19].

The corrosion potential (Ecorr) trends, reported in figure 2.14, showed, up to 24 h immersion, a quick shift towards more positive values for both the alloys, evidence of the formation of a protective corrosion products layer. Successively an almost constant trend was observed. However, AZ31L presented Ecorr values about 50 mV more positive than AZ31C, probably linked to a lower surface area covered by the corrosion products layer.
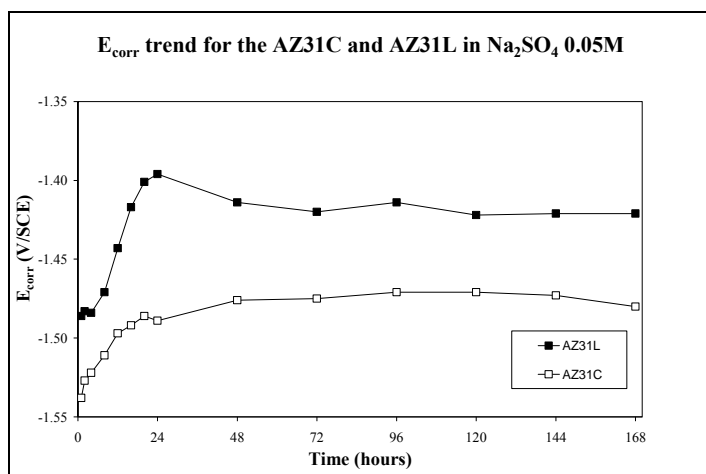

Fig. 2.14 – *Time evolution of Ecorr obtained from the EIS spectra recorded in 0.05 M Na₂SO₄.*

In 0.05 M sodium sulphate (figure 2.15) the R_{CT} value of the AZ31C, starting from 180 Ωcm^2, after an initial fluctuation, tended to increase with time, settling, after 48 h, to a value slightly higher than 200 Ωcm^2. For the AZ31L specimen, the charge transfer resistance, after few immersion hours, tended to decrease and, from the 72 h, immersion it maintained a value around 60 Ωcm^2 up to the end of the test.
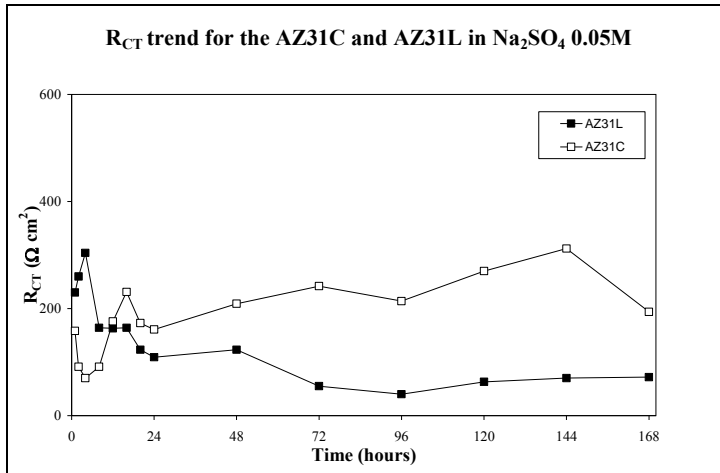
Fig. 2.15 – *Time evolution of R_{CT} obtained from the EIS spectra recorded in 0.05 M Na_2SO_4.*

The evolutions with time of the film resistance (figure 2.16) were similar to the R_{CT} trends. For the AZ31C, R_f, increased, in the first 24 h, from a value of 1400 Ωcm^2 to a value close to 3000 Ωcm^2, maintained till the end of the run. The AZ31L showed a quick increase of R_f in the first 12 h immersion, similarly to the as-cast sample, but successively it presented a certain reduction, stabilizing around 1500 Ωcm^2.

For the AZ31L alloy the film capacitance value (figure 2.17) was almost constant around 18 μFcm^{-2}, whereas, that of the AZ31C, starting form a value of 10 μFcm^{-2}, gradually increased with time, attaining a final value higher than 60 μFcm^{-2}. The increase in C_f for AZ31C in comparison to AZ31L can be related to an increase in the surface covered by a protective layer of corrosion products.
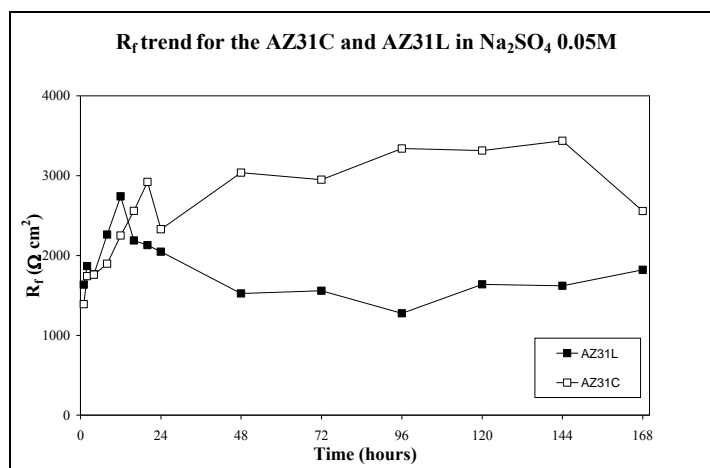
Fig. 2.16 – *Time evolution of R_f obtained from the EIS spectra recorded in 0.05 M Na_2SO_4.*
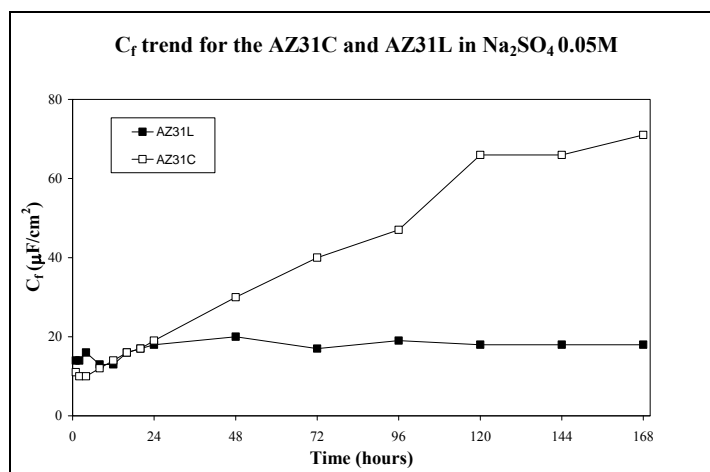

Fig. 2.17 – *Time evolution of C_f obtained from the EIS spectra recorded in 0.05 M Na_2SO_4.*

The polarization resistance (R_p, modulus of the intercept of the capacitive loop with the real axis) trends in sodium sulphate solution for the two alloys are reported in figure 2.21, together with the film resistance trends.
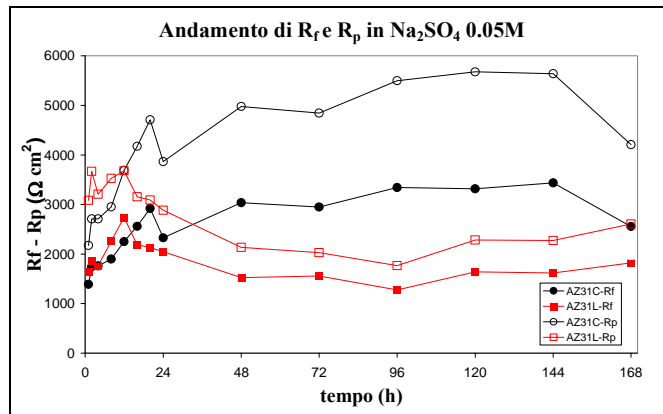
59

Fig. 2.21 – *Time evolution of R_p and R_f obtained from EIS spectra recorded in 0.05 M Na$_2$SO$_4$.*

The difference between R_p and R_f can be considered as the importance of the effect of diffusion trough the corrosion products layer; in fact, some authors [20] observed the presence of an external porous $Mg(OH)_2$ layer. For an immersion time longer than 12 h, a higher hindrance to diffusion trough this layer could be observed for the as-cast AZ31. This phenomenon can be likely attributed to a higher stability of the film for the as-cast process and thus a major protective efficiency. In the more diluted chloride solution, although, for immersion times longer than 24 h, the two AZ31 alloys showed very near film resistance values (figure 2.22); for the as-cast AZ31, the effect of diffusion still played an important role in limiting the corrosion process progress, for all the test period. For the hot rolled alloy, the retarding effect of diffusion, after only 16 h immersion, rapidly decreased and tended to disappeared.
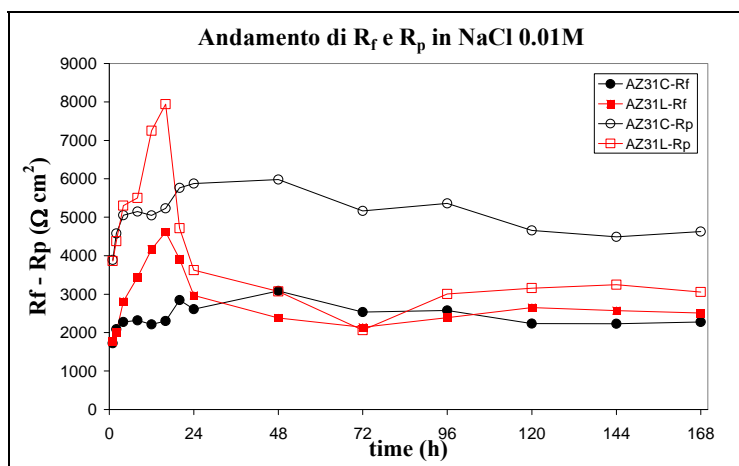
Fig. 2.22 – *Time evolution of R_p and R_f obtained from EIS spectra recorded in 0.01 M NaCl.*

In a more concentrated chloride solution, this effect rapidly vanished from the first immersion hour, for the AZ31L, and after only 2 h, for the AZ31C (figure 2.23).
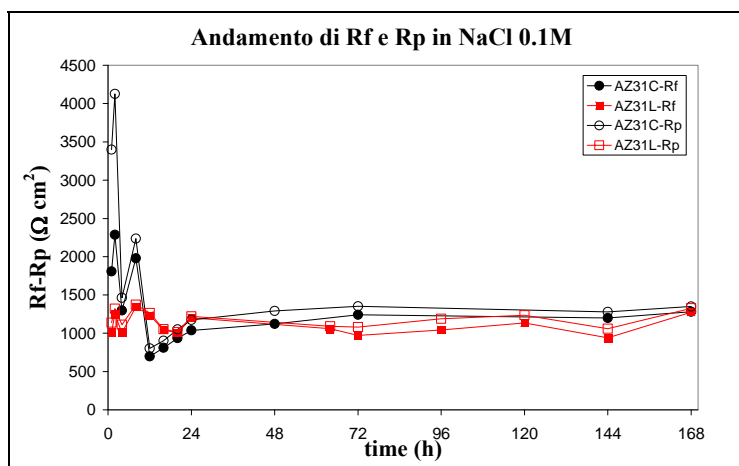

Fig. 2.23 – *Time evolution of R_p and R_f obtained from EIS spectra recorded in 0.1 M NaCl.*

2.4 Conclusions

The analyzed as-cast AZ31 showed a higher corrosion resistance in comparison to the hot rolled AZ31, due to the different distribution and chemical composition of the constituent phases.

For the AZ31C alloy the corrosive attack was localized in the dendrite's core, where the α phase was featured by a lower aluminum content, and left in contact with the solution a surface almost completely constituted by an interdendritic α phase containing a higher aluminum amount. This led to a reduction of the corrosion rate as observed by the electrochemical test results. On the contrary, the hot rolled alloy, having an almost homogeneous Al distribution in the α matrix, did not show this corrosion rate lowering. The α matrix underwent a generalized corrosive attack, sustained by the galvanic coupling with the dispersed β phase particles and the intermetallic compounds. In this case, the corrosive attack, becoming more and more deeper at the matrix-particle interface, could eventually cause the undercut of the cathodic particles.

The polarization curves and the electrochemical impedance measurements showed that the as-cast AZ31 succeed in maintaining a passive state up to 168 h, either in 0.05 M sulphate and in 0.01 M chloride solution, because of its corrosion product layer stability. The hindrance to diffusion trough this film played an important role in limiting the progress of the corrosive attack on the metallic substrate. The corrosion products layer formed on the hot rolled alloy was less stable and protective; in this case, the contribution of hindrance to diffusion on corrosion rate lowering was modest. In fact, in 0.01 M NaCl the corrosion products film lost its protective efficiency after 20 h

immersion, with the occurring of localized corrosion on the metallic substrate. The increasing of chloride concentration (0.1 M) led rapidly to a localized corrosive attack, particularly for the hot rolled AZ31.

References

[65] G. Song, A. Atrens and M. Dargusch, *"Infuence of microstructure on the corrosion of diecast AZ91D"*, Corrosion Science 41 (1999) pp. 249-273.

[66] R. Ambat, N. N. Aung, W. Zhou, *"Evaluation of microstructural effects on corrosion behaviour of AZ91D magnesium alloy"*, Corrosion Science 42 (2000) pp. 1433-1455.

[67] A. Froats, T. Kr. Aune, D. Hawke, W. Unsworth, J. Hillis, *"Corrosion of Magnesium and Magnesium Alloys"*, Corrosion, Vol. 13 ASM Handbook, ASM International (1987).

[68] ASM Handbook vol. 3 Alloy Phase Diagrams, ASM International (1992) p. 2·48.

[69] G. Song, A. Atrens, X. Wu and B. Zhang, *"Corrosion behaviour of AZ21, AZ501 and AZ91 in Sodium Chloride"* Corrosion Science 40 (1998) pp. 1769-1791.

[70] T.V. Padfield, *"Metallography and Microstructures of Magnesium and Its Alloys"*, Metallography and Microstructures, Vol 9, ASM Handbook, ASM International (2004), pp. 801-815.

[71] Mathieu, C. Rapin, J. Hazan, P. Steinmetz, *"Corrosion behaviour of high pressure die-cast and semi-solid cast AZ91D alloys"*, Corrosion Science 44 (2002) pp. 2737-2756.

[72] G. Song, A. L. Bowles, D. H. StJohn, *"Corrosion resistance of aged die cast magnesium alloy AZ91D"*, Material Science and Engineering A366 (2004) pp. 74-86.

[73] M.M. Myshlyaev, H.J. McQueen, A. Mwembela, E. Konopleva, *"Twinning, dynamic recovery and recrystallization in hot worked Mg-Al-Zn alloy"*, Material Science and Engineering A337 (2002) pp. 121-133

[74] B.-P. Zhang, Y.-F. Tu, J.-Y. Chen, H.-L. Zhang et al., *"Preparation and characterization of as-rolled AZ31 magnesium alloy sheets"*, Journal of Materials Processing Technology 184 (2007) pp. 102-107.

[75] G. Galicia, N. Pébère, B. Tribollet, V. Vivier, *"Corrosion Study of an AZ91 Magnesium alloy by EIS and LEIS"* ECS Transactions, (2006), 1 (4), pp. 157-168.

[76] J.H. Nordlien, K. Nisancioglu, S. Ono, N. Masuko, *"Morphology and Structure of Oxide Films Formed on MgAl Alloys by Exposure to Air and Water"*, Journal of Electrochemical Society 143 (1996), pp. 2564-2572

[77] G. Song, A. Atrens, D. StJohn, X. Wu and J. Nairn, *"The anodic dissolution of magnesium in chloride and sulphate solutions"*, Corrosion Science 39 (1997) pp. 1981-2004.

[78] G. Song, A. Atrens, D. StJohn, J. Nairn and Y. Li, *"The electrochemical corrosion of pure magnesium in 1 N NaCl"*, Corrosion Science 39 (1997) pp. 855-875.

[79] N. Pébère, C. Riera and F. Dabosi, *"Investigation of magnesium corrosion in aerated sodium sulphate solution by electrochemical impedante spectroscopy"*, Electrochemical Acta 35 (1990) pp. 555-561.

[80] G. Baril, N. Pébère, *"The corrosion of pure magnesium in aerated and deaerated sodium sulphate solutions"*, Corrosion Science, (2001), 43, pp. 471-484.

[81] F. Dabosi, R. Morancho, N. Pébère and D. Pouteau, *"Investigation of the corrosion and protection of magnesium by AC impedance techinique"*, Proc. 47th Annual World Magnesium Conf. (The international Magnesium Association, Cannes, France, 1990), pp. 51-55.

[82] G. Baril, G. Galicia, C. Deslouis, N. Pébère, B. Tribollet and V. Vivier, *"An Impedance Investigation of the Mechanism of Pure Magnesium Corrosion in Sodium Sulfate Solutions"*, Journal of Electrochemical Society 154 (2) (2007) pp. C108-C113.

[83] G. Baril, C. Blanc, N. Pébère, *"AC Impedance Spectroscopy in Characterizing Time-Dependent Corrosion of AZ91 and AM50 Magnesium Alloys Characterization with Respect to Their Microstructures"* Journal of Electrochemical Society (2001), 148(12), pp. B489-B496.

[84] M. Santamaria, F. Di Quarto, S. Zanna, P. Marcus, *"Initial surface film on magnesium metal: A characterization by X-ray photoelectron spectroscopy (XPS) and photocurrent spectroscopy (PCS)"* Electrochimica Acta 53 (2007) pp. 1314–1324.

Chapter 3

INHIBITION OF THE AZ31 ALLOY CORROSION IN A SYNTHETIC COOLING WATER WITH SODIUM MONO-CARBOXYLATES

3.1 Introduction

Non-toxic linear sodium monocarboxylates can be successfully used as inhibitors for the corrosion of many metals [1-4]. Duloz et al. [1] tested sodium salts of 7-12 carbon atom long mono-carboxylic acids as corrosion inhibitors for rapidly solidified (RS) Mg-3%Zn-15%Al alloy in ASTM D 1387 saline solution and found that sodium undecanoate displayed the highest protective effects, but at very high concentrations (0.02-0.05 M). The inhibiting effects increased by increasing the immersion time and FTIR spectra evidenced the formation of a protective layer of insoluble magnesium undecanoate [1]. Similar salts were also investigated as inhibitors of copper corrosion [2,3]. Furthermore, self-assembled monolayers of carboxylate ions were studied to prevent iron passive film breakdown [4]. In this chapter the ability of sodium salt of mono-carboxylics acids to inhibit the corrosion process of AZ31 Mg alloy in ASTM D 1387 saline solution [5] is investigated. The tested compounds, having the general formula $CH_3(CH_2)_nCOONa$, had the aliphatic chain number *n* ranging between 7 and 15 and were indicated with NaCX (X = 8÷16).

3.2 Experimental part

The electrochemical tests were performed on electrodes obtained from a 5 mm thick AZ31 alloy sheet (nominal composition reported in Chapter 2). The electrodes, room-temperature embedded in Epofix® resin, exposed a surface of 1.5 cm^2 to the aggressive solutions and their electric contact was assured by a copper wire, fixed on the opposite surface. Before the tests, the electrode surface was emery paper (up to n.1000) treated, bi-distilled water rinsed and finally acetone degreased.

The aggressive solution was prepared starting from analytical grade pure salts, following ASTM D 1387 standard; it was constituted by 148 mg/l Na$_2$SO$_4$, 138 mg/l Na$_2$CO$_3$ and 165 mg/l NaCl (pH ≈ 8,1). Pure (Aldrich or Fluka) sodium salts of octanoic (C8, caprylic), decanoic (C10, capric), dodecanoic (C12, lauric), tetradecanoic (C14, myristic) and esadecanoic (C16, palmitic) acids were proved as inhibitors, in concentration ranging, as a function of their solubility, from 10^{-4} to 10^{-2} molar ([$10^{-2} \div 10^{-3}$] for NaC8 and NaC10, [$10^{-4} \div 5 \times 10^{-3}$] for NaC12, [$10^{-4} \div 5 \times 10^{-4}$] for NaC14, and 10^{-4} for NaC16).

All the tests were performed at 25 +/- 0.1 °C. The tests solution was in equilibrium with atmosphere and 100 rpm magnetically stirred.

Starting from the corrosion potential (E$_{CORR}$), independent anodic or cathodic potentiodynamic (0.2 mV/s) polarization curves were recorded, after 1 and 96 h immersion in the various, inhibited or not, solutions. The evolution of the corrosive attack was monitored by EIS technique, by applying a 10 mV rms sinusoidal perturbation, in $10^5 \div 10^{-2}$ (or 10^{-3}) Hz frequency range. All potentials are referred to the saturated calomel electrode (SCE).
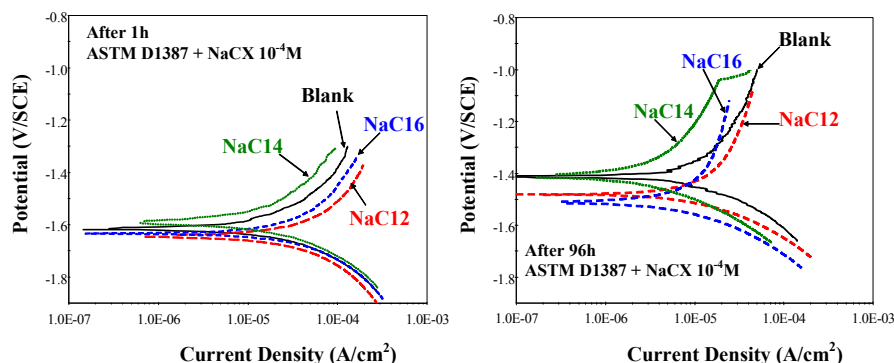
3.3 Results and discussion

3.3.1 Polarization curves

Fig. 3.1 – *Polarization curves recorded on AZ31 electrodes after 1 and 96 h immersion in ASTM D1387 solution in the presence of 10^{-4} M NaCX.*

Figures 3.1 (left and right) report the polarization curves of AZ31 electrodes, recorded after 1 and 96 h in ASTM D1387 solution, in absence and presence of 10^{-4} M NaC12, NaC14, NaC16 (i.e. the higher homologues). After 1 h immersion, among these salts, only NaC14 presented a certain inhibiting action, which regarded the metal anodic dissolution process, while NaC12 and NaC16 interfered, scarcely, with the protective layer formation by magnesium corrosion products precipitation.

With increasing of immersion time, the inhibiting action of NaC14 improved (figure 1 right). Indeed, after 96 h, a further reduction of the anodic polarization currents, accompanied by a contemporaneous decrease of the cathodic ones, was evident. After this time interval, NaC12 and NaC16 slightly succeeded in hindering the cathodic reaction and in this case the corrosion potential, in comparison to the blank, was shifted in the negative direction.
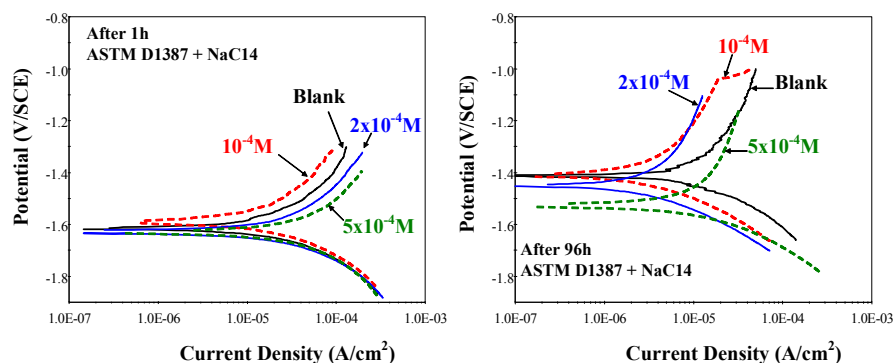
Fig. 3.2 *– Polarization curves recorded on AZ31 electrodes after 1 and 96 h immersion in ASTM D1387 solution in the presence of different NaC14 concentrations.*

At short immersion time (1h), an increase in NaC14 concentration up to 5×10^{-4} M (figure 3.2, left) was detrimental to the anodic process (a feeble stimulating action was found), whereas it didn't exert any influence on the cathodic one. At long immersion times (96h) (figure 3.2, right) a certain inhibiting action was found at 2×10^{-4} M concentration only, while for the higher salt concentration (i.e. 5×10^{-4} M) this effect was not observed.
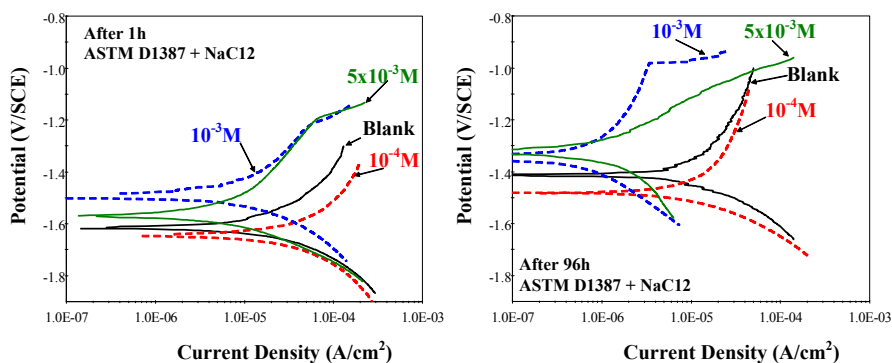

Fig. 3.3 *– Polarization curves recorded on AZ31 electrodes after 1 and 96 h immersion in ASTM D1387 solution in the presence of different NaC12 concentrations.*

The increase in NaC12 concentration from 10^{-4} to 10^{-3} or 5×10^{-3} M caused, initially (1 h), a marked decrease in the anodic polarization currents (figure 3.3, left), with a contemporaneous shift of E_{CORR} towards more positive values; this effect improved for long immersion times. The cathodic polarization currents were markedly reduced in presence of 10^{-3} or 5×10^{-3} M NaC12 concentration (figure 3.3, right), but only after 96 h immersion.
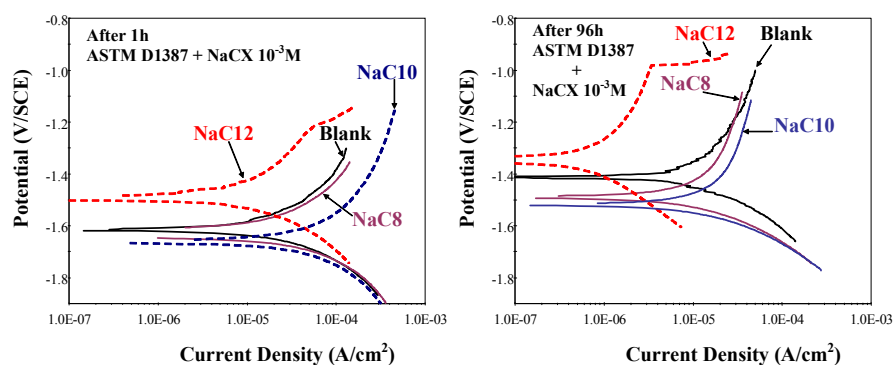

Fig. 3.4 − *Polarization curves recorded on AZ31 electrodes after 1 and 96 h immersion in ASTM D1387 solution in the presence of 10^{-3} M NaCX.*

Figures 3.4 (left and right) show the polarization curves, recorded after 1 and 96 h in synthetic cooling water, in presence of a 10^{-3} M concentration of the lower homologues (i.e. NaC8 and NaC10; NaC12 is introduced exclusively for comparison purposes). After 1 h immersion, the corrosion potential of AZ31 alloy in NaC8 and NaC10 presence was more negative than that of the blank test, due to a stimulation of the anodic reaction. After 96 h, these salts still showed a certain interference with a protective layer formation, as well as a certain inhibiting action towards the hydrogen evolution reaction.

Only when NaC10 was used at 10^{-2} M concentration, a very noticeable inhibition of the anodic reaction was found after 1 h immersion, with a significant shift of E_{CORR} in the positive direction (figure 3.5, left).
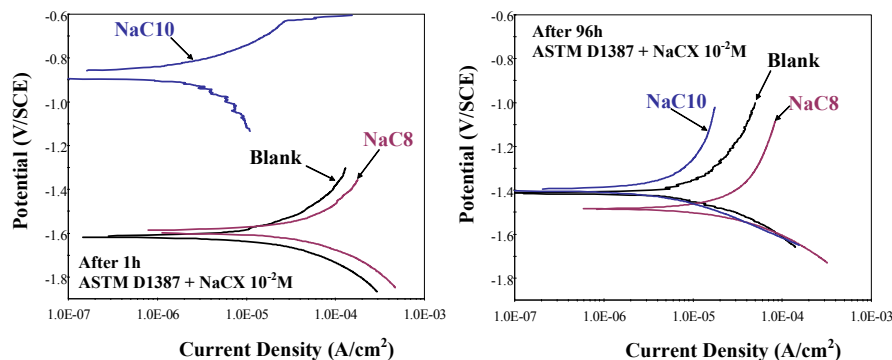

Fig. 3.5 – *Polarization curves recorded on AZ31 electrodes after 1 and 96 h immersion in ASTM D1387 solution in the presence of 10^{-2} M NaCX.*

The considerable inhibiting effect showed after 1 h immersion in presence of a 10^{-2} M NaC10 concentration diminished during the run (figure 3.5, right); after 96 h E_{CORR} was slightly more positive than that of the blank, and the anodic curve, although inhibited, tended to approach those recorded in additive absence. NaC8, at this concentration, never presented a clear inhibiting action, on the contrary after 96 h it showed a certain stimulating effect on the anodic process.

Fig. 3.6 and 3.7 reports the I_{CORR} data (derived from the extrapolation of the cathodic Tafel lines at E_{CORR}), and the corresponding percent inhibiting efficiency values (%IE). The greatest inhibiting action was exerted by NaC12, at 10^{-3} M (or higher: 5×10^{-3} M), which increased by prolonging the immersion time: after 1h immersion its I.E.% was around 70% and it reached a value of 95% after 96h. An increase of I.E.% as a function of immersion time was also found in presence of 2×10^{-4} M and

$1\text{x}10^{-4}$ M of NaC14, but with %I.E. values around 70%. and with NaC16, but with a poor efficiency (I.E. 19%). An opposite trend characterized 10^{-2} M NaC10: in this case %IE was close to 92% after 1h and 70% after 96h. At lower concentration (10^{-3} M), this salt never produced an inhibiting action, as well as NaC8 did.
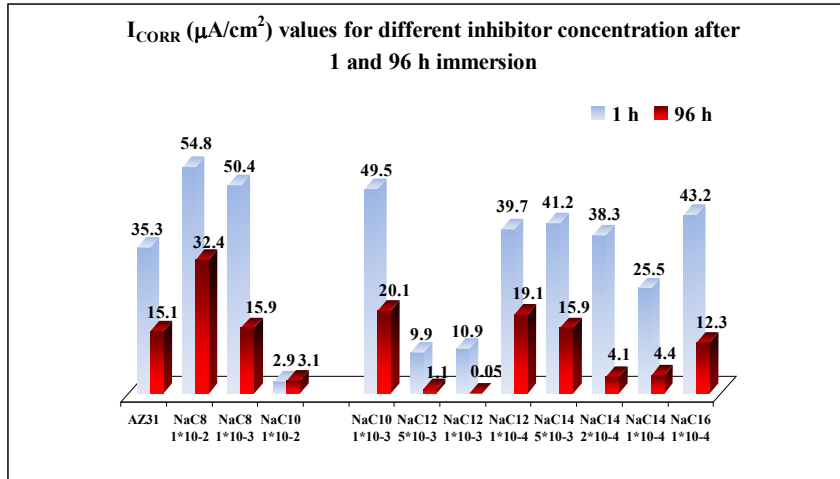

Fig. 3.6 – I_{CORR} *values after 1 and 96 h immersion in ASTM D1387 solution in the presence of different NaCX concentrations.*
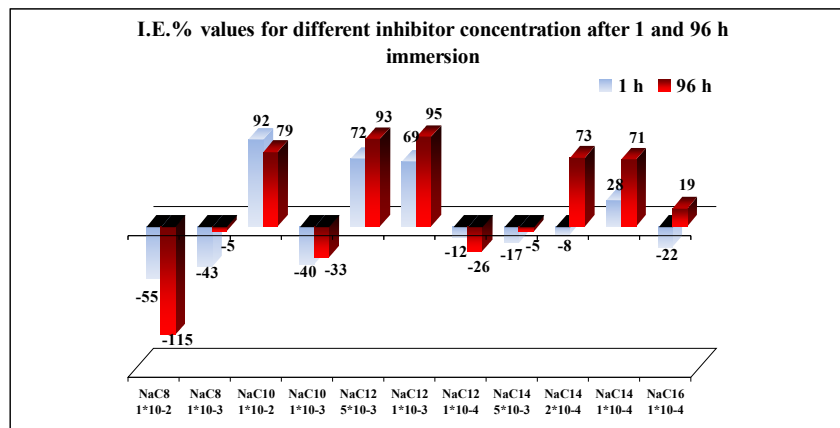

Fig. 3.7 – *E.I.% values after 1 and 96 h immersion in ASTM D1387 solution in the presence of different NaCX concentrations.*

72
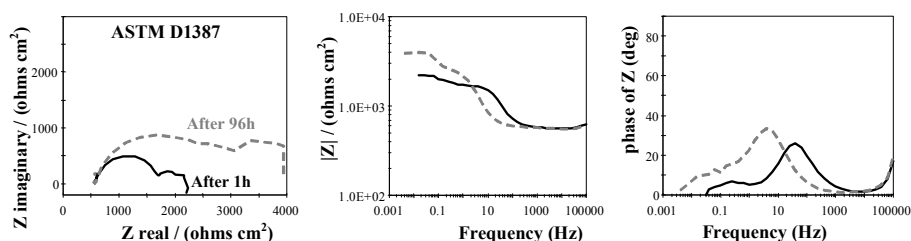
3.3.2 Electrochemical Impedance Spectra

Fig. 3.7 *− EIS spectra of AZ31 electrodes, after 1 and 96h immersion in ASTM D1387 synthetic cooling water.*

EIS spectra (Nyquist and Bode plots) of AZ31 alloy, after 1 and 96 h immersion in ASTM D1387 synthetic cooling water solution, are reported in Figure 3.7. Likely due to the scarce conductance of the test solution, at frequencies higher than 10^4 Hz, these spectra presented the end of a capacitive semicircle, followed by two capacitive semicircles, one at high (*hf*, $10^4 \div 10^1$ Hz) and one at low (*lf*, $10^1 \div 10^{-1}$ Hz) frequency, ending (usually f $<10^{-1}$ Hz) with points in the inductive quadrant. As already discussed in Chapter 2 and reported in [6-8], the *hf* semicircle is usually attributed both to charge transfer and film effect (a magnesium oxide-hydroxide layer) [6-9]. The experimental points of this semicircle can satisfy an Electrical Equivalent Circuit (EEC) constituted by a series of two R-C parallel networks, one representing the charge transfer resistance and a double layer capacitance (R_{CT} and C_{DL}, respectively), the other the film resistance and capacitance (R_F and C_F, respectively) [6-8]. The *lf* semicircle, not analyzed in this case, was associated with ions diffusion through the corrosion product layer, while the inductive behaviour to adsorbed intermediates [6-8]. The diameters of the capacitive semicircles tended to enlarge with increasing in immersion time, whereas that of the inductive loop to disappear.

73

The charge transfer resistance increased mainly in the first 24 h immersion, while the resistance associated to the corrosion product layer almost continuously during the whole testing period (table 3.1); from the values of these resistances, it is evident that AZ31 corrosion process was chiefly controlled by the corrosion product layer.

The increase, as a function of immersion time, of the impedance modulus ($|Z|_{0.01}$) at the low frequency (0.01 Hz), inversely proportional to corrosion rate, was indicative of an increase in film efficiency.

Table 3.1 – *AZ31 electrochemical parameters from impedance spectra in synthetic cooling water.*

Time (h)	R_{CT} (Ωcm^2)	R_F (Ωcm^2)	$(1/|Z|_{0.01}) \times 10^{-5}$ $(\Omega cm^2)^{-1}$
1	75	643	55.6
4	116	854	50.9
12	183	1030	40.4
24	254	1322	32.1
48	249	1461	26.9
72	255	1692	22.7
96	215	1723	25.1

Figure 3.7 shows the evolution of EIS spectra for AZ31 alloy, during the immersion in the synthetic cooling water in presence of the most efficient inhibitor concentrations (10^{-2} M NaC10, 10^{-3} M NaC12 and 10^{-4} M NaC14). Generally these spectra were similar in shape, although larger in size, to that of the unprotected specimen.
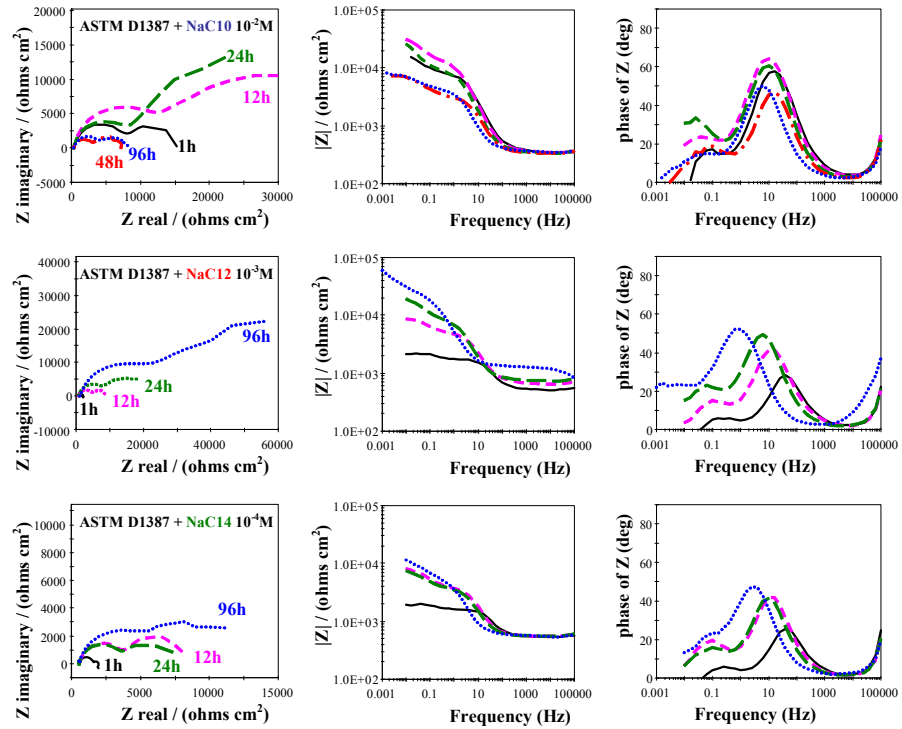
Fig. 3.7 – *Evolution of EIS spectra of AZ31 electrodes during the immersion in ASTM D1387 synthetic cooling water, in the presence of: (a) 10^{-2}M NaC10; (b) 10^{-3}M NaC12; (c) 10^{-4}M NaC14 .*

In comparison to the previous blank test, the size of the *hf* and *lf* capacitive semicircles, for 10^{-2} M NaC10, markedly increased in the first 12 h immersion, then this trend reversed. After 48-96 h, the value of the low frequency impedance modulus was lower than that determined after 1 h; however, $|Z|_{0.01}$ was still superior to that of the blank test, in close agreement with the trend of the polarization curves.

In presence of 10^{-3} M NaC12, the dimension of *hf* capacitive semicircle increased continuously during the run. The *lf* loop was characterized by the same trend too, and after 24 h it changed into an almost pure diffusive component. The diameters of the capacitive loops of AZ31 in 10^{-4} M NaC14 solution increased regularly by increasing the testing time. At the

75

end of the run, in both cases, $|Z|_{0.01}$, which never attained the final values of NaC12, was close to 13 $k\Omega cm^2$.

The parameters determined from the impedance spectra are reported in figure 3.8 and 3.9. The protective action afforded by these substances determined a marked increase in R_F, the resistance of the formed carboxylate salt, rather than to an increase in the charge transfer resistance. A marked increase in R_{CT} was produced only by 10^{-3} M NaC12 after 72-96h immersion, whereas the presence 10^{-2} M NaC10, on the contrary, determined a decreasing of the R_{CT} values in comparison to that of the AZ31 after 12 h immersion.

For 10^{-2} M NaC10, the increase of R_F as a function of time was particularly evident in the first 12 h immersion, successively its value decreased. In the case of 10^{-3} M NaC12, the formation of the protective layer was slower, although this process continued for the whole test period. The development of the protective action of 10^{-4} M NaC14 was as slow as with NaC12, but after 48 h the R_F increase was very limited.
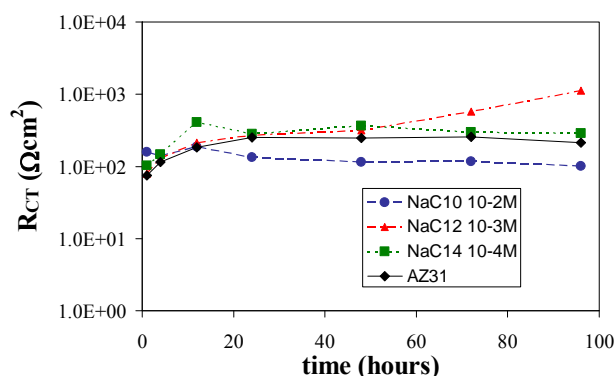

Fig. 3.8 – *R_{CT} trend as a function of time of AZ31 electrodes in ASTM D1387 synthetic cooling water in the presence of 10^{-2}M NaC10, or 10^{-3}M NaC12, or 10^{-4}M NaC14.*
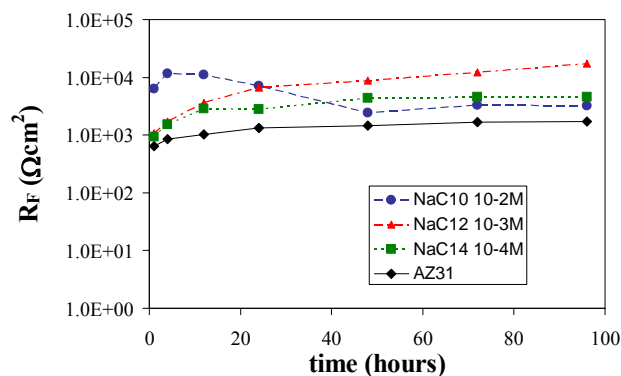
Fig. 3.9 *– R_F trend as a function of time of AZ31 electrodes in ASTM D1387 synthetic cooling water in the presence of $10^{-2}M$ NaC10, or $10^{-3}M$ NaC12, or $10^{-4}M$ NaC14.*

Figure 3.10 compares, as a function of immersion time, $1/|Z|_{0.01}$ values of the blank test with those in the inhibited media. In 10^{-2} M NaC10 solution, the corrosion rate presented its lowest values just in the first test hours, but after 24 hours $1/|Z|_{0.01}$ was augmented, attaining, after 48h, an almost constant value, half that of the blank. In presence of 10^{-3} M NaC12, $1/|Z|_{0.01}$ diminished in the first 24 h immersion from 47 to 5.3 $x10^5$ $\Omega^{-1}cm^{-2}$, arriving, at the end of the test, to 1.7 $x10^5$ $\Omega^{-1}cm^{-2}$. In 10^{-4} M NaC14 solution too, $1/|Z|_{0.01}$ decreased continuously, however in a less marked manner, from about 50 to 7 $x10^5$ $\Omega^{-1}cm^{-2}$.

In figure 3.11 the inhibiting effects obtained from EIS spectra are reported in function of time. With a 10^{-2} M NaC10, a very high protective effect was obtained in the first immersion hours, but after 24 h it decreased attaining an inhibition efficiency of 50%. In presence of a concentration 10^{-3} M of NaC12, the I.E % constantly increased, reaching values close to the 93%. Finally, with a concentration 10^{-4} M of NaC14,

in the first 12 h there was a quick increase in the protective effect, then it maintained a value around the 64 %.

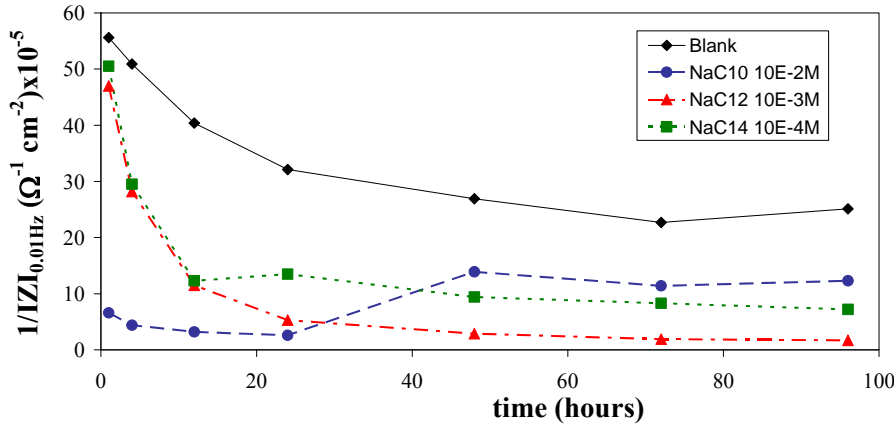***Fig. 3.10*** – *$1/|Z|_{0.01}$ trend as a function of time of AZ31 electrodes in ASTM D1387 synthetic cooling water in the presence of $10^{-2}M$ NaC10, or $10^{-3}M$ NaC12, or $10^{-4}M$ NaC14.*

Fig. 3.11 – *I.E. % trend as a function of time of AZ31 electrodes in ASTM D1387 synthetic cooling water in the presence of $10^{-2}M$ NaC10, or $10^{-3}M$ NaC12, or $10^{-4}M$ NaC14.*
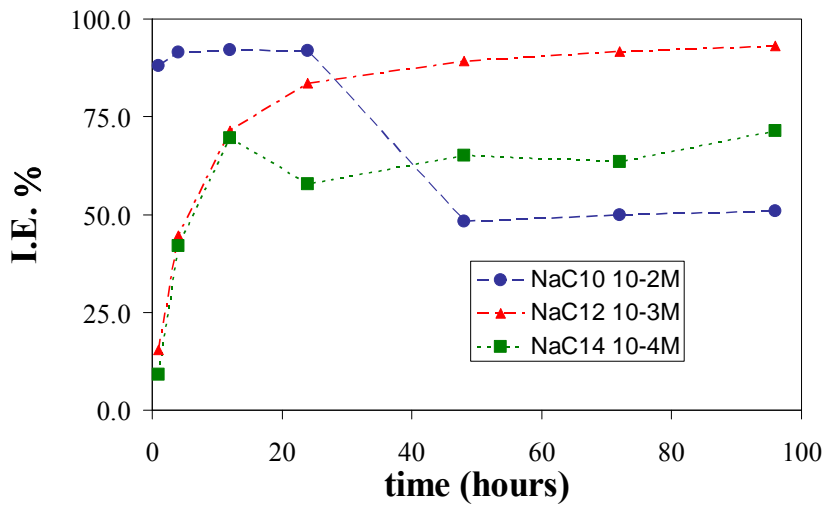
78

Micrographs in figure 3.12, 3.13 and 3.14 show the growth of the magnesium salt layer on AZ31 surface during immersion in the synthetic cooling water. Figure 3.12 shows that the specimen surface was quickly protected by a complete layer of thin magnesium decanoate crystals.

Fig. 3.12 – *Electrode surface after 24 (left) or 96 h (right) immersion in the synthetic cooling water, in the presence of 10^{-2} M NaC10.*

In the case of sodium dodecanoate the formation of the protective layer was slower; in fact, after 24 h (figure 3.13, left), crystals of magnesium laurate did not cover the whole surface, which was, however, fully coated by a thick, although not-homogeneous, layer at the end of the run (figure 3.13, right).

Fig. 3.13 – *Electrode surface after 24 (left) or 96 h (right) immersion in the synthetic cooling water, in the presence of 10^{-3} M NaC12.*

In the presence of sodium tetradecanoate, a layer of magnesium myristate was formed by coarse needle-shaped crystals (figure 3.14, left), which increased in size by increasing in immersion time (figure 3.14, right).
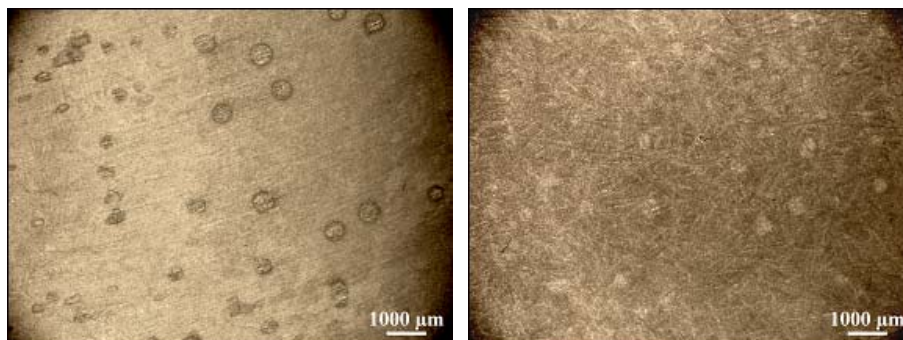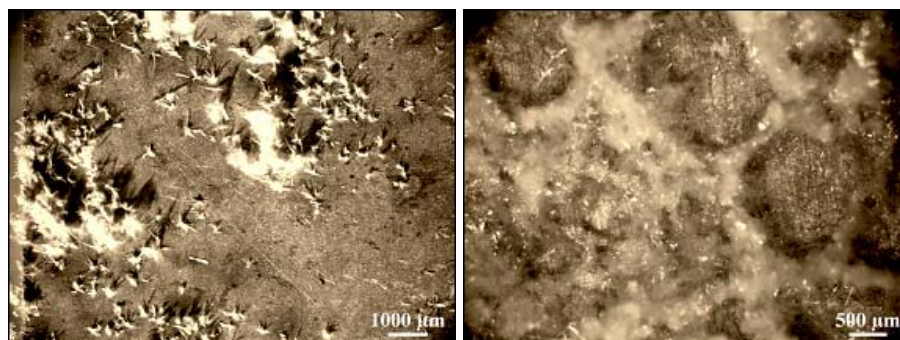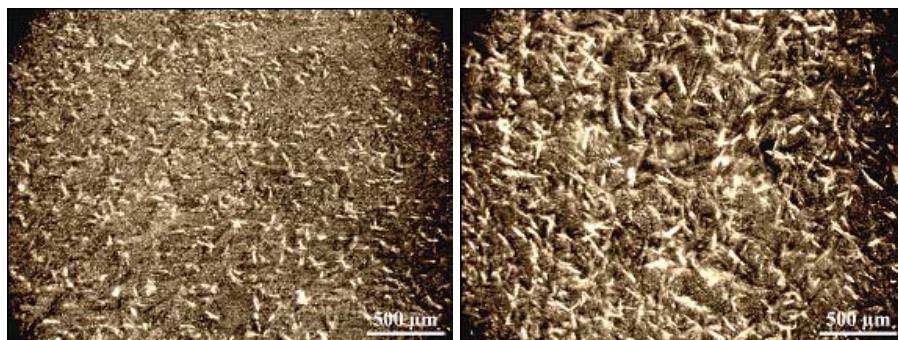

Fig. 3.14 *– Electrode surface after 24 (left) or 96 h (right) immersion in the synthetic cooling water, in the presence of 10^{-4} M NaC14.*

3.3.3 Discussion

Sodium salts of linear mono-carboxylic acids can inhibit corrosion of AZ31 Mg alloy in synthetic cooling water by hindering, chiefly, the anodic reaction. The polarization measurements showed that, for all the salts, a maximum in %IE is reached by increasing their concentration, which, successively, diminish or disappear. After 96h, the optimum molar concentration is 10^{-4} for sodium esadecanoate, $(10^{-4} \div 2x10^{-4})$ for sodium tetradecanoate, $(10^{-3} \div 5x10^{-3})$ for sodium dodecanoate and 10^{-2} for sodium decanoate. In the case of sodium octanoate, only a stimulating effect is observed in the examined concentration interval $(10^{-3} \div 10^{-2})$.

The influence of the aliphatic chain becomes evident by admitting, in agreement with [10], that the inhibiting action of the carboxylic anions is due to a layer of insoluble magnesium carboxylate, precipitated onto the specimen surface. First of all, the aliphatic chain controls the anion

solubility in the solution, as well as the reaction rate of magnesium salt formation, whose solubility should be lower, the longer is the chain. On the basis of these considerations, it is possible to explain the behaviour of the various mono-carboxylic acid salts. Sodium octanoate stimulates the corrosion process because in the solution a sufficient anion concentration for attaining the solubility product of magnesium octanoate is not reached. The salt formation, in its turn, hinders the formation of the protective layer of magnesium corrosion products (magnesium oxide-hydroxides) or enlarges the electrode surface, free from these protective products.

With 10^{-2} M sodium decanoate, the formation of magnesium decanoate rapidly takes place, and in the first immersion times the inhibiting effects are high; however, this protective action successively diminishes because the crystals do not form a very compact layer.

The best inhibiting action is afforded by 10^{-3} M sodium dodecanoate, which rapidly reacts forming a very compact layer in about 12 hours, afterwards the corrosion rates stabilizes at a very low value.

In the presence of 10^{-4} M sodium tetradecanoate, the magnesium myristate forms more slowly and the inhibiting effect increases constantly during 96 h testing.

3.3 Conclusions

The investigation on the influence exerted by sodium salts of linear long-chain mono-carboxylic acids shows that sodium salts of capric, lauric, myristic acids produce an inhibiting action towards AZ31 magnesium alloy corrosion in a synthetic cooling water. The protective action is due to the formation of a layer of insoluble magnesium carboxylates.

The inhibiting efficiency is related to the aliphatic chain length and to the salt concentration. The former influences the formation rate of the protective layer as well as its protectiveness.

%IE of 10^{-2} M NaC10 is around 50-60, that of 10^{-3} M NaC12 over 90, and that of 10^{-4} M NaC14 around 70. NaC8, in 10^{-4}-10^{-3} M concentration range, interferes with the formation of the protective layer of magnesium corrosion products, while NaC16, owing to its scarce solubility, does not afford any protective action.

References

[1] D. Daloz, C. Rapin, P. Steinmetz, G. Michot, *"Corrosion Inhibition of Rapidly Solidified Mg-3% Zn-15% Al Magnesium Alloy with Sodium Carboxylates"*, Corrosion (1988), 54, pp. 444-450.

[2] C. Rapin, P. Steinmetz, J. Steinmetz, *Revue Métall.-CIT*, Feb. 1996, pp. 281-290.

[3] E. Rocca, G. Bertrand, C. Rapin, J.C. Labrune, *"Inhibition of copper aqueous corrosion by non-toxic linear sodium heptanoate: mechanism and ECAFM study"*, Journal of Electro-analytical Chemistry (2001), 503, pp. 133-140.

[4] K. Aramaki, T. Shimura, *"Self-assembled monolayers of carboxylate ions on passivated iron for preventing passive film breakdown"*, Corrosion Science (2004), 46, pp. 313-328

[5] Annual Book of ASTM Standards, ASTM D1348-87, ASTM, Philadelphia, PA (USA), (1986), p. 19103.

[6]   N. Pébère, C. Riera, F. Dabosi, *"Investigation of magnesium corrosion in aerated sodium sulphate solution by electrochemical impedante spectroscopy"*, Electrochimica Acta (1990), 35, pp. 555-561.

[7]   G. Baril, N. Pébère, *"The corrosion of pure magnesium in aerated and deaerated sodium sulphate solutions"*, Corrosion Science, (2001), 43, pp. 471-484.

[8]   G. Baril, C. Blanc, N. Pébère, *"AC Impedance Spectroscopy in Characterizing Time-Dependent Corrosion of AZ91 and AM50 Magnesium Alloys Characterization with Respect to Their Microstructures"*, Journal of Electrochemical Society (2001), 148(12), pp. B489-B496.

[9]   F. Zucchi, V. Grassi, A. Frignani, G. Trabanelli, *"Corrosion behaviour of untreated and termally-treated AS21X Mg alloy in sulphate and chloride media"*, presented at 16th International Corrosion Congress, Beijing, China, 19-24 september 2005, paper 03-Mg-33, CD-ROM.

[10] A. Mesbah, C. Juers, F. Lacouture, S. Mathieu, E. Rocca, M. François, J. Steinmetz, *"Inhibitors for magnesium corrosion: Metal organic frameworks"*, Solid State Science (2007), 9, pp. 322-328.

Chapter 4

PROTECTION OF THE AZ31 MAGNESIUM ALLOY WITH MONO-CARBOXYLATE CONVERSION COATINGS

4.1 Introduction

As already discussed in Chapter 1, the formation of a conversion coating is a method currently applied to protect metallic alloys from corrosion [1]. Some conversion coating treatments, for instance based on Permanganate-Phosphate or Stannate baths [2-7] and rare earth salts [8-11], have been proposed to improve the corrosion resistance of magnesium alloys. On the basis of the results presented in Chapter 3, where sodium salts of mono-carboxylics acids have been studied as corrosion inhibitors, long chain mono-carboxyilate sodium salts were tested also as possible promoters of protective conversion coatings for AZ31 magnesium alloy and their protective action was evaluated in the diluted electrolytic solutions (0.05 M Na_2SO_4 and 0.1 M NaCl). In this case, the tested compounds (general formula $CH_3(CH_2)_nCOONa$) had a aliphatic chain number n ranging between 11 and 17 and were indicated with Cx (x = 12÷18).

The anions of the mono-carboxylic acids should easily bind to an oxide covered metal surface through HSBA interactions [12], and moreover, similarly to other well tested cases [13], a long aliphatic chain, through Van der Waals (VdW) interactions, should lead to the formation of well ordered, highly protective, hydrophobic layers [14].

84

4.2 Experimental part

Square specimens (1.5 cm^2 surface) were cut from a 5 mm thick plate of AZ31 magnesium alloy (nominal composition reported in chapter 2) and embedded in an epoxy resin. Their surfaces were prepared by emery papers up to 1000 grade, washed with distilled water, degreased with acetone and dried with hot air.

The prepared electrodes were dipped (treated) in various solutions of sodium salts of mono-carboxylic acids for 24 h both at room temperature (RT) and 50 °C or for 72 h at RT, dried with a hot air flux and stocked in a drier. The treatment baths were aqueous solutions of sodium salts of mono-carboxylic acids: dodecanoic (Na-C12, sodium laurate, 5×10^{-3} M), tetradecanoic (sodium myristate, Na-C14, 5×10^{-3} M), hesadecanoic (Na-C16, sodium palmitate, 2.5×10^{-3} M) and octadecanoic (Na-C18, sodium stearate, 1×10^{-3} M). The test environments were 0.05 M Na_2SO_4 or 0.1 M NaCl solutions.

Electrochemical tests were performed in a 250 ml volume cell with a three electrode configuration. The reference electrode was a saturated calomel electrode (SCE) and the counter electrode were two platinum wires. All the potentials were referred to the SCE.

Usually the potentiodynamic (0.2 mV sec^{-1} scanning rate) polarization curves were recorded after 1 h immersion of the treated electrodes in 0.05 M Na_2SO_4 solution and after 1, 24 or 216 h immersion in 0.1 M NaCl solution. Electrochemical impedance spectra were acquired in the various solutions at increasing immersion times, within a $10^5 \div 10^{-3}$ Hz frequency range, applying, at the corrosion potential, a 10 mV rms sinusoidal perturbation.

85

Optical Microscope micrographs were taken on specimens at the end of the electrochemical tests in 0.05 M Na$_2$SO$_4$ and 0.1 M NaCl solutions, before and after mechanical removal of the conversion coatings.

4.3 Results and discussion

4.3.1 Polarization curves

The polarization curves of uncoated and coated AZ31 electrodes after 1 h immersion in the sulphate solution allowed us to evaluate the influence that treatment time and bath temperature exerted on the protectiveness of the conversion coatings by short or long aliphatic chain salts (figure 4.1). In the case of the lower homologue, 24h-RT treatment formed a layer that scarcely hindered only the cathodic process. By prolonging the treatment time to 72 h or incrementing the treatment temperature, the Na-C12 coatings continued to inhibit the same reaction but in a slightly better way. In fact, in every case, the corrosion potential of treated specimens shifted towards more negative values, in comparison to the blank.
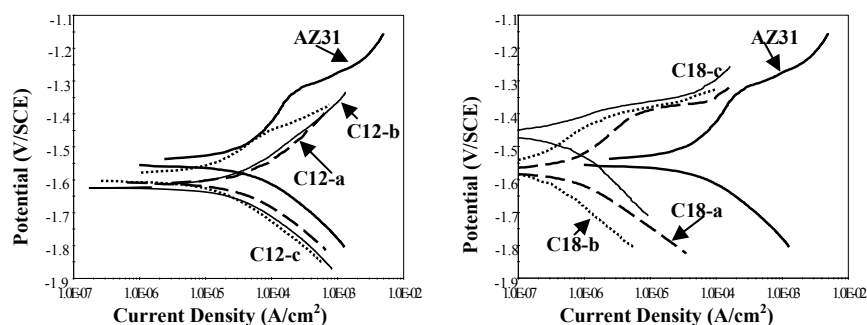

Fig. 4.1 – *Polarization curves recorded, after 1 h immersion in 0.05 M Na$_2$SO$_4$, on AZ31 electrodes treated for 24 (a) and 72 h (b) at RT and for 24 h at 50 °C (c), in a 0.005 M Na-C12 (left) or 0.001 M Na-C18 (right) baths.*

The inhibition of the anodic process with the Na-C12 compound was only realized by a 50 °C treatment, even if the effect was quite poor.

At all the treatment conditions, the higher homologue built a layer which markedly hindered the anodic magnesium oxidation reaction, the best results were obtained by increasing both the treatment time and temperature. Furthermore, these coatings inhibited the cathodic process more efficiently than the lower homologue did, and a net improvement was achieved by lengthening the RT treatment time from 24 to 72 h. In any case, with the Na-C18 treatments, the cathodic and anodic currents were more than two orders of magnitude lower than those of the blank.

Figure 4.2 illustrates the influence that the aliphatic chain length exerted on the performances of the conversion coatings: in general the protective action of the mono-carboxylate salts was improved by increasing the number of carbon atoms of the chain. For instance, this increase caused a more sensitive reduction in the cathodic currents. This effect was improved by prolonging the treatment temperature to 50 °C.
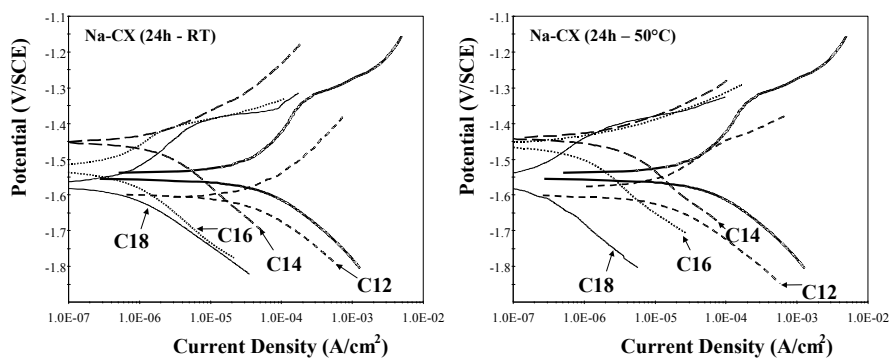

Fig. 4.2 *– Polarization curve, recorded, after 1 h immersion in 0.05 M Na$_2$SO$_4$, on AZ31 electrodes treated for 24 h at RT (left) and for 24 h at 50 °C (right) in the various baths.*

87

While the coatings formed with the Na-C12 treatment bath never succeeded in reducing the polarization currents of the anodic reaction, the presence of a longer alkyl chain was necessary in order to promote the formation of a layer able to produce a marked inhibition of the anodic process. Indeed, Na-C14, Na-C16 and Na-C18 coatings shifted the anodic polarization curves to much lower current density values (more than one order of magnitude) than those of the untreated specimen. These effects were maintained at higher treatment temperature.

The protective effects of these coatings were also confirmed in the more aggressive chloride solution (0.1 M NaCl). As an example, figure 4.3 compares the polarization curves of AZ31 specimens treated in Na-C12 or Na-C18 baths at 50 °C for 24 h.
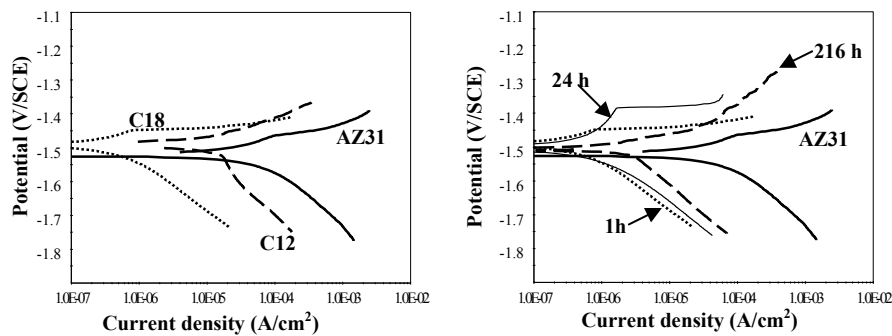
Fig. 4.3 – *Polarization curve recorded on AZ31 electrodes treated for 24 h at 50 °C in a 0.001 M Na-C18 and a 0.005 M Na-C12 solution, after 1 h immersion in 0.1 M NaCl (left), and treated for 24 h at 50 °C in a 0.001 M Na-C18 bath after different immersion times (1, 24, 216 h) in 0.1 M NaCl (right).*

The cathodic and anodic polarization curves of coated specimens shifted towards the lower current values with increasing of alkyl chain length; in the case of the cathodic process, this shift for the Na-C18 treated electrode was around two orders of magnitude, while that of the Na-C12 it was around one order of magnitude; in the case of the anodic process

these values became around three orders of magnitude, or one order of magnitude, respectively. Also in the presence of Cl⁻ anions, magnesium carboxylate salts clearly showed the tendency to form a very protective layer, as evidenced by the initial very high slope of the anodic reaction, although the carboxylate film breakdown was retarded in a narrower potential interval than in the sulphate solution. The protective effects of stearate coating lasted for a long time and the decrease in their efficiency mainly involved the anodic process. In fact, from 1 to 216 h the cathodic polarization currents increased solely three-fold, while the anodic ones by well over ten-fold.

4.3.2 Electrochemical Impedance Spectra

Figure 4.4 shows the impedance spectra of AZ31 electrodes, treated in Na-C12 or NaC-18 baths for different times and temperatures, recorded after 1 h immersion in the electrolytic solution.
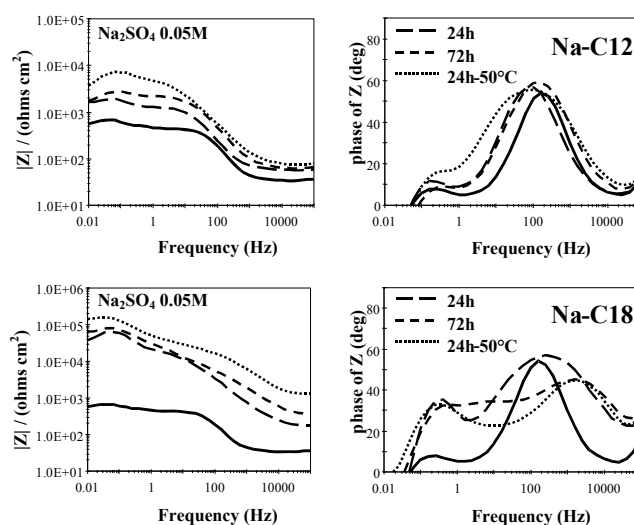

Fig. 4.4 *– EIS spectra recorded after 1 h immersion in   0.05 M Na₂SO₄ on AZ31 electrodes treated with Na-C12 and Na-C18 carboxylic salts for 24 and 72 h at RT, or for 24 h at 50 °C.*

89

Like untreated specimens, AZ31 treated electrodes presented, in the capacitive quadrant, two, more or less well defined, loops (sometimes ending with very low frequency points in the inductive quadrant). The increase in the intercept of these loops with the real axis (Rp, the polarization resistance, inversely proportional to the corrosion rate), in comparison to the blank, confirmed that the corrosion resistance afforded by magnesium carboxylate layers was superior to that of the natural magnesium corrosion product layer. The polarization resistance, i.e. the corrosion resistance, was improved by lengthening the treatment time from 24 to 72 h, as well as by augmenting the bath temperature to 50 °C. Figure 4.5 compares EIS spectra recorded, after 1 h immersion in 0.05 M sulphate solution, on AZ31 electrodes treated for 24 h at 50 °C with the sodium salts of the various mono-carboxylic acids.
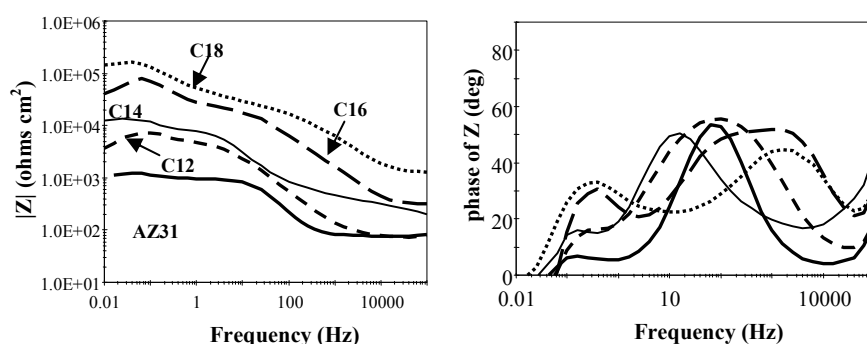
Fig. 4.5 – *EIS spectra of Na-C12, Na-C14, Na-C16 and Na-C18 treated AZ31 specimens after 1 h immersion in 0.05 M Na$_2$SO$_4$.*

These spectra confirmed the results of the polarization curves; in fact, the polarization resistance shifted to higher values by increasing the alkyl chain length: with Na-C12 Rp (7.3 kΩcm^2) was about one order of magnitude higher than that of the blank (1.2 kΩcm^2) and with Na-C18 (156 kΩcm^2) over two orders of magnitude.

As already discussed in Chapter 2, neglecting the lowest frequency range, the untreated AZ31 electrode presented in the phase angle vs. frequency Bode plot two time constants: one (high frequency, hf) at around 10^2 Hz, attributed to the charge transfer process and to the corrosion products layer formation, and the other (low frequency, lf) around 10^{-1} Hz, to the diffusion through this layer [15-18]. At all the temperatures and treatment times, the spectra of Na-C12 treated electrode were always characterized by a phase angle vs. frequency diagram shape which was very similar to that of the blank, even if with a larger phase angle distribution, i.e. by the same time constants (τ) of the blank (10^2 and 10^{-1} characteristic frequencies). In Na-C14 spectra two τ could be observed, that at hf, with a characteristic frequency around 10 Hz, and that at lf around 10^{-1} Hz. Na-C18 spectra showed two well defined time constants: while the lf one maintained its 10^{-1} Hz characteristic value, the characteristic frequency of the hf time constant moved from 10^2 Hz to over 10^3 Hz by prolonging the treatment time or by increasing the bath temperature. Na-C16 spectra seemed to be characterized by a time constant overlapping in the $10^2 \div 10^3$ Hz frequency range, still presenting the lf τ at 10^{-1} Hz.

In general, the shape of the lower homologues impedance spectra were very similar to that of the untreated AZ31 (time constants with 10^2 and 10^{-1} Hz characteristic frequencies), and this evidenced the presence of a very defective layer. With higher homologues, for prolonged treatment times or high bath temperature, i.e. for very efficient treatments, the hf time constant characteristic frequency was over 10^3 Hz; this latter time constant could be ascribed to an almost complete magnesium carboxylate

layer, and can be considered to represent the response of the carboxylate film, in terms of electrolyte resistance in the pores of the film (R_F) and film capacitance (C_F), to the applied sinusoidal perturbation, as it was found in similar cases [19, 20].

In order to extract the carboxylate layer parameters, the equivalent circuit (EC) of a defective coating (figure 4.6) was used to simulate the EIS spectra (from about 10^4 to 10^1 Hz for Na-C16 and Na-C18 treated electrodes, and to 1 Hz for Na-C14 and Na-C12 treated ones).
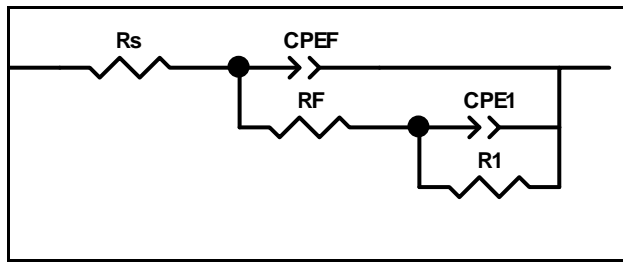
Fig. 4.6 *– Equivalent circuit (EC) used to simulate the EIS spectra*

This EC was characterized by a R_F-C_F parallel combination in which, in series with R_F, a second R_1-C_1 parallel combination was placed. R_1-C_1 represented the corrosion process on the unprotected alloy surface and the related double layer capacitance, respectively. Constant Phase Elements (CPE), instead, of pure capacitances were used in the model in order to take into account the non ideal behaviour of the film. CPE values were converted into capacitances by means of the parameters obtained from the fitting [21].

Table 4.1 – *Film parameters after 1 h immersion in 0.05 M Na$_2$SO$_4$ calculated from EIS spectra recorded on (24h-50°C) Na-C14, Na-C16 and Na-C18 treated AZ31 electrodes.*
   a)   *Approximated values*

Treatment	R$_F$ (kΩcm^2)	C$_F$ (µFcm^{-2})
Na-C12	0.04	7.5 [a]
Na-C14	0.6	3.2 [a]
Na-C16	3.7	0.3
Na-C18	19	0.06

Table 4.1 compares the parameters of the conversion coatings for various homologues determined after 1 h immersion in the sulphate solution.

The film resistance (R$_F$) increased with the increase in the carbon chain length, while C$_F$ decreased. Na-C18 treated electrode showed the highest R$_F$ value (i.e. the most efficient layer) and the lowest C$_F$ value, while the R$_F$ value for Na-C12 was extremely low, practically irrelevant. It can, therefore, be assumed that the stearate layer (10^3 Hz hf τ) was the widest and the most protective, characterized by very few small unprotected points of the metal substrate, at variance with the much less efficient laurate layer (with a negligible R$_F$ value and the same hf τ of the blank).

Nevertheless, during the immersion in the electrolytic solution, the low frequencies impedance modulus of Na-C18 treated electrode diminished, initially quickly (figure 4.7), then very slowly.
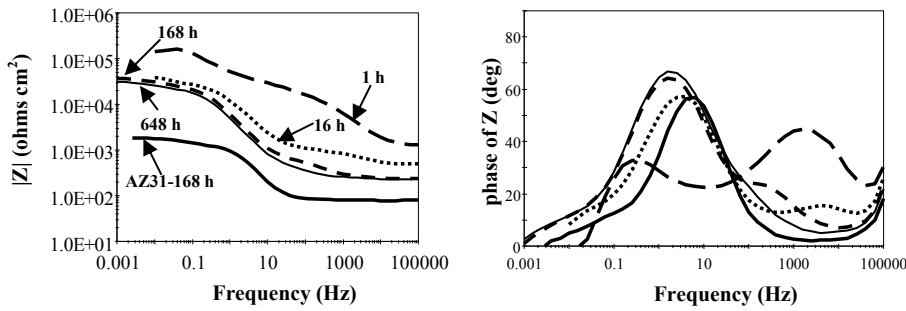
Fig. 4.7 – *EIS spectra of Na-C18 treated AZ31specimens, after 1, 16, 168, 648 h immersion in 0.05 M Na₂SO₄.*

The film resistance (figure 4.8) decreased rapidly (within 16 h) to very low values, around 0.8 kΩcm² (much lower than the corresponding Rp, and close to the resistance of corrosion product layer of the blank), while the film capacitance increased (figure 4.9), but attaining values much lower than those of the blank (about two orders of magnitude, 0.15 μFcm⁻² and 18 μFcm⁻², respectively).

Fig. 4.8 – *R$_F$ evolution of (24h-50°C) Na-C18 layer during 24 h immersion in 0.05M Na₂SO₄ solution.*

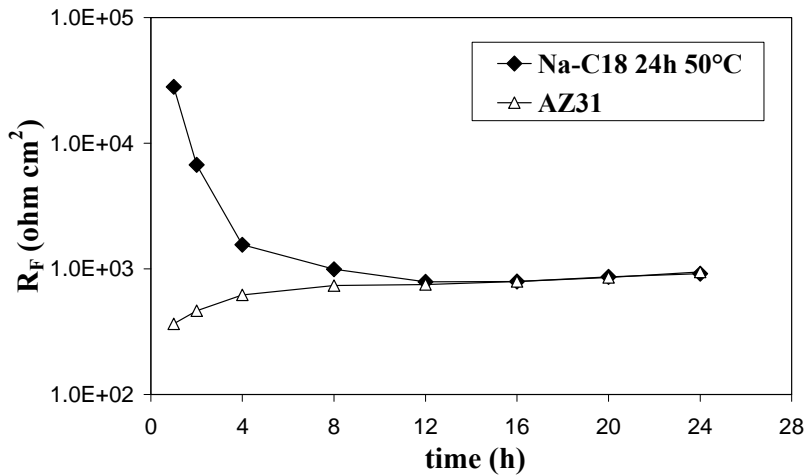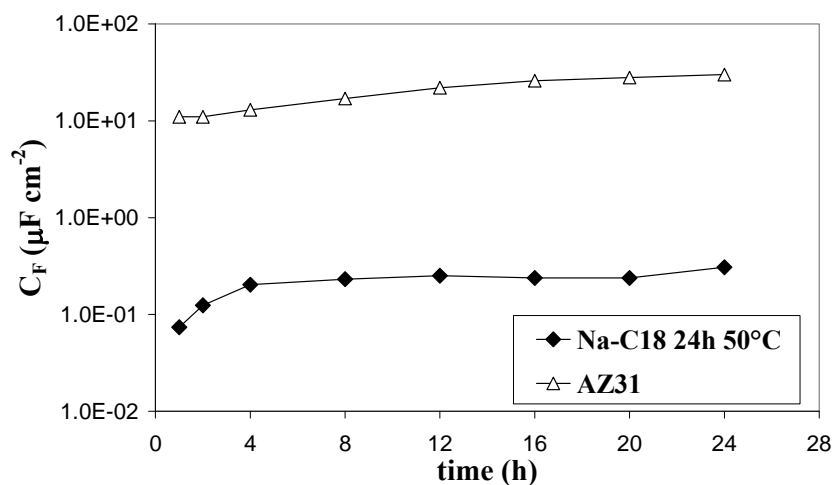***Fig. 4.9*** *– C_F evolution of (24h-50°C) Na-C18 layer during 24 h immersion in 0.05M Na_2SO_4 solution.*

In this time interval (figure 4.7), the phase angle amplitude of 10^3 Hz time constant decreased (while that of $10^0 \div 10^{-1}$Hz increased, with a contemporaneous shift towards higher frequencies, those of the blank). After 168h, 10^3 Hz τ had disappeared and was substituted by that at 10^2 Hz. At longer testing times EIS spectra shape became almost equal to that of untreated AZ31 alloy.

In spite of this marked decrease in R_F, Rp for Na-C18 treated specimens remained very high (figure 4.10): initially Rp was around 156 kΩcm^2, but rather quickly it worsened (like R_F), attaining a plateau value around 34 kΩcm^2, and no further sign of deterioration was experienced for over 800 hours.

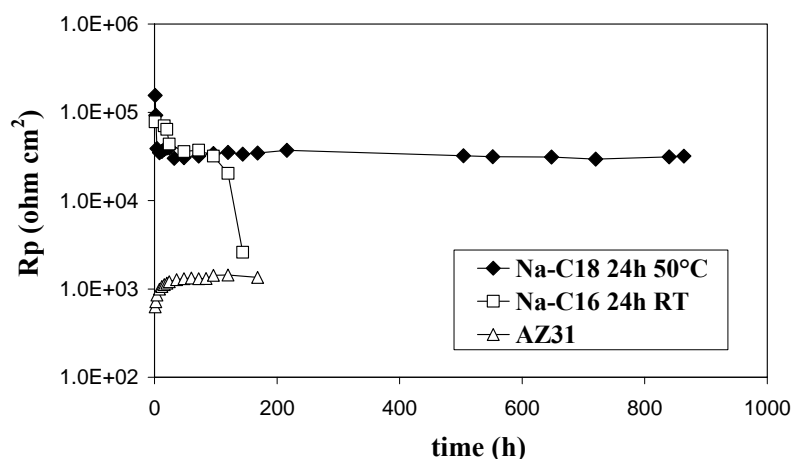***Fig. 4.10*** *– Trend, in 0.05 M Na₂SO₄ solution of Rp values, obtained from EIS measurements, for 24h-50°C Na-C18 or for 24h-RT Na-C16 treated AZ31 electrodes.*

It can be observed that the final Rp value of the Na-C18 treated electrode was still more than one order of magnitude superior to that of the blank; in fact, on untreated AZ31 electrode, Rp increased in the first 24 h immersion, to stabilize at around 1 $k\Omega cm^2$.

Although a not particularly efficient treatment (low bath temperature, short treatment time, e.g. Na-C16, RT, 24 h) could initially produce a very protective coating (Rp=78 $k\Omega cm^2$), nevertheless, R_F was not particularly high (3.7 $k\Omega cm^2$). Then, fairly quickly (within a few hours), the coating characteristics worsened and Rp decreased to a plateau value around 36 $k\Omega cm^2$ while R_F to a meaningless value, less than 0.3 $k\Omega cm^2$. In this case, the last Rp value was maintained for a short time interval, around a hundred hours and, successively, a very rapid and complete coating deterioration ensued, so that the polarization resistance arrived close to the value of the blank.

The EIS shape differentiation in function of the carboxylic anion carbon chain length is easily observed from the normalized Nyquist diagrams (normalized by the maximum of impedance module [22, 23]) presented in figure 4.11.

While for lower homologues (Na-C12, Na-C14) the normalized Nyquist plot (NNP) was similar to that of the blank, for higher homologues (Na-C16, Na-C18) NNP showed a much wider lf loop (whose characteristic frequency, 0.1 Hz, was close to that proper of the untreated electrode). In the case of the untreated electrode, the hf semicircle was related to the layer of natural magnesium corrosion products, while in the case of the latter homologues the hf loop could be attributed to a layer formed by magnesium carboxylates. Since the lf semicircle for the blank was related to a diffusion stage (i.e. the diffusion of Mg^{2+} ions through the corrosion product layer [16, 18]), it is likely that, for the higher homologues, the influence of the carboxylate layer towards the corrosion process was chiefly linked to greater hindrance to diffusion. However, during the immersion in the aggressive environment, for the penetration of this electrolytic solution in the carboxylate layer, the dimension of lf part decreased and NPP became similar to that of the blank, as reported for Na-C18 in figure 4.12.
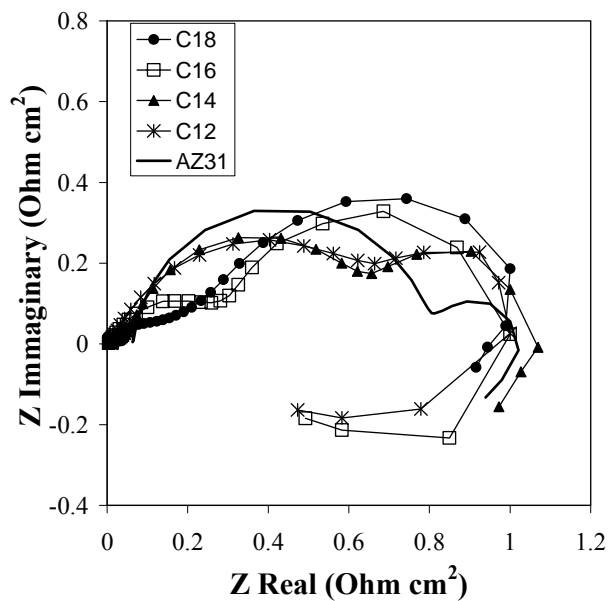
Fig. 4.11 *– Normalized Nyquist plots for Na-C12, Na-C14, Na-C16 and Na-C18 treated AZ31 electrodes after 1 h immersion in 0.05 M Na₂SO₄.*
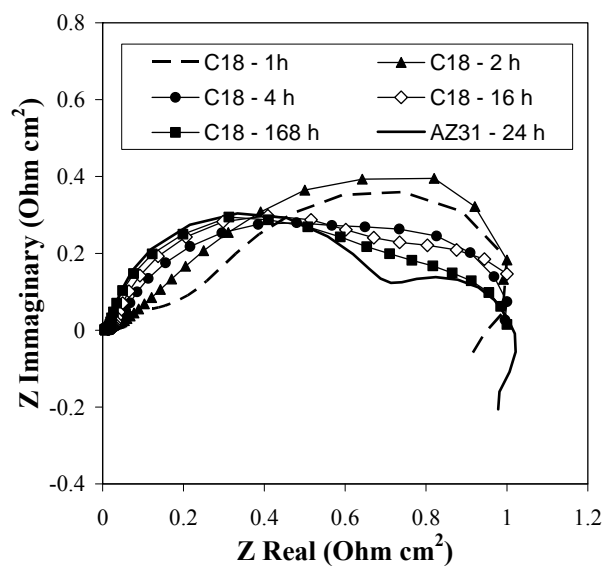
Fig. 4.12 *– Normalized Nyquist plots for Na-C18 treated AZ31 electrode during the immersion in 0.05 M Na₂SO₄.*

Some micrographs taken at the end of the runs showed that, both in the sulphate (figure 4.13) and chloride solution (figure 4.14), the corrosive attack did not develop all over the specimen surface, but it interested only isolated points, usually located near to the specimen edge, where the conversion coating was likely to be less adherent.
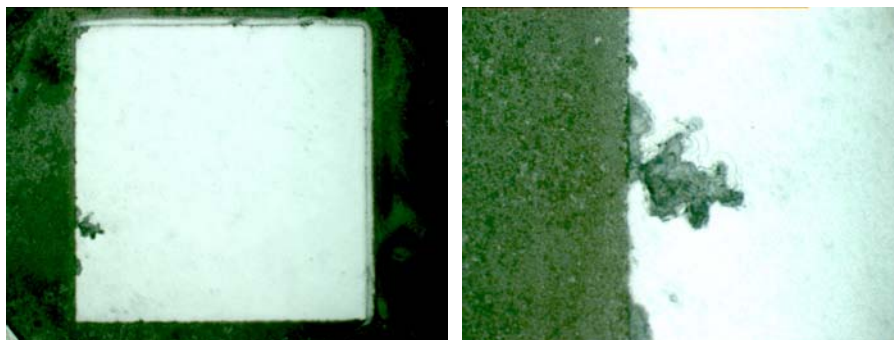
Fig. 4.13 *– Appearance of 24h-50°C Na-C18 treated electrodes, after 216 h immersion in 0.1 M NaCl solution.*
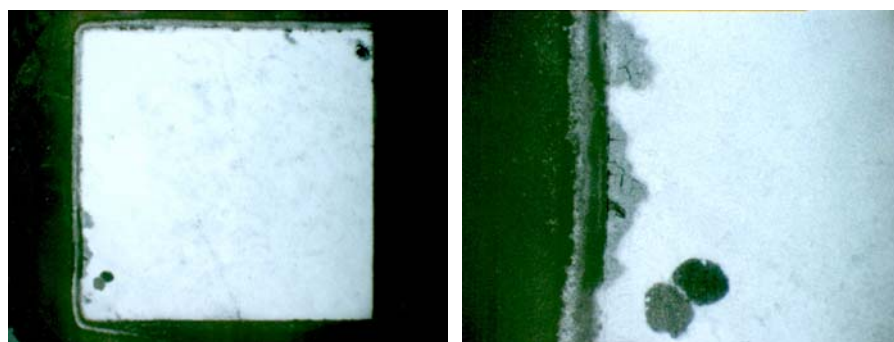
Fig. 4.14 *– Appearance of 24h-50°C Na-C18 treated electrodes, after 864 h immersion in 0.05 M Na₂SO₄ solution.*

4.3.3 Discussion

In the case of sodium salts of long-chain mono-carboxylic acids, for magnesium, it may be hypothesised that a certain likeness exists between the formation of an inhibitor film [24] and the building of conversion coatings. Both cases (which require a long time) deal with the formation of a layer of insoluble carboxylates more protective than the oxides-hydroxides spontaneously forming on the magnesium surface in aqueous media. As a general rule, the hydrophobicity and the insolubility of the carboxylate layer should augment by increasing the alkyl chain length, and this should determine an improvement in its protective performances. In the present research, both impedance and potentiodynamic polarization measurements show that the longer the aliphatic chain of carboxylate anion, the more protective the coatings are, in agreement with what was previously found on their behaviour as inhibitors for aliphatic chain length ranging from 7 to 11 carbon atoms [25].

In the conversion coatings, the marked diminution in the cathodic currents by the increase in the alkyl chain length can be explained by a wider metal surface covered with long chain carboxylate magnesium salts. At this purpose, for example, it was found that 10^{-4} M Na-C14 allowed the formation of well-shaped and more-ordered crystals on magnesium surface (that increased in size by increasing the immersion time), which more completely and evenly covered the metallic surface [21]. This effect was attributed to the stronger VdW interactions between long alkyl chains. At the same time, the parallel diminution in the values of the carboxylate film capacitance (C_F) in the impedance measurements can be accounted for by the formation of a thicker layer, since, for long

chain compounds, the value of the dielectric constant ε_r (inversely proportional to the film capacitance) can be considered as almost independent of the number of carbon atoms of the chain [26, 27].

The increase in thickness should lead to a reduction in the interconnected porosity, and, in fact, lower homologues presented the same time constants of the unprotected specimen, while higher homologues presented (for instance, after sufficiently long treatments) a new hf τ at 10^3 Hz, which can be assigned to an almost complete, poorly defective magnesium carboxylate layer. Moreover, the formation of thicker, less defective, less soluble and more hydrophobic layers by higher homologues should account for the increased capacity of their coating in hindering the anodic magnesium oxidation reaction so efficiently.

The time constants from impedance measurements showed that the protective effects of the almost complete stearate layer masked the corrosion processes occurring on a few small areas of the metal substrate, whereas, for the laurate treated electrode, the corrosion processes occurring on a larger surface area masked the carboxylate layer behavior. Thus, it can be assumed that at the beginning of the run the layers of the lower homologues slowed down the corrosion process through coverage of the metal surface, whereas those of the higher homologues interfered with the process also by exerting a strong hindrance to diffusion, as shown by the much wider lf loop in the corresponding NNP plots. To this regard, reference may be made to the fact that Z.L. Lu et al [28] recently determined that a laurate film formed on steel surface in neutral environment also behaved as a diffusive barrier limiting the charge transfer process.

101

However, with the elapsing of time, the quick capacitance increase and resistance decrease in impedance measurements showed that the aggressive solution can easily diffuse even through these very efficient layers. While in the case of lower homologues the solution entrance led to a net diminution of the protected surface (i.e. a net diminution in impedance spectra size), for higher homologues the impedance modulus, remained much higher than that of the untreated specimen, indicating a very limited diminution in the protected area. In fact, the cathodic polarization curves of stearate coatings showed a very limited increase during long immersion in chloride media.

Nevertheless, in spite of the limited coverage decrease, the permeated electrolytic solution was sufficient to have a strong affect on the protective performances of the carboxylate layer; in fact, the anodic polarization currents increased noticeably (i.e. the anodic reaction was much less efficiently inhibited) and, in these circumstances, the same time constants of the blank appeared, while the diffusion hindrance effects became less evident.

4.4 Conclusions

By using aqueous solutions of sodium salts of mono-carboxylic acids it is possible to build, on magnesium, a protective conversion coating, formed by magnesium mono-carboxylate insoluble salts. Such conversion treatments require fairly long times, which can be reduced by raising the bath temperature.

The corrosion resistance of the conversion coating increases by increasing the alkyl chain length, which renders the magnesium mono-carboxylate layer wider, more insoluble and more hydrophobic. The

longer this chain, the thicker and less defective the coating, the wider the protected metallic surface. A long chain allows the formation of a layer able to markedly inhibit not only the cathodic but also the anodic process. In the case of very efficient treatments (long alkyl chain, high bath temperature), the conversion coating maintains excellent protective performances for very long times (for instance, over 800 h in diluted sulphate solutions).

References

[1]   J.E. Gray, B. Luan, *"Protective coatings on magnesium and its alloys — a critical review"*, Journal of Alloys Compounds (2002), 336, pp. 88-113.

[2]   M.A. M.A Gonzáles-Núñez, C.A. Núñez-Lopez, P. Skeldon, G.E. Thompson, H. Karimzadeh, P. Lyon, T.E. Wilks, *"A non-chromate conversion coating for magnesium alloys and magnesium-based metal matrix composites"*, Corrosion Science (1995), 37, pp. 1763-1772.

[3]   H. Huo, Y. Li, F. Wang, *"Corrosion of AZ91D magnesium alloy with a chemical conversion coating and electroless nickel layer"*, Corrosion Science (2004), 46, pp. 1467-1477.

[4]   C.S. Lin, H.C. Lin, K.M. Lin, W.C. Lai, *"Formation and properties of stannate conversion coatings on AZ61 magnesium alloys"*, Corrosion Science (2006), 48, pp. 93-109.

[5]   H. Umehara, M. Takaya, S. Terauchi, *"Chrome-free surface treatments for magnesium alloy"*, Surface and Coating Technology (2003),169-170, pp. 666-669.

[6]   C.S. Lin, C.Y. Lee, W.C. Li, Y.S. Chen, G.N. Fang, *"Formation of Phosphate/Permanganate Conversion Coating on AZ31 Magnesium Alloy"*, Journal of Electrochemical Society (2006), 153(3), B90-B96.

[7]   F. Zucchi, A. Frignani, G. Grassi, G. Trabanelli, C. Monticelli, *"Stannate and permanganate conversion coatings on AZ31 magnesium alloy"*, Corrosion Science (2007), 49, pp. 4542-4552.

[8]   M.F. Montemor, A.M. Simões, M.G.S. Ferreira and M.J. Carmezim, *"Composition and corrosion resistance of cerium conversion films on the AZ31 magnesium alloy and its relation to the salt anion"*, Applied Surface Science 254 (6) (2008), pp.1806-1814.

[9]   M. Dabala, K. Brunelli, E. Napolitani, M. Magrini, *"Cerium-based chemical conversion coating on AZ63 magnesium alloy"*, Surface and Coatings Technology 172 (2003), pp.227-232.

[10]   K. Brunelli, M. Dabala, I. Calliari, M. Magrini, *"Effect of HCl pre-treatment on the corrosion resistance of cerium-based conversion coatings on magnesium and magnesium alloys"*, Corrosion Science 47 (2005), pp.989-1000

[11]   A.L. Rudd, C. B. Breslin, F. Mansfeld, *"The corrosion protection afforded by rare earth conversion coatings applied to magnesium"*, Corrosion Science 42 (2) (2000), pp.275-288.

[12]   K. Aramaki, T. Shimura, *"Self-assembled monolayers of carboxylate ions on passivated iron for preventing passive film breakdown"*, Corrosion Science (2004), 46, pp. 313-328.

[13]   A.Ulman, *"Formation and Structure of Self-Assembled Monolayers"* Chemical Reviews (1996), 96, pp. 1533-1544.

104

[14] Y. Liu, Z. Yu, S. Zhou, L. Wu, *"Self-assembled monolayers on magnesium alloy surfaces from carboxylate ions"*, Applied Surface Science (2006), 252, pp. 3818-3827.

[15] N. Pébère, C. Riera, F. Dabosi, *"Investigation of magnesium corrosion in aerated sodium sulphate solution by electrochemical impedante spectroscopy"*, Electrochimica Acta (1990), 35, pp. 555-561.

[16] G. Baril, N. Pébère, *"The corrosion of pure magnesium in aerated and deaerated sodium sulphate solutions"*, Corrosion Science (2001), 43, pp. 471-484.

[17] G. Baril, C. Blanc, N. Pébère, *"AC Impedance Spectroscopy in Characterizing Time-Dependent Corrosion of AZ91 and AM50 Magnesium Alloys Characterization with Respect to Their Microstructures"*, Journal of Electrochemical Society (2001), 148(12), pp. B489-B496.

[18] G. Baril, G. Galicia, C. Deslouis, N. Pébère, B. Tribollet and V. Vivier, *"An Impedance Investigation of the Mechanism of Pure Magnesium Corrosion in Sodium Sulfate Solutions"*, Journal of Electrochemical Society (2007), 154 (2) pp. C108-C113.

[19] G. Boisier, A. Lemure, N. Pébère, N. Portail, M. Villatte, *"Corrosion protection of AA2024 sealed anodic layers using the hydrophobic properties of carboxylic acids"*, Surface and Coatings Technology (2009), 203, pp. 3420-3426.

[20] S.V. Lamaka, M.F. Montemor, A.F. Galio, M.L. Zheludkevich, C. Trindade, L.F. Dick, M.G.S. Ferreira, *"Novel hybrid sol–gel coatings for corrosion protection of AZ31B magnesium alloy"*, Electrochimica Acta (2008), *53*, pp. 4773-4783.

[21] C.H Hsu, F. Mansfeld, *"Concerning the use of constant phase elements (CPEs) in the analysis of impedance data"*, Corrosion (2001), 57, pp. 747-748.

[22] G. Baril, G. Galicia, C. Deslouis, N. Pébère, B. Tribollet and V. Vivier, *"An Impedance Investigation of the Mechanism of Pure Magnesium Corrosion in Sodium Sulfate Solutions"*, Journal of Electrochemical Society 154 (2) (2007) pp. C108-C113.

[23] H. Ardelean, I. Frateur, P. Marcus, *"Corrosion protection of magnesium alloys by cerium, zirconium and niobium-based conversion coatings"*, Corrosion Science (2008), 50, pp.1907-1918.

[24] E. Rocca, G. Bertrand, C. Rapin, J.C. Labrune, *"Inhibition of copper aqueous corrosion by non-toxic linear sodium heptanoate: mechanism and ECAFM study"*, Journal of Electro-analytical Chemistry (2001), 503, pp. 133-140.

[25] F. Zucchi, V. Grassi, F. Zanotto, *"Sodium monocarboxylates as inhibitors of AZ31 alloy corrosion in a synthetic cooling water"*, Materials and Corrosion (2009), 60(3), pp. 199-205.

[26] G.K. Jennings, T-H. Yong, J.C. Munro, P.E. Laibinis, *"Effect of Chain Length on the Protection of Copper by n-Alkanethiols"* Langmuir (1998), 14(21), pp. 6130-6139.

106

[27] G.K. Jennings, T-H. Yong, J.C. Munro, P.E. Laibinis, *"Structural Effects on the Protective Properties of Self-Assembled Monolayers Formed from Long-Chain w-Alkoxy-n-Alkanethiols on Copper"* Journal of the American Chemical Society (2003), 125, pp. 2950-2957.

[28] Z.L. Lu, Y.B. Qiu, X.P. Guo, *"Study of inhibition performance and adsorption behaviour of lauric acid on N80 steel in acidic and near neutral environments"*, Corrosion Engineering Science and Technology (2009), 44(1), pp. 43-50.

Chapter 5

PROTECTION OF THE AZ31 MAGNESIUM ALLOY WITH CERIUM MODIFIED SILANE COATINGS

5.1 Introduction

In Chapter 1 silane treatments have been reported as a possible alternative technology to the use of pre-treatments based on Cr(VI)-containing formulations and have been successfully tested with magnesium alloys too [1-5] . Silane treatments lead to the formation of a thin organic protective layer that act as a physical barrier delaying the ingress of aggressive species towards the metallic surface; moreover, they can build strong bonds with the metallic substrate, providing a good adhesion between the varnish and the metal, also in critical conditions such as in wet environments [6].

The main feature of silanes is the formation of a metallo-siloxane bond (Si-O-Me), due to the condensation process between silanol groups (SiOH, derived from silane hydrolysis) and the hydrated metal surface (MeOH). The Me-O-Si covalent bonds lead to a good anchoring of the silane layer to the metal substrate. Moreover, in the reticulation step, silanol groups can condensate each other forming siloxane bonds and thus build thick polymeric metallo-organic protective layers [7-9].

Montemor and Ferreira [10], observed that the protective effects of the silane coating could be improved by adding to the silane pre-treatment baths some species, such as cerium salts, which displayed inhibition properties on magnesium corrosion processes [11, 12]. In particular, the scanning vibrating electrode technique (SVET) evidenced that cerium

ions could inhibit the corrosion processes at the artificially damaged areas in the silane film [10].

Zucchi et al. [3] studied the possibility to obtain a protective coating on a magnesium alloy by 3-mercapto-propyl-trimethoxysilane (PropS–SH), but its protective performances decayed after only 24 hours in a 0.05 M Na_2SO_4 solution. However, formerly, these researchers showed that a PropS-SH treatment bath could built a very efficient layer on copper surface [13]. In this case the marked corrosion protection was attributed to the strong bond between the mercapto group and the copper surface.

In order to increase the scarce protective performance of the PropS-SH coating, the treatment bath was modified adding an aqueous solution of 10^{-2}M or 10^{-1}M $Ce(NO_3)_3$. In this Chapter the results about the protective effects of these cerium modified silane pre-treatments are reported.

5.2 Experimental part

Square specimens were cut from a 5 mm thick plate of AZ31 magnesium alloy and embedded in an epoxy resin allowing the exposition of a area of 1.5 cm^2. Their surfaces were prepared by emery papers up to 1000 grade, washed with distilled water, degreased with acetone and dried with hot air.

The electrodes were initially pre-treated in a 10% HF solution for 60 sec, hot air dried and then immersed for 30 sec in the silane bath; after a hot air flux drying, they were finally cured for 1 hour at 100 °C.

The treatment bath was a hydroalcoholic solution of 3-mercapto-propyl-trimethoxy-silane (PropS-SH) (90%/5%/5%, vol./vol./vol., 95° ethylic alcohol/water/silane), which was also modified with an aqueous solution of 10^{-2} M or 10^{-1} M $Ce(NO_3)_3$ (90%/5%/5%, vol./vol./vol., 95° ethylic

alcohol/cerium nitrate/silane) in order to obtain a Ce^{+3} ions concentration of 5×10^{-4} M or 5×10^{-3} M. In order to favour silane hydrolysis, the baths were utilized after different aging times from their preparation (from 24 to 168 h).

Electrochemical tests were performed in a 250 ml volume cell and the aggressive solution was 0.1M NaCl.

Anodic and cathodic potentiodynamic (0.2 mV sec^{-1} scanning rate) polarization curves were recorded on independent specimens starting from the corrosion potential. Electrochemical impedance spectra were performed in the $10^5 \div 10^{-3}$ Hz frequency range, applying, at the corrosion potential, a 10 mV rms sinusoidal perturbation.

FT-IR spectra were acquired on pure silane and on AZ31 specimens treated with the above described silane baths.

5.3 Results and discussion

5.3.1 Preliminary results

Figure 5.1 collects the polarization curves recorded on AZ31 electrodes treated with the un-modified or 5×10^{-4} M $Ce(NO_3)_3$ modified silane bath, after different aging times (after 24, 72 and 168 h from solutions preparation).
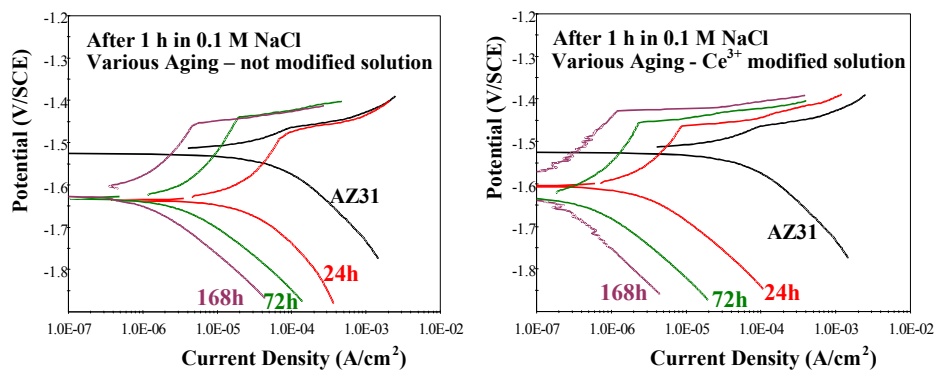
Fig. 5.1 – *Polarization curves recorded in 0.1M NaCl on AZ31 electrodes treated in a not modified (left) or 5x10^{-4} M Ce(NO_3)_3 modified (right) Prop-SH bath, for different aging times .*

When AZ31 was treated in the un-modified bath (figure 5.1, left), the increasing of bath aging time determined a marked and constant improvement in efficiency of the silane coating, which hindered both the anodic and cathodic processes.

The presence of $5x10^{-4}$M Ce(NO_3)_3 in the treatment bath further on improved the inhibiting effects (figure 5.2, right); in fact, by a 168 h aging, the corrosion current of AZ31 treated with the modified solution was more than two order of magnitude lower than that of the untreated specimen, while that of AZ31 treated with the not modified solution was a little over one order of magnitude (Table 5.1).

Table 5.1 reports the corrosion current (i_{CORR}) and the inhibition efficiency (%I.E.) values obtained from the polarization curves of AZ31 electrodes treated in the different silane baths for different aging times, together with the corresponding pH values.

Table 5.1 – I_{CORR} and I.E. % obtained from polarization curves recorded in 0.1M NaCl on AZ31 electrodes treated in a not modified or $5x10^{-4}$ M $Ce(NO_3)_3$ modified PropS-SH bath, for different aging times.

PropS-SH solution aging (hours)	Ce^{+3} 5x10^{-4}M			No Ce^{+3}		
	i_{CORR} ($\mu A/cm^2$)	I.E. %	pH	i_{CORR} ($\mu A/cm^2$)	I.E. %	pH
AZ31	57	-	-	57	-	-
24	2.9	95%	5.48	22	61%	8.22
72	0.65	98.9%	3.50	4.2	93%	5.80
168	0.14	99.8%	3.14	1.3	98%	4.50

Due to silane hydrolysis continuous progress, the pH of the un-modified PropS-SH solution decreased during the aging step and contemporaneously the bath efficiency increased. After only 24 h from the preparation, the modified silane bath presented a pH value noticeably decreased in comparison to that of the sole silane; probably the presence of Ce^{3+} ions quickened the Si-O-CH$_3$ group hydrolysis. This effect continued with the increase in the aging time, determining a progressive bath acidification and a contemporaneous increment of the inhibition effects. After an aging time of 168 h, the Ce^{3+} modified solution had a pH value of 3.14 with an inhibition efficiency of 98.8%, whereas the un-modified silane bath exhibited a pH value of 4.5 with an inhibition effect of 98%. Therefore, to avoid the influence of pH variation, all the silane baths were pH 4 acidified with sulphuric acid addition.

In order to better understand the effect of Ce^{3+} ion presence on the coating features, FT-IR spectra were acquired on AZ31 specimens treated in the silane bath, not modified (pH 8.22) or modified (pH 5.48) with 5×10^{-4} M $Ce(NO_3)_3$, after 24 h from their preparation (figure 5.2).
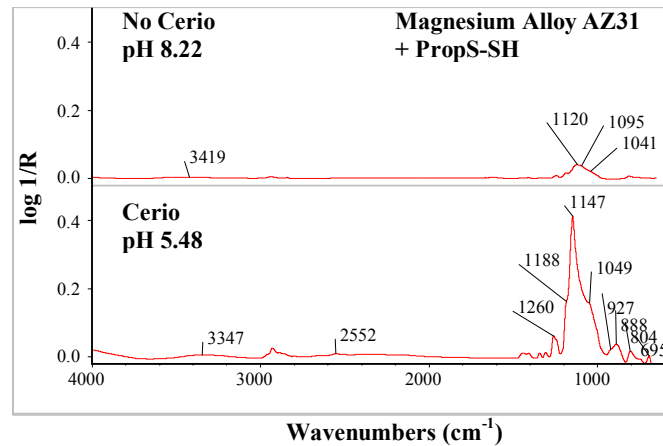

Fig. 5.2 *– FT-IR spectra acquired on AZ31 specimens treated with a 5×10^{-2} M $Ce(NO_3)_3$ modified silane solution (pH 5.48) and with a not modified silane solution (pH 8.22).*

From a first analysis it can be observed that the $Ce(NO_3)_3$ modified bath treated specimen presented higher peaks, that of the sole silane one. The spectra of figure 5.2 were expanded in different scale ranges and compared also with FT-IR spectra acquired on pure silane and on specimens treated with a not modified silane solution, whose pH was regulated to 6.01 value (figure 5.3).
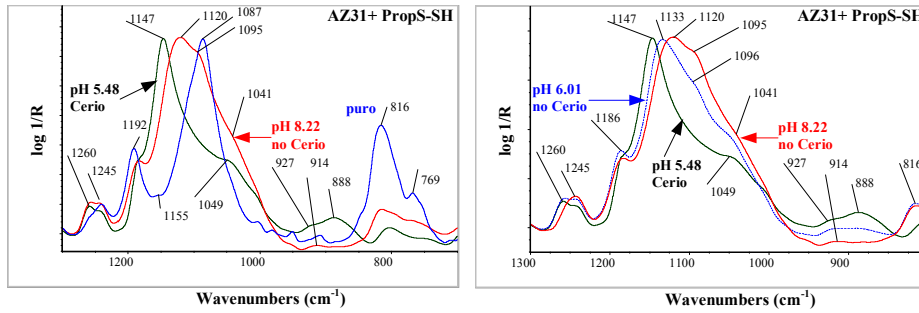
Fig. 5.3 – *FT-IR spectra acquired on pure silane and on AZ31 specimens treated with a 5×10^{-2} M Ce(NO$_3$)$_3$ modified silane solution (pH 5.48) and with a not modified silane solution (pH 8.22)(left) or with a not modified silane solution which pH was regulated at 6.01 (right).*

A 1087 cm^{-1} peak was detectable in the pure silane FT-IR spectra and was associated to the Si-OCH$_3$ bond stretching. This peak tended to disappear in AZ31 spectra with the decreasing of the bath pH value, because of the progressive Si-O-CH$_3$ group hydrolysis and Si-OH groups condensation to form Si-O-Si bonds (peaks around 1147 and 1049 cm^{-1}). The comparison between FT-IR spectra acquired on specimens treated with a not modified PropS-SH solution (24 h; pH 8.22 and 168 h; pH 4.5 hydrolysis time, figure 5.4), evidenced an intensification of the peaks associated to Si-O-Si bonds (around 1147 and 1050 cm^{-1}) for the longer hydrolysis time.
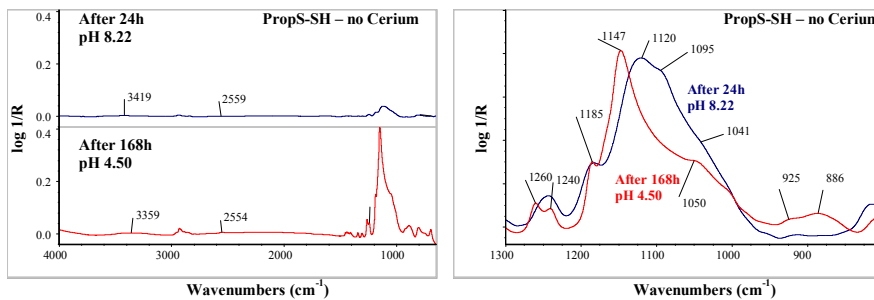

Fig. 5.4 – *FT-IR spectra acquired on AZ31 specimens treated with a not modified silane utilized after 24 h (pH 8.22) and 168 h (pH 4.5) from its preparation.*

In order to avoid the hydrolysis effect, FT-IR spectra were acquired on specimens treated with pH 4 regulated - 24 h aged baths (figure 5.5). The final pH value was 3.40 for the sole silane solution and 3.16 for the silane solution with Ce^{3+} ions.
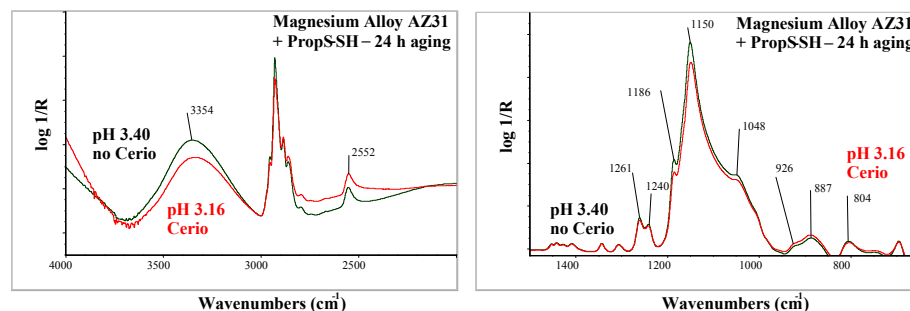

Fig. 5.5 *– FT-IR spectra acquired on AZ31 specimens treated with a not modified and modified silane bath after a pH value regulation at 4 and 24 h aged.*

The spectra were very similar, thus, apparently, for the same pH and aging time conditions, the Ce^{3+} ions presence did not seem to have any influence on coating features. From a qualitative point of view, the 2550 cm⁻¹ band, detectable in both the spectra and attributed to the S-H bond stretching, showed that the SH group seemed not to form any bond with the metal substrate. The presence of O-H bonds (peaks around 3300 and 926 cm⁻¹) suggested that not all the Si-OH groups were involved in condensation and reticulation process to build-up Si-O-Si bonds, during the curing step-stage (100 °C for 1 h).
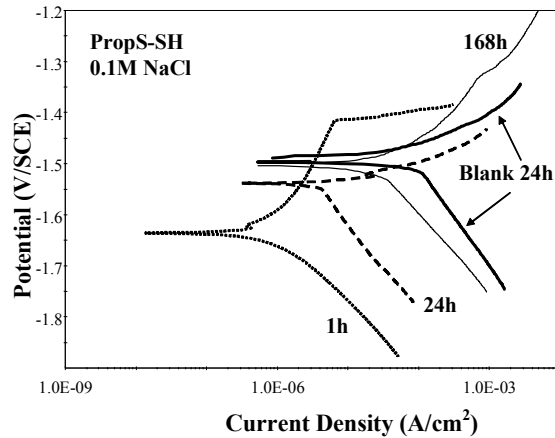
5.3.2 Polarization curves

Fig. 5.6 – *Polarization curves of PropS-SH coated AZ31 recorded after 1, 24 and 168 h immersion in 0.1M NaCl.*

In comparison to unprotected AZ31, PropS-SH coating formed on AZ31, after 1 h immersion in the chloride solution (figure 5.6), succeeded in reducing the cathodic polarization currents of hydrogen evolution by about two orders of magnitude and it was also more efficient than the original magnesium corrosion product layer towards magnesium oxidation process; as a matter of fact, in the first potential interval, the anodic polarization curve presented a very high slope with currents markedly lower than those of the blank.

The passive state was maintained up to a certain potential (breaking potential around − 1.4 VSCE), where an abrupt current increase took place. However, such a protective action showed a limited duration; in fact, only after 24 h immersion, the cathodic currents resulted increased and at the end of the test (7 d) they were close to those of the untreated AZ31. The same trend was experienced on the anodic process, where, after 168 h, the protective effects were almost completely lost.

Figure 5.7 collects the polarization curves recorded, after 1 and 168 h immersion in 0.1 M NaCl, on AZ31 electrodes treated with the $5x10^{-4}$M or $5x10^{-3}$M Ce^{3+} modified baths together with that of the sole PropS-SH treated and the untreated AZ31.
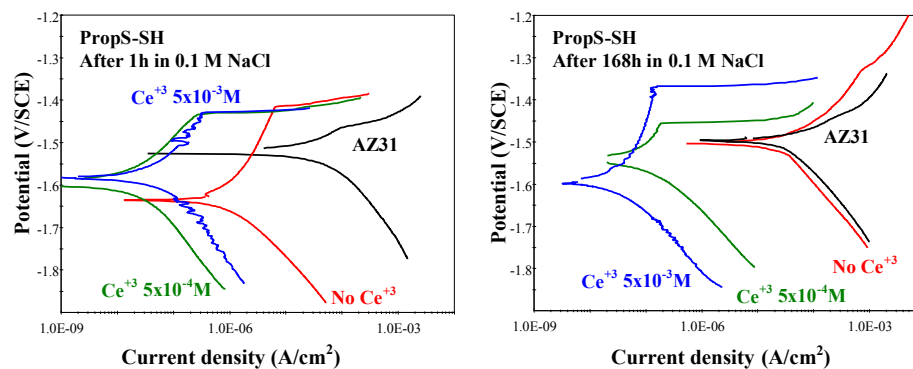

***Fig. 5.7** – Polarization curves recorded, after 1(left) or 168 (right) h in 0.1M NaCl, on AZ31 electrodes treated with un-modified and Ce^{3+} $5x10-4$ or $5x10^{-3}$M modified PropS-SH baths.*

The addition of Ce^{3+} ions to the silane baths, led to a significant improving of the silane coating protective performance. As a matter of fact, the corresponding polarization curves, recorded after 1 h immersion in 0.1 M, were shifted towards current values noticeably lower than that of the sole silane treated electrodes, in particular, when the Ce^{3+} ions concentration was $5x10^{-4}$ M, Ce^{3+} ions presence in the treatment baths made the silane coatings not only more protective, but also more stable (table 5.2). In fact, at the end of the test, the inhibiting effects were practically maintained, even if with a little i_{CORR} increasing in the case of the $5x10^{-4}$ M Ce^{3+} modified bath. Moreover, in presence of a higher Ce^{3+} concentration ($5x10^{-3}$M), these effects resulted further on enhanced, as evidenced by a 50 mV positive shift of the breakdown potential and by the increased slope of the anodic curve.

Table 5.2 – I_{CORR} *and E.I.% values obtained from polarization curves recorded after 1 and 168 h in 0.1M NaCl on AZ31 electrodes treated with the different silane baths.*

Treatment	After 1h in 0.1M NaCl		After 168h in 0.1M NaCl	
	i_{CORR} $(\mu A/cm^2)$	I.E. %	i_{CORR} $(\mu A/cm^2)$	I.E. %
AZ31	57	-	37	-
PropS-SH	1.48	97.4%	23.9	35.4%
PropS-SH + Ce^{+3} 5x10^{-4}M	0.03	99.95%	0.14	99.62%
PropS-SH + Ce^{+3} 5x10^{-3}M	0.09	99.84%	0.05	99.86%

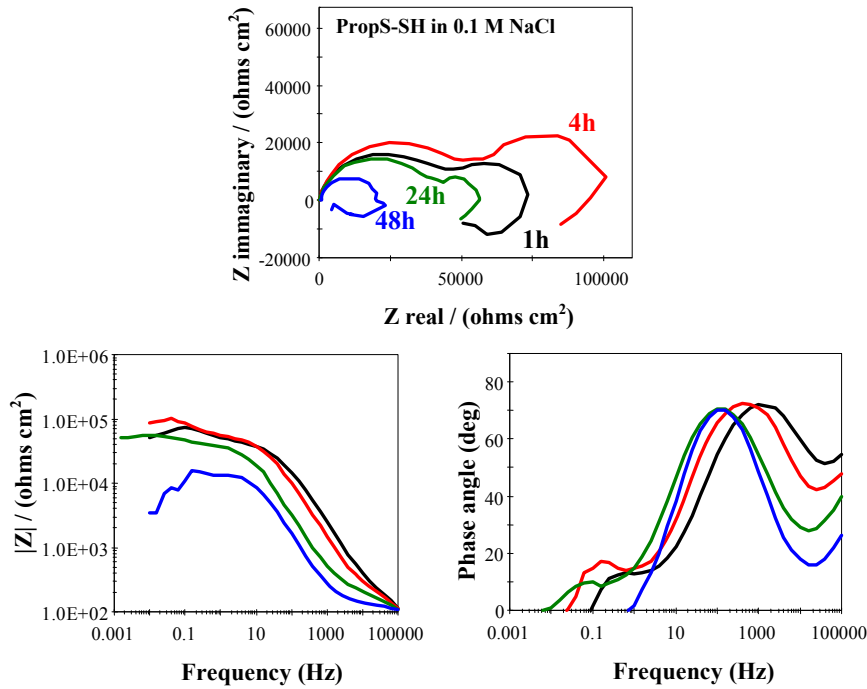## 5.3.3 Electrochemical Impedance Spectra

Fig. 5.8 – *EIS spectra recorded, after 1, 4, 24, 48 h immersion in 0.1 M, on AZ31 electrodes treated with a not modified PropS-SH bath.*

As already exposed in the preceding Chapters, the impedance spectra of the untreated AZ31 showed, at the beginning of the test (1 h), two time constants, one at 10^2 Hz, attributed to the charge transfer process and film resistance, and one around 10^{-1} Hz, linked to the Mg^{2+} diffusion trough the corrosion product layer [14-16]. After 1 h of exposure to the electrolytic solution, the presence of a PropS-SH coating increased the low frequencies impedance modulus (considered as the Polarization Resistance, Rp) of almost two orders of magnitude in comparison to that of the untreated AZ31 (figure 5.8). As a matter of fact, only the electrolytic resistance inside the pores was valuable, and, as affirmed by Murray [17], with the decreasing of the protective layer coverage the coating capacitance also decreases and may not be measurable at frequencies below 1 MHz. Two time constants were clearly discernible in these spectra: one at *hf* (characteristic frequency around 10^3 Hz), that was associated to the electrochemical processes occurring at the bottom of the pores [18], and the second (characteristic frequency around 10^{-1} Hz), observed also in the untreated AZ31 spectra. However, the sole silane bath built on AZ31 electrode a very defective coating: its spectra, after only 1 h immersion, showed, at the highest frequencies ($10^4 \div 10^5$ Hz), a resistive response, due to the high conductivity of the electrolyte solution inside the pores.

With increasing of immersion time, the barrier effect of the sole silane coating further decreased, as observable from the diminution of the impedance modulus at lower frequencies. The *hf* time constant shifted to lower frequencies, because of the worsening of silane film characteristics, i.e. increasing of defectiveness, porosity enlargement and

coalescence. The corrosion processes occurring on many large areas of the metal substrate (the areas reached by solution) masked the protective effect of the sole silane film, thus the EIS spectra became similar to that of the untreated AZ31. Moreover, after only 48 h, the quick worsening of the coating protective features lead to a localized corrosion attach on the metal substrate, thus the time constant around 0.1 Hz was no more detectable.
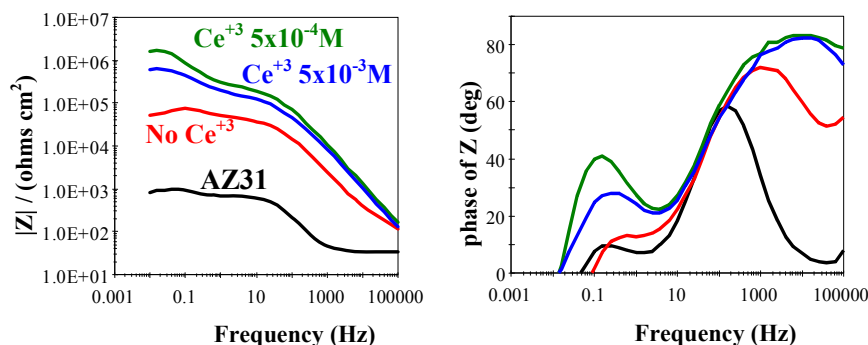

Fig. 5.9 – *Bode EIS spectra recorded, after 1 h immersion in 0.1 M, on AZ31 electrodes treated with modified or not modified PropS-SH baths*

Figure 5.9 compares the impedance spectra (Bode format) recorded, after 1 h immersion in 0.1 M NaCl solution, on electrodes treated in PropS-SH silane solution, also modified with the two different $Ce(NO_3)_3$ concentrations ($5x10^{-3}$ M e $5x10^{-4}$ M). When $Ce(NO_3)_3$ was added to the treatment baths, the low frequencies impedance modulus value of PropS-SH coating was further on increased by an additional order of magnitude. In this case, the capacitive response at high frequencies, due to the lowered defectiveness and porosity, represented the dielectric properties of the obtained coatings; the *hf* time constant, with a characteristic frequency at 10^4 Hz, was attributed to coating capacitance and pore resistance [19-20], and the 10^{-1} Hz time constant, (having a

120

higher phase angle value respect to that of the blank or of the sole silane treated electrode) to the diffusion of water and ions trough the micro pores that likely characterize an almost complete coating before the development of conductive pathways ("interconnected electrolyte filled micro pores") [21].

Fig. 5.10 *– EIS spectra recorded, after 1, 4, 24, 72 h immersion in 0.1 M, on AZ31 electrodes treated with a $5x10^{-4}$ M Ce^{3+} modified PropS-SH bath.*

When a $5x10^{-4}$ M $Ce(NO_3)_3$ solution was added to the silane bath, the initial (1h) protective performances were maintained for almost 24 h (figure 5.10), then a decreasing in the impedance modulus was found, however in a much more limited way in comparison to the sole silane treated electrode. After only 4 h of immersion, a $10^3 \div 10^2$ Hz time constant was detectable and with increasing of time, became more evident with a frequency shift to lower values. As previously reported,

121

this time constant can be likely linked to the corrosion processes occurring on the metal substrate (at the bottom of the pores) reached by the electrolyte, as conductive pathways were formed in the coating. The *lf* time constant also shifted to lower values and the corresponding capacitive semicircle progressively tended towards a more depressed shape. Indeed, since with proceeding of the corrosive process the corrosion products precipitate on the metal substrate building a porous layer [22], after a long immersion time, it can be supposed that the *lf* time constant was linked to the diffusion of the Mg^{2+} ions through the corrosion product layer, as it is reported for the untreated AZ31 [23, 24].
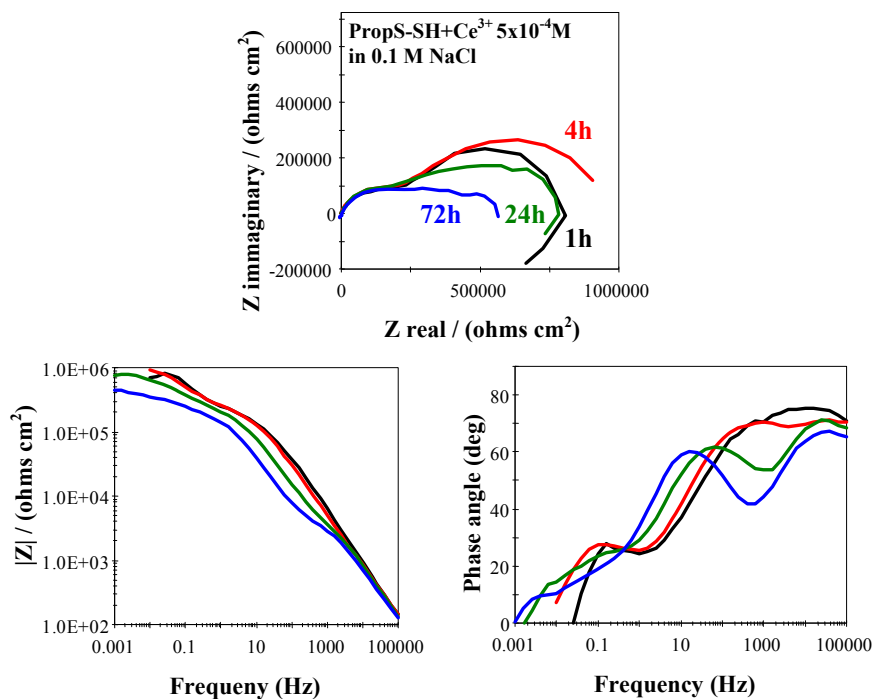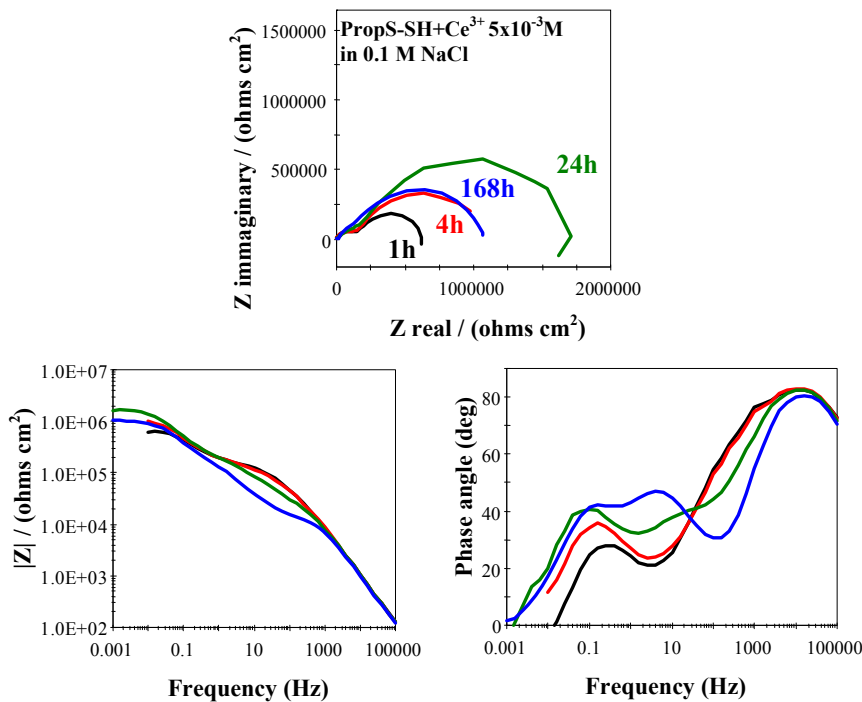

Fig. 5.11 *– EIS spectra recorded, after 1, 4, 24, 168 h immersion in 0.1 M, on AZ31 electrodes treated with a $5x10^{-3}$ M Ce^{3+} modified PropS-SH bath.*

When the Ce^{3+} ions concentration was increased up to $5x10^{-3}$ M, the high protective effect of the coating was practically maintained up to the end of the run with an impedance modulus at lower frequencies still having a value of 10^6 Ωcm^2 (figure 5.11). In this case, the 10^3-10^2 Hz time constant appeared after a longer immersion period (24 h) than in the case of the lower Ce^{3+} concentration, while the *lf* time constant practically maintained its characteristic frequency and the corresponding capacitive semicircle maintained a large diameter amplitude.

It can be supposed that after a short immersion time the number of conductive pathways was very low, thus the corrosion process in this very limited area of the metal substrate was masked by the behaviour of the protective coating. As a matter of fact, the large angle phase distribution observable for the EIS spectra of Ce^{3+} modified coatings in the first immersion hours, can be considered as two time constant overlapping, so that the 10^4 Hz and 10^2 Hz time constants became distinguishable later. As a consequence a two Randle elements circuit showed in figure 5.12 was adopted to analyse the EIS spectra in the $[10^5 \div 10^1$ Hz] or $[10^5 \div 10^0$ Hz] frequency range: R_s was the solution resistance, R_{po} the pore resistance and CPE_C the coating capacitance, R_1 and CPE_1 represented the corrosion process on the unprotected alloy surface and the related double layer capacitance, respectively.

As it was done for the analysis of EIS spectra of AZ31 electrodes covered by carboxylate conversion coating in Chapter 4, Constant Phase Elements (CPE), instead of pure capacitances were adopted in order to take into account the non ideal behaviour of the film. CPE values were converted into capacitances by means of the parameters obtained from the fitting [25].

123
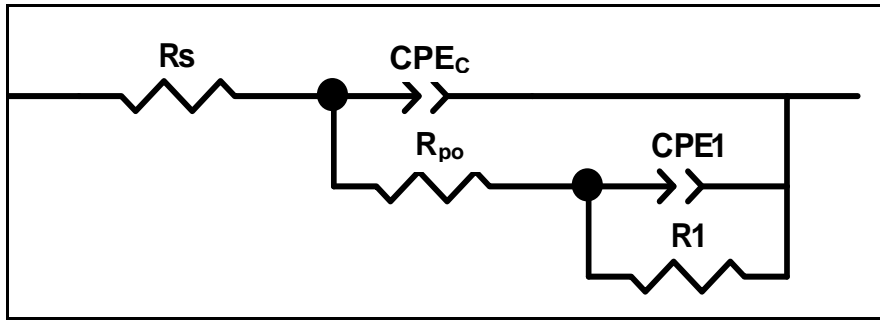
Fig. 5.12 *– Equivalent circuit (EC) used to simulate the EIS spectra.*

Figure 5.13 reports the pore resistance evolution during the 168 h immersion for the three tested silane coatings. The sole silane coating showed very low R_{po} values from the first immersion hours (512 Ωcm^2 after 1 h), due to its high porosity and defectiveness. The pore resistance gradually decreased with time and after 48 h immersion its value was negligible.

Fig. 5.13 *– R_{po} time evolution obtained from EIS spectra recorded in 0.1M NaCl on AZ31 treated with modified and not modified PropS-SH baths.*

With presence of Ce^{3+} ions in the treatment bath the R_{po} values of the formed silane coatings noticeably increased.

124

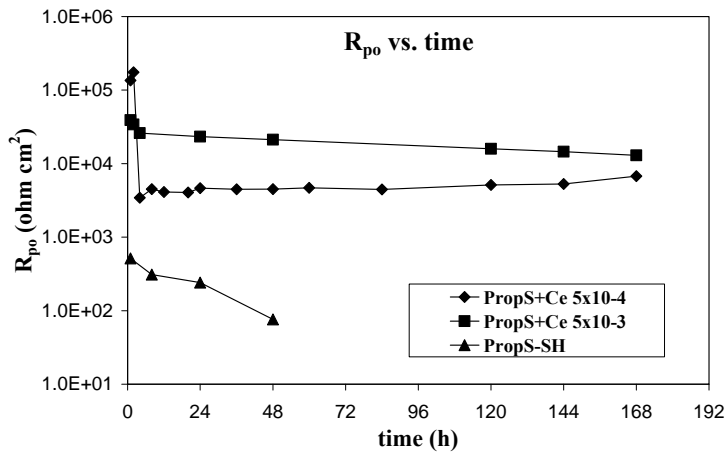In this case of the more diluted Ce^{3+} concentration, the pore resistance quickly decreased to 3.5 kΩcm^2 in the first 4 h immersion and contemporaneously the 10^2 Hz time constant became distinguishable. In the succeeding hours, R_{po} maintained an almost constant vale around 4.7 kΩcm^2. On the contrary, when Ce^{3+} concentration was higher, the R_{po} value showed a very limited reduction in the first immersion hours (from 39 kΩcm^2 after 1 h to 26 kΩcm^2 after 4 h). At the end of the run, after an almost constant trend, it exhibited still a relatively high value (13 kΩcm^2).

Figure 5.14 shows the evolution with time of the coating capacitance. Both the Ce^{3+} modified silane coatings, in the first immersion hours, presented very low capacitance values (around 23 nFcm^{-2} after 1 h).

Fig. 5.14 – C_c *time evolution obtained from EIS spectra recorded in 0.1M NaCl on AZ31 treated with modified PropS-SH baths (Ce^{3+} concetration 5x10^{-4}M and 5x10^{-3} M.*

After 20 h immersion, the C_c of the coating of the more diluted Ce^{3+} ions silane bath, showed a progressive increasing, likely due to electrolyte solution penetration and reached, at the end of the run, a value of 100 nFcm^{-2}. At the higher Ce^{3+} ions concentration, the C_c exhibited an

almost constant value up to 168 h immersion, evidencing a relevant film stability and a high inertia to electrolyte penetration.

Figure 5.15 and 5.16 show the trend of the resistance (R_1) and capacitance (C_1) value attributed to the corrosion processes occurring on metal substrate reached by the aggressive solution.

Fig. 5.15 *– R_1 time evolution obtained from EIS spectra recorded in 0.1M NaCl on AZ31 treated with modified and not modified PropS-SH baths.*

In the case of the sole silane coating, R_1 (44 kΩcm^2, after 1 h immersion) reached a value of 58 kΩcm^2 after 8 h, then it quickly decreased, attaining a value of 1.1 kΩcm^2 at the end of the test, close to the values of untreated AZ31 [26]. When Ce^{3+} ions were added to silane bath, R_1 resulted noticeably enhanced; with the more diluted Ce^{3+} concentration, R_1, in the first 24 h, had a certain increase (from 180 to 220 kΩcm^2), then it slowly decreased, attaining, after 84 h, a value around 150 kΩcm^2. With a higher Ce^{3+} concentration, R_1, starting from about the same previous values (140 kΩcm^2 after 1 h), was characterized by corresponding higher R_1 values (around 330 kΩcm^2).
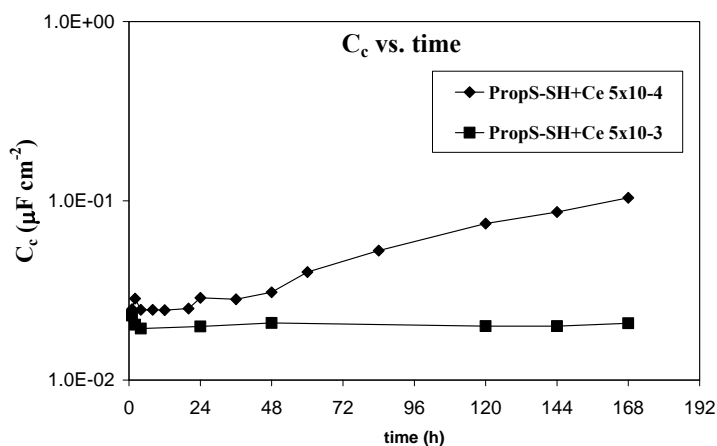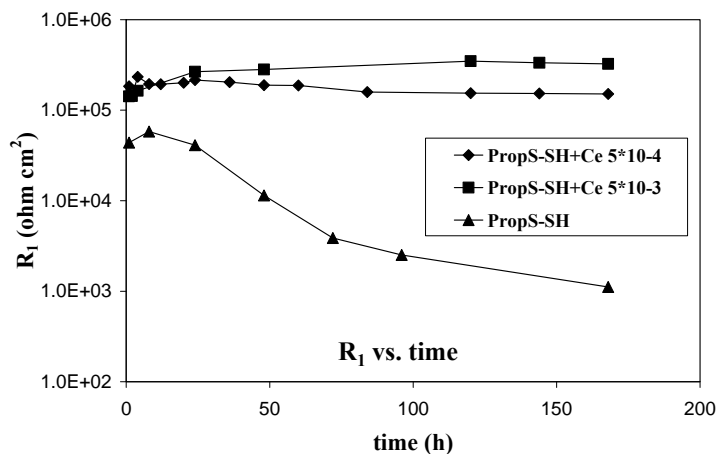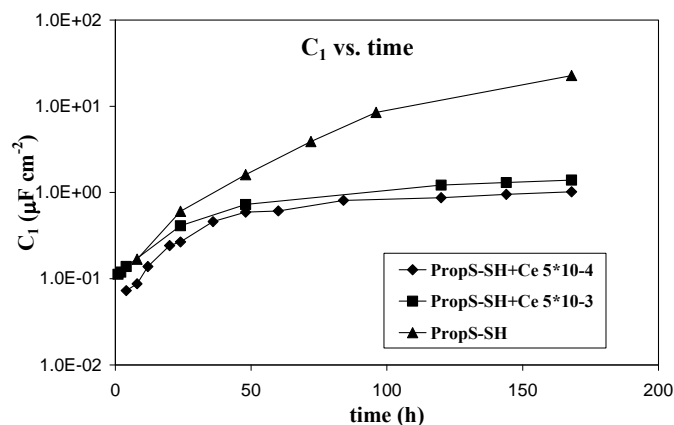
Fig. 5.16 *– C_1 time evolution obtained from EIS spectra recorded in 0.1M NaCl on AZ31 treated with modified PropS-SH baths (Ce^{3+} concetration 5x10^{-4}M and 5x10^{-3} M.*

C_1 of the sole silane treatment started from a very low value, but it rapidly increased attaining, after 168 h, a value of 23 µFcm^{-2} very near to the values measured for the untreated AZ31 (around 10 µFcm^{-2} after 1 h and 40 µFcm^{-2} after 168 h) [26]. Also in the case of the modified treatments baths, C_1 was very low at the beginning of the EIS measurements, then it showed a gradual increasing; anyway it attained values that were more than one order of magnitude lower than that of the sole silane treatment (1 and 1.4 µFcm^{-2} for the 5x10^{-4} and 5x10^{-3} M Ce^{3+} concentration respectively).

The presence of cerium ions increases the pore resistance and decreases the capacitance of the silane film and therefore these species enhance the coating barrier properties. The presence of a high frequency capacitive behaviour in the EIS spectra of the cerium modified silane film suggests that the porosity and/or conductivity of the film decrease and that the thickness increases. Increased film thickness was found for sol–gel coatings doped with cerium [27]. It is reported in literature [28–30] that

127

Ce^{3+} ions can be converted in Ce^{4+} ions in solution by oxygen. These ions can substitute some of the Si atoms in the silane film, leading to the formation of a modified Si–O–Ce network [27]. Moreover, as already reported in Chapter 1, cerium nitrate was demonstrated to provide a "self-healing" effect to the silane coating [31]. In fact, once local damages occur, Ce^{3+} ions, incorporated in the silane network, readily diffuse to these areas in an aqueous environment and precipitate on the "damaged" metal by forming protective Ce^{3+} hydroxides in situ [32]. The inhibiting effect of Ce^{3+} was also suggested to be promoted by a local increase of pH at the cathodic sites that disrupts the siloxane network, releasing Ce^{3+} ions. These species precipitate as insoluble hydroxides on the cathodic sites that surround the defect, hindering the reduction reactions [32].

5.4 Conclusions

The protective effect obtained with a sole PropS-SH treatment decayed after few hours of immersion of the AZ31 specimens in a 0.1 M NaCl solution, because the electrolyte rapidly penetrated through pores and defects that characterized the mercapto derivative silane coating .

Cerium ions rendered the silane coatings less porous and defective and thus more protective. This effects persisted with high results for all the test, particularly with presence of a higher $Ce(NO_3)_3$ concentration in the treatment bath.

The higher Ce^{3+} modified silane coating stability may be also linked to the precipitation of very insoluble cerium hydroxide corrosion product at the damaged areas, which hinder the corrosion activity ("self-healing effect").

128

References

[1]   F. Zucchi, A. Frignani, V. Grassi, A. Balbo, G. Trabanelli *"Organo-silane coatings for AZ31 magnesium alloy corrosion protection"* Materials Chemistry and Physics, 110 (2008), pp. 263–268.

[2]   A.L.K. Tan, A.M. Soutar, I.F. Annergren, Y.N. Liu, *"Multilayer sol–gel coatings for corrosion protection of magnesium"*, Surface and Coatings Technology, 198 (2005), pp. 478-482.

[3]   F. Zucchi, V. Grassi, A. Frignani, C. Monticelli, G. TrabanellI, *"Influence of a silane treatment on the corrosion resistance of a WE43 magnesium alloy"*, Surface and Coatings Technology, 200 (2006), pp. 4136-4143.

[4]   R. Supplit, T. Koch, U. Schubert, *"Evaluation of the anti-corrosive effect of acid pickling and sol–gel coating on magnesium AZ31 alloy"*, Corrosion Science 49 (2007), pp. 3015-3023.

[5]   A.N. Khramov, J.A. Johnson, *"Phosphonate-functionalized ORMOSIL coatings for magnesium alloys"*, Progress in Organic Coatings (2009), 65, pp. 381-385.

[6]   S. Rossi, F. Deflorian, *"Innovative Pretreatment of Metals to improbe the Adhesion Strength of the Organic Coatings: Silanes"*, Pitture e Vernici – European Coatings 1 (2006), pp.47-63.

[7]   W.J. van Ooij, D. Zhu, *"Electrochemical Impedance Spectroscopy of Bis-[Triethoxysilypropyl]Tetrasulfide on Al 2024-T3 Substrates"*, Corrosion (2001), 57, pp. 413-427.

[8]   A. Franquet, C. Le Pen, H. Terryn, J. Vereecken, *"Effect of bath concentration and curing time on the structure of nonfunctional thin organosilane layers on aluminium"*, Electrochimica Acta (2003), 48, pp. 1245-1255.

[9]   R. Duarte, A.M. Cabral, M.F. Montemor, J.C.S. Fernandes, M.G.S. Ferreira, Keynote: *"Environmentally friendly pre-treatments for aluminium alloys"*, in: Proc. 15th Int. Corros. Congress, Granada, Spain, 22-27 September 2002, CD-ROM publication.

[10] M.F. Montemor, M.G.S. Ferriera, *"Electrochemical study of modified bis- [triethoxysilylpropyl]tetrasulfide silane films applied on the AZ31 Mg alloy"*, Electrochimica Acta (2007), 52, pp. 7486-7495.

[11] K. Brunelli, M. Dabalà, I. Calliari, M. Magrini, *"Effect of HCl pre-treatment on corrosion resistance of cerium-based conversion coatings on magnesium and magnesium alloys"*, Corrosion Science (2005), 47, pp. 989-1000.

[12] M. Dabalà, K. Brunelli, E. Napolitani, M. Magrini, *"Cerium-based chemical conversion coating on AZ63 magnesium alloy"*, Surface & Coating Technology (2003), 172, pp. 227-232.

[13] F. Zucchi, V. Grassi, A. Frignani, G. Trabanelli, *"Inhibition of copper corrosion by silane coatings"*, Corrosion Science (2004), 46, pp. 2853–2865.

[14] N. Pébère, C. Riera, F. Dabosi, *"Investigation of magnesium corrosion in aerated sodium sulphate solution by electrochemical impedante spectroscopy"*, Electrochimica Acta (1990), 35, pp. 555-561.

[15] G. Baril, N. Pébère, *"The corrosion of pure magnesium in aerated and deaerated sodium sulphate solutions"*, Corrosion Science (2001), 43, pp. 471-484.

[16] G. Baril, G. Galicia, C. Deslouis, N. Pébère, B. Tribollet and V. Vivier, *"An Impedance Investigation of the Mechanism of Pure Magnesium Corrosion in Sodium Sulfate Solutions"*, Journal of Electrochemical Society (2007), 154 (2), pp. C108-C113.

[17] J. N. Murray, *"Electrochemical test methods for evaluating organic coating on metals: an update. Part III: Multiple test parameter measurements"*, Progress in organic coating (1997), 31, pp. 375-391.

[18] D. Loveday, P. Peterson, B. Rodgers; *"Evaluation of organic coatings with electrochemical impedande spectroscopy. Part 2: Application of EIS to coatings"*, JCT Coatings-tech (2004), Vol. 1, pp. 88-93.

[19] S.V. Lamaka, M.F. Montemor, A.F. Galio, M.L. Zheludkevich, C. Trindade, L.F. Dick, M.G.S. Ferreira, *"Novel hybrid sol–gel coatings for corrosion protection of AZ31B magnesium alloy"*, Electrochimica Acta (2008), 53, pp. 4773-4783.

[20] Hongwei Shi, Fuchun Liu, En-hou Han *"Corrosion protection of AZ91D magnesium alloy with sol-gel coating containing 2-methyl piperidine"*, Progress in Organic Coatings (2009), 66, pp.183–191.

[21] S. Skale, V. Doleček, M. Slemnik, *"Substitution of the constant phase element by Warburg impedance for protective coatings"*, Corrosion Science (2007), 49, pp. 1045–1055.

[22] M. Santamaria, F. Di Quarto, S. Zanna, P. Marcus, *"Initial surface film on magnesium metal: A characterization by X-ray photoelectron spectroscopy (XPS) and photocurrent spectroscopy (PCS)"* Electrochimica Acta (2007), 53, pp. 1314–1324.

[23] G. Baril, N. Pébère, *"The corrosion of pure magnesium in aerated and deaerated sodium sulphate solutions"*, Corrosion Science (2001), 43, pp. 471-484.

[24] G. Baril, G. Galicia, C. Deslouis, N. Pébère, B. Tribollet and V. Vivier, *"An Impedance Investigation of the Mechanism of Pure Magnesium Corrosion in Sodium Sulfate Solutions"*, Journal of Electrochemical Society (2007), 154 (2), pp. C108-C113.

[25] C.H Hsu, F. Mansfeld, *"Concerning the use of constant phase elements (CPEs) in the analysis of impedance data"*, Corrosion (2001), 57, pp. 747-748.

[26] F. Zanotto, V. Grassi, A. Frignani, F. Zucchi, *"Influenza della microstruttura sul comportamento a corrosione di una lega di magnesio AZ31"*, Atti del 32° Convegno Nazionale dell'AIM, Ferrara 24-26 settembre (2008), (CD-ROM).

[27] M. Garcia-Heras, A. Jimenez-Morales, B. Casal, J.C. Galvan, S. Radzki, M.A. Villegas, *"Preparation and electrochemical study of cerium–silica sol–gel thin films"*, Journal of Alloys and Compounds (2004), 380, pp. 219-224.

[28] S.A. Hayes, P.Yu, M.J. O'Keefe, T.J. O'Keefe, J.O. Stoffer, *"The Phase Stability of Cerium Species in Aqueous Systems"*, Journal of Electrochemical Society (2002), 149, pp. C623-C630.

[29] P.Yu, S.A. Hayes, T.J. O'Keefe, M.J. O'Keefe, J.O. Stoffer, *"The Phase Stability of Cerium Species in Aqueous Systems"*, Journal of Electrochemical Society (2006), 153, pp. C74-C79.

[30] P. Yu, T.J. O'Keefe, *"The Phase Stability of Cerium Species in Aqueous Systems"*, Journal of Electrochemical Society (2006), 153, pp.C80-C85.

[31] V. Palanivel, Y. Huang, W. J. van Ooij, *"Effects of addition of corrosion inhibitors to silane films on the performance of AA2024-T3 in a 0.5M NaCl solution"*, Progress in Organic Coatings (2005), 53, pp. 153–168.

[32] M.F. Montemor, M.G.S. Ferreira, *"Electrochemical study of modified bis-[triethoxysilylpropyl] tetrasulfide silane films applied on the AZ31 Mg alloy"*, Electrochimica Acta (2007), 52, pp. 7486-7495.

Chapter 6

PROTECTION OF THE AZ31 MAGNESIUM ALLOY WITH SILANE COATINGS MODIFIED WITH NANOPARTICLE OXIDES

6.1 Introduction

As discussed in Chapter 5, an improvement of the silane layer protective characteristics could be reached by reducing its defectiveness; this can be obtained also by adding the silane bath with small (nanosized) particles [1]. In fact, it was reported that a silane coating on aluminium alloy could be thickened and strengthened by silica particle addition [1, 2]. The positive synergistic combination of silane and Ceria or Zirconia nanoparticles was experienced on a galvanised steel too [3, 4], as well as on a carbon steel [4]. It was found that these particles reduced the defectiveness and increased the silane layer thickness. Moreover, it has been determined that microsilica addition promoted also an increase in the hardness of BTSPA coating [5]. In every case there was always an optimum nanoparticle concentration [2, 5].

In Chapter 5 the addiction of $Ce(NO_3)_3$ solutions to the 3-mercapto-propyl-trimethoxysilane (PropS–SH) treatment bath determined an increasing of its protective performances. This Chapter intends to show the results obtained by protecting the AZ31 magnesium alloy with the PropS-SH coating loaded with different nanoparticle oxides (Cerium, Zirconium, Titanium and Cerium-Zirconium oxide).

6.2 Experimental part

Square specimens were cut from a 5 mm thick plate of AZ31 magnesium alloy and embedded in an epoxy resin allowing the exposition of a area of 1.5 cm^2. Their surfaces were prepared by emery papers up to 1000 grade, washed with distilled water, degreased with acetone and dried with hot air. These coupons were initially pre-treated in a 10% HF solution for 60 sec, hot air dried and then immersed for 30 sec in the silane bath; after a hot air flux drying, they were finally cured for 1 hour at 100 °C.

The treatment bath was a hydroalcoholic solution (90%/5%/5%, ethylic alcohol/water/silane) of 3-mercapto-propyl-trimethoxy-silane (PropS-SH), which was also modified with an aqueous nanopowder suspensions of 5000 ppm of Cerium oxide (particle size < 25 nm) or Zirconium oxide (particle size < 50 nm) or Titanium oxide (particle size < 25 nm) or Cerium-Zirconium oxide (particle size < 50 nm) (90%/5%/5%, ethylic alcohol/nanoparticle oxide aqueous suspension/silane) in order to obtain a final nanoparticle concentration of 250 ppm. All products are from Aldrich. The silane solutions were regulated at pH 4 by H_2SO_4 addition, maintained under stirring condition for 12 hours and utilized for filming treatment after 48 hours from its preparation.

Electrochemical tests were performed in a 250 ml volume cell and the aggressive solution was 0.1M NaCl. The potentiodynamic polarization curves were recorded by applying a 0.2 mV sec^{-1} scanning rate and electrochemical impedance spectra were performed in the $10^5 \div 10^{-3}$ Hz frequency range, applying, at the corrosion potential, a 10 mV rms sinusoidal perturbation.

6.3 Results and discussion
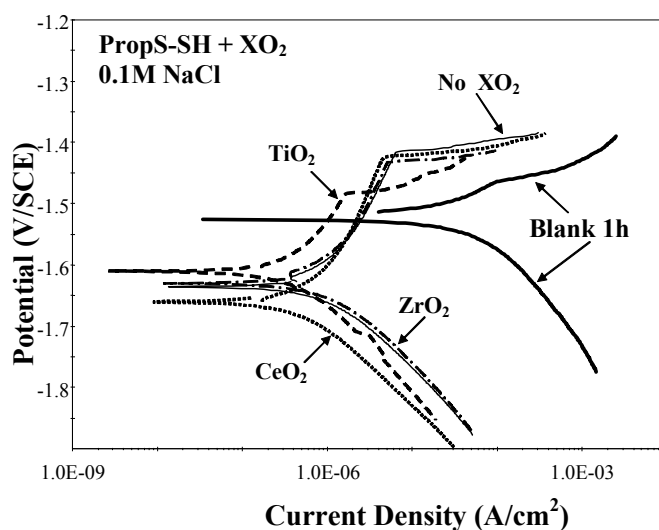
6.3.1 Polarization curves

Fig. 6.2 – *Polarization curves recorded after 1 h immersion in 0.1M NaCl of AZ31 coated by nano-oxide modified and not modified (No XO₂) PropS-SH solution.*

In Chapter 5 the effect of the sole PropS-SH treatment on the AZ31 magnesium alloy was already presented: this treatment showed protective performances that decay quite rapidly with time. The addition of the nano-oxides to the treatment bath improved the performances of the silane coating (figure 6.2); the presence of CeO_2 strengthened the protective action of the PropS-SH layer towards the cathodic reaction, while the presence of TiO_2 also towards the anodic process, although in a lower potential interval (E_{BR} was around 50 mV less positive than that of the sole silane layer). The presence of ZrO_2 afforded no particular advantages.

136

Table 6.1 collects the values of the corrosion current density (i_{CORR}), corrosion potential (E_{CORR}) and inhibition efficiency (I.E.%) determined by the potentiodynamic polarization curves after 1 h immersion. The presence of Titania and Ceria almost three-fold reduced i_{CORR} value, in comparison to that of the sole PropS-SH layer, and the resulting inhibition effect was 99%.

Table 6.1 – *i_{CORR}, I.E.%, and E_{CORR} values obtained from the polarization curves recorded after 1 h immersion in 0.1M NaCl of AZ31 treated with PropS-SH solutions modified with different nanoparticle oxides.*

Treatment	*Nanoparticle Concentration /(ppm)*	*i_{CORR} ($\mu A/cm^2$)*	*I.E. %*
Blank	-	57	-
PropS-SH	-	1.48	97.4%
PropS-SH+ ZrO₂	*250*	1.29	97.7%
PropS-SH + CeO₂	*250*	0.57	99.0%
PropS-SH + TiO₂	*250*	0.52	99.1%

The greatest effect caused by these oxides was to slow down the decay of the protective performances (or even to improve them) that affected PropS-SH coating. However with the addiction of ZrO_2, the inhibition of both the anodic and cathodic processes obtained after 24 h (figure 6.3), resulted reduced after 168 h, especially for the anodic reaction whose polarization curve shifted to currents value almost equivalent to that of the untreated AZ31.
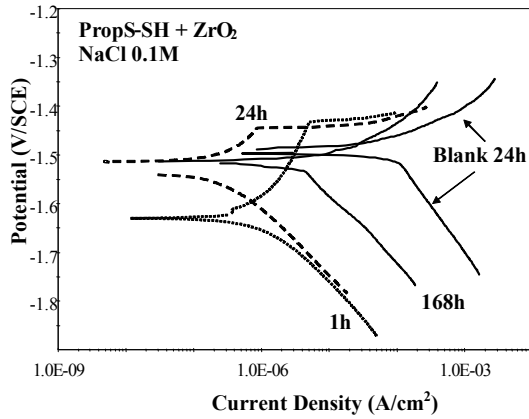
Fig. 6.3 *– Polarization curves recorded, after 1, 24 and 168 h immersion in 0.1M NaCl, on AZ31 coated by PropS-SH bath modified with Zirconim nano-oxide.*

Although, after 168 h immersion, the anodic currents of TiO_2 modified coating (figure 6.4) resulted increased in comparison to that measured after 1 h, the formed layer showed a certain protectiveness also after 168 h. The cathodic currents showed a high increase after 168 h, however still presenting lower values than that of the blank.
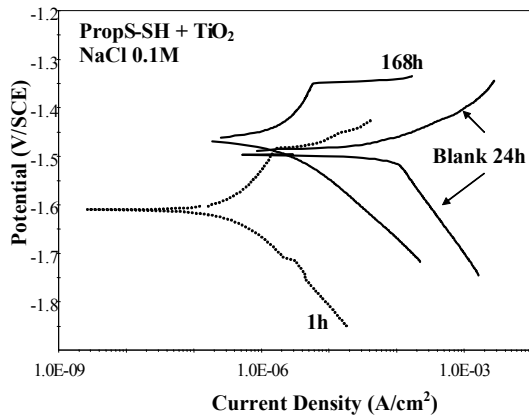

Fig. 6.4 *– Polarization curves recorded, after 1 and 168 h immersion in 0.1M NaCl, on AZ31 coated by PropS-SH bath modified with Titanium nano-oxide.*

138

The treatment bath that better succeeded in maintaining the protective performance of the modified PropS-SH coating up to 168 h was that added with CeO_2 nano-oxide (figure 6.5).
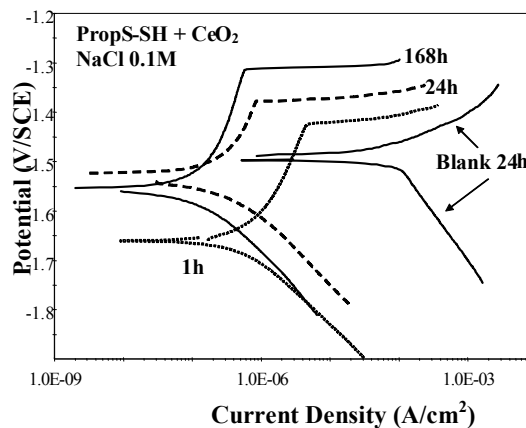

Fig. 6.5 *– Polarization curves recorded, after 1 and 168 h immersion in 0.1M NaCl, on AZ31 coated by PropS-SH bath modified with Cerium nano-oxide.*

In this case, after 168 h immersion, the cathodic curve current values resulted still three order of magnitude lower than that of the untreated AZ31 and the anodic process inhibition resulted increased from 1 to 168 h, with current values decreased of about one order of magnitude. The CeO_2 modified silane coating stability was practically maintained up to 168 h.

A further improvement of the protective performance and stability of the silane coating was obtained with the addition of 250 ppm or 500 ppm of Cerium-Zirconium oxide to the treatment bath; in fact, after 1 h immersion (figure 6.6), the cathodic and anodic currents resulted shifted to lower values in comparison to that of the silane coating modified with Ceria, and with a concentration of 250 ppm there was also a slight ennoblement of the breakdown potential (E_{BR}).

139

Fig. 6.6 – Polarization curves recorded, after 1 h immersion in 0.1M NaCl, on AZ31 coated by PropS-SH bath modified with, Cerium or Cerium-Zirconium nano-oxide (250 ppm) or Cerium-Zirconium nano-oxide (500 ppm).

With increasing of immersion time, in the case of a Cerium-Zirconium concentration of 250 ppm, the cathodic polarization curves remained almost unchanged during the whole time interval (figure 6.7) and the action exerted on the anodic process still continued for all the test (168 h): during this interval the anodic currents decreased by about one order of magnitude and E_{BR} ennobled by around 50 mV.
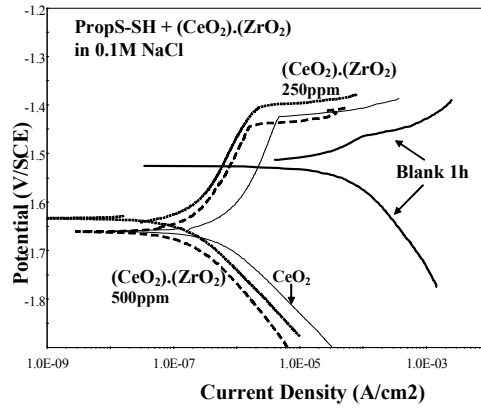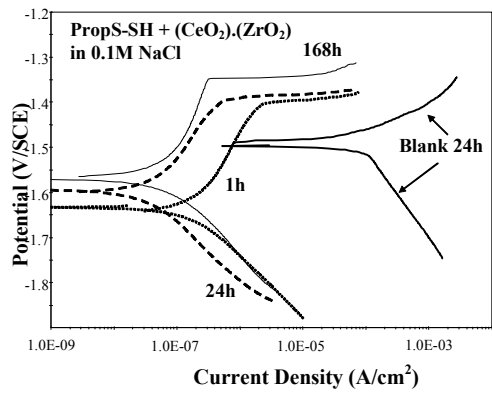

Fig. 6.7 – Polarization curves recorded, after 1 h immersion in 0.1M NaCl, on AZ31 coated by PropS-SH bath modified with, 250 ppm of Cerium-Zirconium nano-oxide.

140

Table 6.2 collects the icorr values and the inhibition efficiency obtained from polarization curves after 1, 24 and 168 h immersion in 0.1M NaCl, for the various treatment baths. The corrosion rate value of the AZ31 electrode covered by the 250 ppm Cerium-Zirconium oxide modified silane coating, after 1 h immersion, was 0.18 $\mu A/cm^2$, i.e. a third of the value of PropS-SH + CeO_2 coated AZ31 specimen, and after 7 d it was further on reduced to 0.07 $\mu A/cm^2$, whereas that of the PropS-SH + CeO_2 coated AZ31 specimen to 0.12 $\mu A/cm^2$. Although, after 1 h immersion, a 500 ppm addiction of Cerium-Zirconium oxide to the PropS-SH bath determined a corrosion rate of the AZ31 specimen equal to 250 ppm Cerium-Zirconium oxide one (0.18 $\mu A/cm^2$), after 168 h, there was a slight worsening in its inhibition efficiency.

Table 6.2 – i_{CORR} *Values obtained from polarization curves recorded after 1, 24, 168 h immersion in 0.1M NaCl.*

Treatment		After 1h in NaCl 0.1M		After 24h in NaCl 0.1M		After 168h in NaCl 0.1M	
	Conc. (ppm)	*icorr ($\mu A/cm^2$)*	*I.E. %*	*icorr ($\mu A/cm^2$)*	*I.E. %*	*icorr ($\mu A/cm^2$)*	*I.E. %*
Blank	-	57	-	86	-	37	-
PropS-SH	-	1.48	97.4	3.65	95.8	23.9	35.4
+ ZrO₂	250	1.29	97.7	0.40	99.5	3.50	90.5
+ CeO₂	250	0.57	99.0	0.32	99.6	0.12	99.7
+ TiO₂	250	0.52	99.1	0.34	99.6	2.38	93.6
+ (CeO₂)·(ZrO₂)	250	0.18	99.7	0.03	99.97	0.07	99.8
+ (CeO₂)·(ZrO₂)	500	0.18	99.7	0.11	99.9	0.21	99.4

6.3.2 Electrochemical Impedance Spectra

In Chapter 5 the EIS spectra acquired on the AZ31 specimen treated with the sole PropS-SH bath has been already discussed: the initial good performances of the formed coating soon worsened, as a matter of fact there was a progressive reduction of the *hf* semicircle, with the disappearance, after 48 h immersion, of the *lf* one, due to a local breakdown of the protective layer. At the end of the test the Rp value (impedance modulus calculated at low frequency, before the inductive behaviour) was close to that of the blank (895 $\Omega.cm^2$ [6]).

The EIS spectra recorded on the AZ31 electrodes treated with the PropS-SH bath modified with ZrO_2 (figure 6.6) or TiO_2 (figure 6.7) nano-oxide were very similar to that obtained with the sole PropS-SH treatment, but with Rp values, at the beginning of the test, a little improved in comparison to that of the sole silane treatment. As observed for the PropS-SH coating, the EIS spectra of the Zirconia modified PropS-SH showed, at the highest frequencies ($10^4 \div 10^5$ Hz), a resistive response, due to the high conductivity of the electrolyte solution inside the pores, evidencing the fact that the coating was very porous and defective and characterized by a rather low stability. In fact, also in this case, after 48 h immersion, the *lf* capacitive semicircle was not anymore detectable due to a local breakdown of the layer.

Fig. 6.6 *– EIS spectra recorded, after 1, 4, 24, 48 h immersion in 0.1 M, on AZ31 electrodes treated with a ZrO₂ nano-oxide modified PropS-SH bath.*

Fig. 6.7 *– EIS spectra recorded, after 1, 4, 24, 48 h immersion in 0.1 M, on AZ31 electrodes treated with a TiO₂ nano-oxide modified PropS-SH bath.*

In the first immersion hours, Ceria also displayed an almost resistive response (figure 6.8). However after 24 h immersion a time constant at very high frequencies resulted well defined, whose characteristic frequency was initially around 10^5 Hz, and then 10^4 Hz (after 168 h). As already discussed in Chapter 5, this *hf* time constant is likely representative of a capacitive response, due to the lowered defectiveness and porosity of the Ceria modified coatings [7]. The presence of a 10^2 Hz time constant, likely linked to the corrosion processes occurring on the metal substrate (see Chapter 5), persisted for almost all the run, but at the end it merged with the *lf* time constant (1÷0.1 Hz).
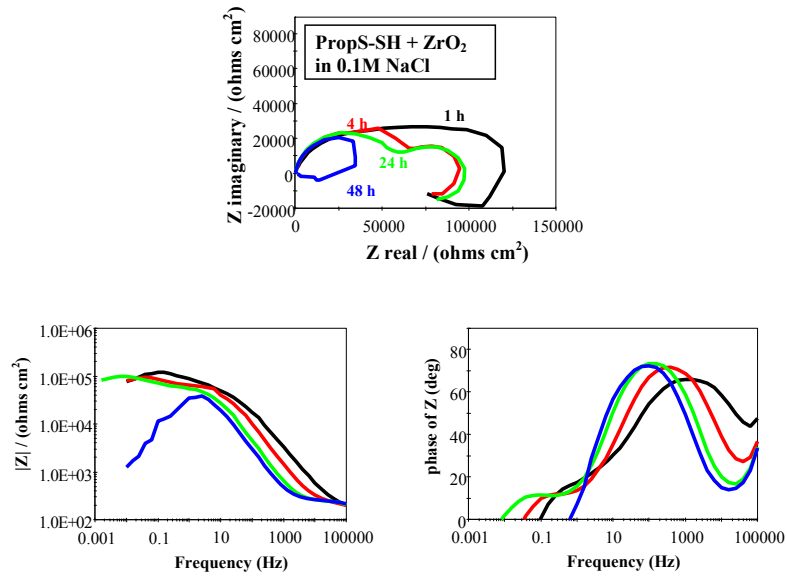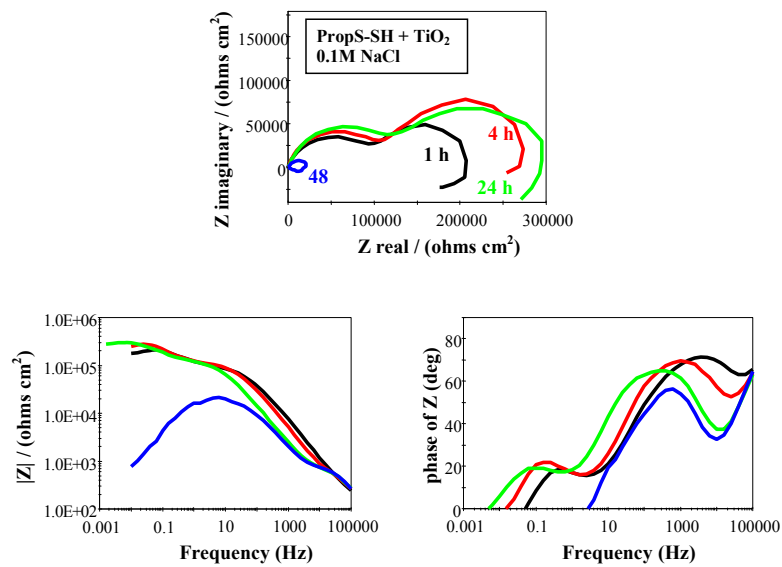

Fig. 6.8 – *EIS spectra recorded, after 1, 4, 24, 168 h immersion in 0.1 M, on AZ31 electrodes treated with a CeO₂ nano-oxide modified PropS-SH bath.*

The *lf* semicircle diameter, noticeably increased from 4 to 24 h, in fact Rp passed from 60 to 250 kΩcm² , and then it remained almost constant up to 168 h. It was reported in Chapter 5 that this latter time constant might be linked to the diffusion of water and ions trough the micro-pores

144

that likely characterize an almost complete coating, when conductive pathways are very few [8], or to the diffusion of Mg^{2+} ions through the corrosion product layer, when, due to electrolyte penetration, conductive pathways become active and the electrochemical reactions occur on metallic substrate [8, 9]. The modification of PropSH-SH solution with Cerium-Zirconium oxide confirmed the presence of 10^5 Hz time constant (figure 6.9), observable for all the test duration, thus the capacitive response, indicative of a low defective and porous coating was present since the first immersion hours. However, the 10^2 Hz time constant was detectable too. With this oxide, PropS-SH coating improved its efficiency particularly during the first 24 h immersion, when Rp increased from 275 to over 1100 kΩcm². Afterwards there was a certain decrease; however, at the end of the run, Rp was close to 500 kΩcm².
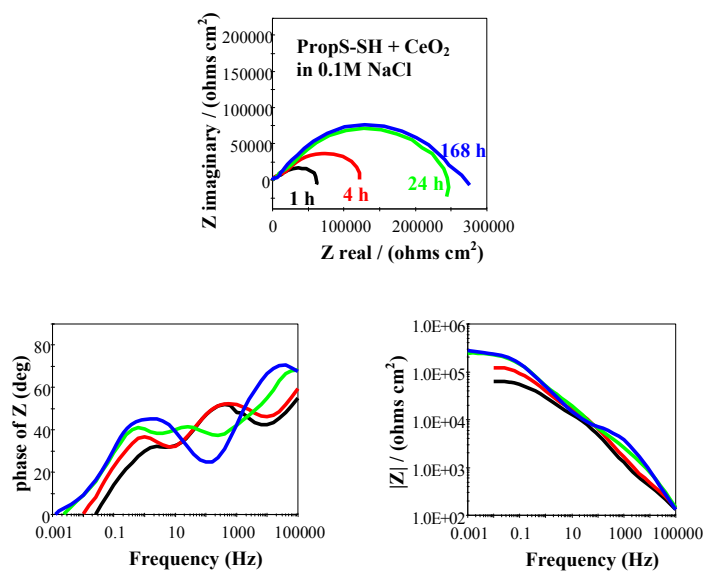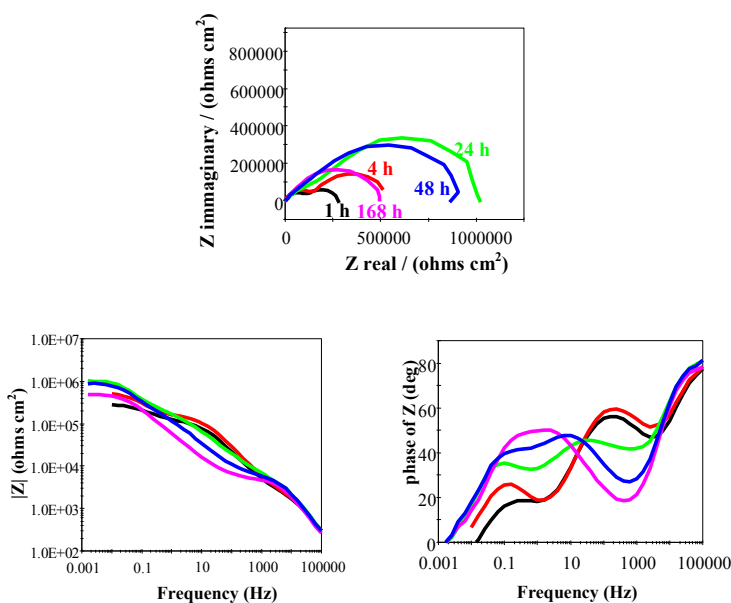

Fig. 6.9 – *EIS spectra recorded, after 1, 4, 24, 48, 168 h immersion in 0.1 M, on AZ31 electrodes treated with a (CeO₂)·(ZrO₂) nano-oxide modified PropS-SH bath.*

Table 6.3 collects the values of Rp for the various coatings obtained by EIS measurements during 7 d (168 h) immersion in 0.1M NaCl, while Table 6.4 the Inhibiting Efficiency (I.E.%) ones.

It can be clearly seen that the protective action of PropS-SH layer lasted for not longer than few days; in fact, Rp soon decreased rapidly and after 3-4 d immersion this action was almost completely disappeared.

Although, at the beginning, Titania proved to be the most efficient nanopowder, nevertheless in a short time its influence decreased. However, at the end of the experiment, PropS-SH coating, loaded with Titania, reduced AZ31 corrosion process by over one order of magnitude (like Zirconia did).

Table 6.3 – *Rp values obtained from EIS spectra recorded in 0.1M NaCl.*

Time in NaCl 0.1N (hours)	Rp (Ωcm^2)					
	PropS-SH	*PropS-SH + ZrO$_2$*	*PropS-SH + CeO$_2$*	*PropS-SH + TiO$_2$*	*PropS-SH + (CeO$_2$)·(ZrO$_2$)*	
	250 ppm				*250 ppm*	*500 ppm*
1	50203	42420	77325	207372	284688	184470
4	95448	94842	121876	275616	516672	372130
24	56285	97363	246444	295756	1251360	473770
48	11726	34861	258060	20724	859824	396000
72	3812	13451	263604	14032	639216	367620
96	2567	9169	262812	13122	549216	317020
168	1108	8837	276012	6192	493344	258940

Between the preceding oxides, Ceria was, in the whole, the most efficient one, because it almost completely stopped the PropS-SH layer decay. In fact, Ceria loaded PropS-SH coating maintained a very high protective action for the whole testing time and at the end of the run the coating inhibition efficiency was over 99% (around 99.7%). A further improvement in the coating performances could be obtained with Cerium-Zirconium oxide. This coating efficiency was very high since the first immersion hour (99.7%) and was maintained up to the end of the test. In this case the optimum oxide amount was 250 ppm.

Table 4 – *I.E.% values obtained from EIS spectra recorded in 0.1M NaCl.*

Time / (hours)	I.E.%					
	PropS-SH	PropS-SH + ZrO_2	PropS-SH + CeO_2	PropS-SH + TiO_2	PropS-SH + $(CeO_2)\cdot(ZrO_2)$	
	250 ppm				*250 ppm*	*500 ppm*
1	*98.2*	*97.9*	*98.8*	*99.6*	*99.7*	*99.5*
4	*99.1*	*99.1*	*99.3*	*99.7*	*99.8*	*99.8*
24	*98.4*	*99.1*	*99.6*	*99.7*	*99.9*	*99.8*
48	*92.4*	*97.4*	*99.7*	*95.7*	*99.9*	*99.8*
72	*76.5*	*93.3*	*99.7*	*93.6*	*99.9*	*99.8*
96	*65.1*	*90.2*	*99.7*	*93.2*	*99.8*	*99.7*
168	*19.2*	*89.9*	*99.7*	*85.5*	*99.8*	*99.6*

Impedance spectra have shown that the XO_2 nanoparticle presence augmented the barrier properties of the PropS-SH coating on AZ31 magnesium alloy, as it has been previously found by some authors in the

case of other type of alloys [1, 3, 4]. It is well known that a coating efficiency depends on its thickness and on defects presence: the lower the thickness and the higher the defects number, the lower the efficiency. Although till now the PropS-SH coatings thicknesses have not been measured, it is likely that also in our case these nanopowders have increased the PropS-SH layer thickness. Contemporaneously, this should have also reduced the possibility of interconnected porosity presence, that allows an easy entrance of the aggressive solution to the underlying AZ31 substrate. At the same time it is likely that these powders, incorporated in the defects, can limit the access of the electrolytic solutions or can lead to a pores plugging. In fact, the same authors considered a pinholes concentration decrease or a pore-blocking effect a possible justification for the increasing of the silane layer corrosion resistance. Moreover, Montemor and co-workers [4] in a study about the role played by CeO_2 and $CeO_2 \cdot ZrO_2$ added as fillers to a silane coating treatment applied to galvanized steel, reported that CeO_2 nanoparticles are characterized by a fluorite structure that easily develop oxygen vacancies, making these nanoparticles highly reactive. They suggested that when silica network decomposes, due to a local pH increasing on the cathodic sites, nanoparticles are released into the solution and might precipitate forming complexes with species derived from the anodic activity. These more stable corrosion products decrease the active area available slowing down the corrosion activity. Thus they concluded that CeO_2 and $CeO_2 \cdot ZrO_2$ nanoparticles play an active role in the corrosion protection performance when they are added to silane coatings.

148

6.4 Conclusions

✓ Loading with 250 ppm nanosized powders of Zirconium, Titanium, Cerium oxides improves the protective performances of 3-mercapto-propyl-trimethoxy-silane (PropS-SH) coating, both as efficiency and as persistence.

✓ The sequence of increasing ability is: Zirconia, Titania, Ceria.

✓ A further improvement can be reached with Cerium-Zirconium oxide. Optimum concentration is 250 ppm.

References

[1] M.L. Zheludkevich, R. Serra, M.F. Montemor, I.M. Miranda Salvado, M.G.S. Ferreira, *"Corrosion protective properties of nanostructured sol–gel hybrid coatings to AA2024-T3"*, Surface Coating Technology (2006), 200, pp. 3084-3094.

[2] V. Palanivel, D. Zhu, W.J. van Ooji, *"Nanoparticle-filled silane films as chromate replacements for aluminum alloys"*, Progress in Organic Coatings (2003), 43, pp. 384-392.

[3] M.F. Montemor, A.M. Cabral, M.L. Zheludkevich, M.G.S. Ferreira, *"The corrosion resistance of hot dip galvanized steel pretreated with Bis-functional silanes modified with microsilica"*, Surface Coating Technology (2006), 200, pp. 2875-2885.

[4] M.F. Montemor, W. Trabelsi, S.V. Lamaka, K.A. Yasaku, M.L. Zheludkevich, A.C. Bastos, M.G.S. Ferreira, *"The synergistic combination of bis-silane and $CeO_2 \cdot ZrO_2$ nanoparticles on the electrochemical behaviour of galvanised steel in NaCl solutions"*, Electrochimca Acta (2008), 53, pp. 5913-5922.

[5]   P.H. Suegama, A.A.C. Recco, A.P. Tschiptschin, I.V. Aoki, *"Influence of silica nanoparticles added to an organosilane film on carbon steel electrochemical and tribological behaviour"*, Progress in Organic Coatings (2007), 60, pp. 90-98.

[6]   F. Zanotto, V. Grassi, A. Frignani, F. Zucchi, *"Influenza della microstruttura sul comportamento a corrosione di una lega di magnesio AZ31"*, Proc. of 32nd AIM National Congress, Ferrara, Italy, September 24-26, 2008, (CD-ROM publication).

[7]   J. N. Murray, *"Electrochemical test methods for evaluating organic coating on metals: an update. Part III: Multiple test parameter measurements"*, Progress in organic coating (1997), 31, pp. 375-391.

[8]   S. Skale, V. Doleček, M. Slemnik, *"Substitution of the constant phase element by Warburg impedance for protective coatings"*, Corrosion Science (2007), 49, pp. 1045–1055.

[9]   G. Baril, G. Galicia, C. Deslouis, N. Pébère, B. Tribollet and V. Vivier, *"An Impedance Investigation of the Mechanism of Pure Magnesium Corrosion in Sodium Sulfate Solutions"*, Journal of Electrochemical Society (2007), 154 (2), pp. C108-C113.

Conclusions

This thesis illustrates the main topics that I have faced during my PhD research activity concerning corrosion behaviour of magnesium alloys, in particular AZ31 alloy, and the anti-corrosion methods, such as corrosion inhibition and surface treatments, for the protection of the AZ31 alloy from corrosion.

The results discussed in Chapter 2 showed that the analyzed as-cast AZ31 magnesium alloy exhibited a higher corrosion resistance in comparison to the hot rolled AZ31, due to the different distribution and chemical composition of the constituent phases.

In Chapter 3 environmentally friendly sodium salts of capric (decanoic), lauric (dodecanoic), myristic (tetradecanoic) acids produced an inhibiting action towards AZ31 magnesium alloy corrosion in a synthetic cooling water, due to the formation of a layer of insoluble magnesium carboxylates.

By means of aqueous solutions of sodium salts of long mono-carboxylic acids was possible to build a protective conversion coating on AZ31 magnesium alloy (Chapter 4). In particular, sodium stearate (sodium salt of octadecanoic acid) displayed the higher protective effect.

Finally, the protective performance of coatings obtained by treating the AZ31 specimens in 3-mercapto-propyl-trimethoxysilane baths could be improved by adding cerium nitrate (Chapter 5) or nanoparticle oxides (Chapter 6). In the latter case the best protective performance were obtained by loading the PropS-SH silane coating with 250 ppm of Cerium or Cerium-Zirconium nano-oxides.

List of publications

International Journals

- ➤ F. Zucchi, V. Grassi, F. Zanotto [*], *"Sodium monocarboxylates as inhibitors of AZ31 alloy corrosion in a synthetic cooling water"*, Materials and Corrosion, 60, No. 3, 2009, pp. 199-205.
- ➤ Frignani, V. Grassi, F. Zucchi and F. Zanotto*, *"Mono-carboxylate conversion coatings for AZ31 Mg alloy protection"*, Materials and Corrosion (2010), DOI: 10.1002/maco.200905615.

Proceedings of Nationals and International Conferences

- ➤ F. Zanotto, V. Grassi, A. Frignani, F.Zucchi., *"Influenza della microstruttura sul comportamento a corrosione di una lega di magnesio AZ31."*, Atti del 32° Convegno Nazionale dell'AIM, Ferrara, 24-26 Settembre 2008.
- ➤ F. Zanotto, V. Grassi, A. Frignani, F.Zucchi, *"Caratteristiche protettive di rivestimenti di 3-mercapto-1-trimetossisilil-propano modificati con cerio e depositati su lega di magnesio AZ31."*, Atti delle Giornate Nazionali sulla Corrosione e Protezione, Udine, 24-26 Giugno 2009.

➢ F. Zanotto, V. Grassi, A. Frignani, C. Monticelli, A. Balbo, F. Zucchi, *"Corrosion behaviour of AZ31 magnesium alloy pre-treated with silane solutions modified with nanoparticle oxides."* Proceedings of EUROCORR 2009, 6-10 September 2009, Nice, France.

Other Publications

➢ F. Zucchi, F. Zanotto, V. Grassi, *"Comportamento a corrosione delle principali leghe di magnesio di interesse industriale."*, Atti della Giornata di Studio: Il magnesio e le sue leghe: caratteristiche, processi e applicazioni, AIM, 29 febbraio 2008, Vicenza.